

Through-the-Earth Magnetic Induction Communication and Networking: A Comprehensive Survey

Honglei Ma, Erwu Liu, *Senior Member, IEEE*, Wei Ni, *Fellow, IEEE*, Zhijun Fang, Rui Wang, Yongbin Gao, Dusit Niyato, *Fellow, IEEE*, and Ekram Hossain, *Fellow, IEEE*

Abstract—Magnetic induction (MI) communication (MIC) has emerged as a promising candidate for underground communication networks due to its excellent penetration capabilities. Integration with Space-Air-Ground-Underground (SAGUI) networks in next-generation mobile communication systems requires a well-defined network architecture. A recent discovery in MIC research, MI fast fading, remains in its early stages and presents unique challenges. This paper provides a comprehensive survey on through-the-earth (TTE) MIC, covering MI applications, channel modeling, point-to-point MIC design, relay techniques, network frameworks, and emerging technologies. We compare various MIC applications to highlight TTE-specific challenges and review the principles of channel modeling, addressing both MI slow fading and MI fast fading, along with its potential impact on existing MIC theories. We conduct a fine-grained decomposition of MI channel power gain into four distinct physical parameters, and propose a novel geometric model to analyze MI fast fading. We also summarize MI relay techniques, examine crosstalk effects in relay and high-density networks, and explore key research tasks within the OSI framework for a holistic MI network protocol in SAGUI. To bridge the gaps identified, we propose a MIC framework that supports TCP/IP and Linux, enabling full implementation of existing and emerging MIC solutions. This framework empowers researchers to leverage Linux resources and deep learning platforms for accelerated development of MIC in SAGUI networks. Remaining research challenges, open issues, and promising novel techniques are further identified to advance MIC research.

Index Terms—Magnetic induction (MI), underground wireless

This work is supported in part by grants from the National Science Foundation of China (Nos. 42171404, 62271352), in part by Shanghai Engineering Research Center for Blockchain Applications And Services (No. 19DZ2255100), in part by Seatrium New Energy Laboratory, Singapore Ministry of Education (MOE) Tier 1 (RT5/23 and RG24/24), the NTU Centre for Computational Technologies in Finance (NTU-CCTF), and the RIE2025 Industry Alignment Fund-Industry Collaboration Projects (IAF-ICP) (Award I2301E0026), administered by A*STAR, and in part by the Fundamental Research Funds for the Central Universities under Grant 22120250094.

H. Ma, Z. Fang, and Y. Gao are with the School of Electronic and Electrical Engineering, Shanghai University of Engineering Science, Shanghai, China (e-mail: holyma@yeah.net, Zjfang@gmail.com, gaoyongbin@sues.edu.cn).

E. Liu and R. Wang are with the College of Electronic and Information Engineering, Tongji University, Shanghai, China. R. Wang is also with the Shanghai Institute of Intelligent Science and Technology, Tongji University, Shanghai, China (e-mail: erwu.liu@ieee.org, ruiwang@tongji.edu.cn).

W. Ni is with the School of Engineering, Edith Cowan University, Perth, WA 6027, and the School of Computer Science and Engineering, The University of New South Wales, Sydney, NSW 2033, Australia (e-mail: wei.ni@ieee.org).

D. Niyato is with the College of Computing and Data Science, Nanyang Technological University, Singapore 639798 (e-mail: dniyato@ntu.edu.sg).

E. Hossain is with the Department of Electrical and Computer Engineering, University of Manitoba, Winnipeg, Manitoba, Canada (e-mail: Ekram.Hossain@umanitoba.ca).

(Corresponding author: E. Liu)

DOI: 10.1109/COMST.2025.3623258

communication, through-the-earth (TTE), fast fading, network architecture, TCP/IP.

TABLE I
ACRONYMS AND DEFINITIONS

Acronym	Full name / Definition
*/ **/ ***	Low / Medium / High (priority used in tables and figures)
AF	Amplified-and-forward
AG	Aboveground
APO	Antenna position and orientation
AUV	Autonomous underwater vehicle
AVI	Antenna vibration intensity
BAN	Body area network
BCS	Boundary Chi-square (Boundary χ^2)
BCH	Bose, Ray-Chaudhuri, Hocquenghem
CDF	Cumulative distribution function
CLO	Cross-layer optimization
CLT	Central limit theorem
CMG	CMIC achievable rate gain
CMI	Cooperative magnetic induction
CMIC	Cooperative magnetic induction communication
CMIC-1NR	CMIC with one non-aligned relay
CMIC- n AR	CMIC with multiple aligned relays
CSI	Channel state information
CSMA	Carrier sense multiple access
DF	Decode-and-forward
DMI	Direct magnetic induction
DWE	dynamic weighted evolution/learning
EMW	Electromagnetic wave
EMWC	Electromagnetic wave communication
EPR	Effective payload ratio
FEC	Forward error correction
FEM	Finite element method
FF	Filter-and-forward
FSOC	Free-space optical communication
GAN	Generative adversarial networks
GTS	Guaranteed time slot
IP-HC	Internet protocol header compression
IoV	Internet of Vehicles
JSCC	Joint source-channel coding
KVL	Kirchhoff's voltage law
LLM	Large language model
LLC	Logical link control
Ly	Layer
MAC	Medium access control
M ² I	Metamaterial-enhanced magnetic induction
MCD	MI Linux character device
MCNSI	MI communication-navigation-sensing integrated
MI	Magnetic induction
MIC	Magnetic induction communication
MIMO	Multiple-input multiple-output
MND	MI Linux network device
MPRIA	MI passive relay array
NFC	near field communication
OSI	Open Systems Interconnection
P2P	Point-to-point
PDF	Probability density function
PSD	Power spectral density
RL	Reinforcement learning
RPMA	Rotating permanent magnet antenna
RTT	Round-trip time
Rx	Receive
SAGUMI	Space-Air-Ground-Underground multi-network integration
SISO	Single-in single-out
SNR	Signal-to-noise ratio
TCP / IP	Transmission control protocol / Internet protocol
TMR	Tunneling Magnetoresistance
ToA	Time of arrival
TTE	Through-the-earth
Tx	Transmit
UDP	User datagram protocol
UG	Underground
UG-WSN	Underground wireless underground sensor network
UW-WSN	Underwater wireless sensor network
VMI	Vehicle magnetic induction
VLF-LA	Very low frequency and a larger antenna
WSN	Wireless sensor network

I. INTRODUCTION

A. Underground Communication and TTE Communication

As human activities increasingly extend into underground environments, and reliable underground communication has become essential for applications, such as resource exploration, disaster rescue, underground blasting, and robotic operations in hazardous scenarios [1]. DARPA launched the Subterranean Challenge in 2017 to drive innovation in mapping, navigation, and search solutions for complex underground spaces, including tunnel systems, urban underground areas, and natural caves [2]. One of the primary challenges in this initiative was ensuring robust underground communication. As next-generation mobile communication technologies, such as 6G [3], evolve, underground communication is expected to play a critical role in integrated networks, where protocols, such as TCP/IP, will be indispensable for enabling essential functionalities, such as dynamic passwords, node registration, and licensing approval by regional authorities (e.g., national security centers). However, without standardized protocols, these advanced features are nearly impossible to achieve.

TABLE II
NOTATION AND DEFINITION

Definition [†]	Notation
Basic parameters	See Table III
Probability	$\mathbb{P}(\cdot)$
Expectation	$\mathbb{E}(\cdot)$
Imaginary unit $\sqrt{-1}$	j
Source/Tx	S
Destination/Rx	D
Relay	R
(-) of source/Tx antenna	$(\cdot)_S$
(-) of destination/Rx antenna	$(\cdot)_D$
(-) of relay antenna	$(\cdot)_R$
(-) of link $S \rightarrow D$	$(\cdot)_{SD}$
Magnetic moment by antenna S	\mathbf{m}_S
Channel power gain [of link $S \rightarrow D$]	G_{SD}
Circuit gain [of link $S \rightarrow D$]	\mathcal{C}_{SD}
Space gain [of link $S \rightarrow D$]	\mathcal{S}_{SD}
Eddy gain [of link $S \rightarrow D$]	\mathcal{E}_{SD}
Polarization gain or MI fast fading [of link $S \rightarrow D$]	J_{SD}
Mutual inductance [of link $k \rightarrow l$]	M_{kl}
Compensated in-device gain/loss [for link $S \rightarrow D$]	\mathbb{N}_{SD}
Wavenumber in the medium	k_0
Horizontal vibration angle [of the antenna S]	ϕ_S
Vertical vibration angle [of the antenna D]	θ_D
Average AVI [of antenna S]	σ_S
Boundary of the antenna vibration	ς
Dirac's function	$\delta_{pu}(\cdot)$
Overall circuit impedance [of coil S]	Z_S
Current or divisor [at coil/antenna S]	I_S
PSD [of Tx S]	P_{Sf}
Noise power	N_o
Capacitance of match capacitor for f_0 [at coil S]	C_{CS}
Resistance of the load	R_L
Resistance [of coil S]	R_{CS}
Time or time slot [of Tx S]	t_S
Inductance [of coil S]	L_{CS}
Bandwidth	B_w
Function of 3-dB bandwidth	$B_w(\cdot)$
3-dB bandwidth for CMIC-1NR using AF	B_{AF}
Achievable rate [of link/system $S \rightarrow D$]	\mathfrak{C}_{SD}

[†] The brackets [] represents the optional part. For example, the average AVI [of antenna S] is denoted by σ_S . Optionally, the average AVI [of antenna D] is denoted by σ_D .

Despite its importance, underground communication has received significantly less research attention compared to aboveground technologies such as electromagnetic wave communication (EMWC). It remains a bottleneck in applications ranging from general underground operations to DARPA's

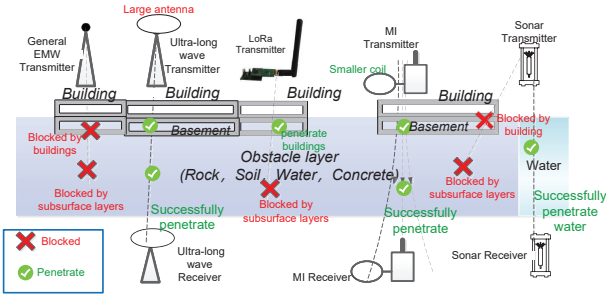


Fig. 1. Comparison of the penetration abilities of communication approaches. Green and red texts indicate the advantages and disadvantages, respectively. Performance and deployment comparisons are presented in Table IV.

robotic systems and next-generation multi-network integration, particularly when supporting TCP/IP protocols. Known as through-the-earth (TTE) communication due to its ability to penetrate over 10 m of soil and rock, this technology is especially critical for scenarios such as mining and drilling, where depths often exceed 1,000 m. Notably, the Kola Superdeep Borehole even extends beyond 12,000 m [4]. During disasters, when EMWC and wired infrastructures are often rendered inoperative, TTE communication's flexible deployment capabilities can expedite rescue operations, potentially saving countless lives.

Fig. 1 illustrates various TTE communication techniques with their performance and deployments compared in Table IV. General EMW signals are limited in penetration and may fail to reach basement levels. Acoustic communication systems are unsuitable for TTE communication due to severe multipath effects in complex underground materials [5]. Ultra-long wave (ULW) radio-based communication, though capable of penetrating deeper, requires kilometer-scale antennas, which are impractical in confined underground spaces [6]. In contrast, MIC has proven effective for a wide range of underground applications. Time-varying magnetic fields experience less attenuation than EMWs [7], and MIC antennas (coils) are compact compared to ULW devices. For instance, an 8-meter diameter MIC antenna can achieve a TTE communication range of up to 310 m [8], while smaller antennas (less than 1 m in diameter) are sufficient for shorter distances, making them suitable for vehicle-mounted applications. This flexibility enables mobile MI networks, ideal for emergency rescue operations [9], [10].

The MIC uses a modulated magnetic field generated by a transmitter antenna. This field is received by a receiver coil or magnetic sensor, which demodulates it into symbols. The Wrathall team accomplished an underwater MIC in 1999 using a 3 kHz field [17]. Since then, MIC has been explored as an alternative for underground (UG) WSNs. In 2006, Akyildiz *et al.* [18], [19] summarized various UG-WSN scenarios, including soil monitoring, underground water monitoring, pipe leak detection, intruder detection, rescue personnel localization, and building load-bearing pressure detection. Sun *et al.* [12] introduced MIC into UG-WSNs with a small device featuring a 10 cm coil in 2010. Recently, researchers have expanded on applications of the non-coil-based MIC and large-scale MI networks. For example, Zhang *et al.* [20] developed a rotating permanent magnet antenna (RPMA) array device for

TABLE III
KEY PARAMETERS, SYMBOLS, AND THEIR DEFAULT VALUES FOR SIMULATIONS IN THIS PAPER

Parameters	Symbol [†]	Default values	Unit	Refs.	Related simulations in this survey
Tx or CMI coil radius	a_{cS}	0.6	meter	[11]	Figs. 4, 11, 12, 19, 21, 22
Rx coil radius	a_{cD}	0.4	meter	[11]	Fig. 11, 12
Number of turns of Tx or CMI coils	N_S	15	-	[11]	Figs. 11, 12, 19, 21, 22
Number of turns of Rx coil	N_D	30	-	[11]	Fig. 11, 12
Coil resistance	ρ_w	0.166	Ω / m	[8], [11]	Figs. 11, 12, 19, 21, 22
Tx Power	P_s, P_S	5	Watt	[7], [11]	Figs. 11, 12, 19, 21, 22
Resonance (center) frequency	f_0	10000	Hz	[7], [11]	Figs. 19, 22
Carrier frequency	f	10000	Hz	[7], [11]	Figs. 19, 22
Tx coil orientation	θ_s	0	-	[12]	Figs. 7, 8, 11, 12, 19, 21, 22
DMI Rx coil orientation	θ_D	π	-	[12]	Figs. 11, 12, 19
VMI Rx coil orientation	θ_D	$-\frac{\pi}{2}$	-	[9]	Fig. 7
Ambient noise PSD	$N_{o,f}$	-103	$\text{dBm} / 2 \text{ kHz}$	[12]	Figs. 11, 12, 19, 21, 22
Permeability of medium	μ_u	$4\pi \times 10^{-7}$	H / m	[7], [13]	Figs. 11, 12, 19, 21, 22, 29
Conductivity of medium	σ_u	10^{-2}	S / m	[7], [13]	Figs. 11, 12, 19, 21, 22
Permittivity of medium	ϵ_u	6.978×10^{-11}	F / m	[13]	Figs. 11, 12, 19, 21, 22, 29
Distance between S and D	d_{SD}	60	meter	[7]	Figs. 19, 21, 22

[†] In this paper, Italic subscript ‘f’ indicates “(·) per Hz”. All the normal (upright) subscripts indicate the description which does not represent any number or node ID.

TABLE IV

COMPARISON OF MIC AND OTHER COMMUNICATIONS IN PERFORMANCE AND DEPLOYMENT DIMENSIONS FOR UNDERGROUND ENVIRONMENTS

Performance [†]	MIC	EMWC	Acoustic	Wired	Hybrid
Comm. ranges (m)	0.1~1,700	<10 ($f=300\text{MHz}$) [12]	<50 m (Position) [14]	> 10,000	-
Data rates (kbps)	< 10 ($d_{SD} > 50 \text{ m}$)	< 100 ($d_{SD} > 5 \text{ m}$) [15]	5~17.8 [16]	>1,000	-
Channel dependency	Conductivity, antenna vibration	Multipath, conductivity, permittivity,	Multipath, Doppler effect, sound noise	Cable properties and length, shielding, connection quality	Interference, protocols, power control
Antenna/device size (m)	0.1~4 radius coil	> 10,000 (VLF antenna) [6]	<1	>10,000 (including cables)	Smaller antenna for subsystems
Deployment costs	Low	High	Medium	Extremely High	High
Maintenance costs	Low	High	High	High	High
System complexity	Medium	High	High	Low	High
Disaster resilience	Strong	Weak	Medium	Medium	Strong
Maturity levels	Low	High	Medium	High	Medium

[†] Optical communication is omitted due to its zero communication range underground.

TABLE V
RELATED SURVEYS AND THEIR DIFFERENCES FROM THIS SURVEY

Aspects	Refs.	Most important contribution	Differences from this survey
UG communications	[21]–[29]	Issues of acoustic wave communication, EMWC, wired communication, mud pulse telemetry communication and MIC for UG-WSNs	Diluting comprehensiveness due to non-exclusive to MICs, and no exploration of issues of the MI fast fading, RPMA
MICs	[30]	Reference book covering antennas, channels, performance, and protocols related to MICs	No exploration of issues of MI fast fading, RPMA and routing algorithm
Underground MICs	[15], [31]	Issues for general MI UG-WSNs, primarily concerning short-to-mid range MICs	No exploration of issues of MI fast fading, RPMA, a complete MI network architecture
Underwater MICs	[16], [32]	Fundamental issues and advances in underwater MICs	No exploration of issues of MI fast fading, RPMA, and a complete MI network architecture
TTE MICs	This survey	Fundamental issues and advances in underground MIC, primarily concerning long-range MICs, MI fast fading, and a complete MI network architecture	-

the through-the-sea MIC application in 2023, and Ma *et al.* [11] focused on MI multi-cellular networks in 2024.

B. Related Surveys and Motivations of This Survey

While many surveys on underground communication have been published as listed in Table V, only a handful of the surveys have focused on underground MICs. For example, Sharma *et al.* [31] reviewed MIC research until 2017 for non-conventional media applications. They introduced the applications and advantages of MICs and briefly introduced the channel modeling of the P2P MIC and a hardware testbed for MIC research. Kisseleff *et al.* [15] conducted a comprehensive review of underground MIC studies up to that point. Although their work primarily focused on P2P MIC and MI waveguide issues, they also discussed physical protocols such as channel estimation and node deployments. Recently, Liu *et al.* [30] offered a thorough introduction to general MICs in a monograph. This monograph covers the basic concepts and theories of background, developments, antennas, channels, performance, and protocols related to MICs proposed before 2020.

Compared to this current survey, the existing review [31] has overlooked multi-node MICs. The survey [15] does not comprehensively review MI network architectures and the issues of mobile MIC, including the data link layer, network layers, RPMA, and MI fast fading. The monograph [30] does not review MI network architectures and MI fast fading, especially the recent routing algorithms and RPMA developed in the past five years.

However, the surveys conducted since 2020 have not yet provided comprehensive reviews on expanded MIC techniques, such as MAC and routing protocols for a large-scale MI network and a novel mechanical antenna. This is due to the great surge in mobile MICs, mechanical antennas, and upper-layer MI research since 2020. Moreover, almost all existing articles on MICs presented the common conclusion that the MI channel is a quasi-static and predictable channel without a small-scale fading. These articles also include the surveys (e.g., [15], [32]) and reviews (e.g., [31]). However, several studies have described the MI fast fading channel recently. The common conclusion may no longer hold.

Although most related articles claim that their research on

MIC is compatible with TTE communication, few surveys and reviews highlight the potential or specific issues and methodologies when existing MIC techniques are applied in TTE or long-distance MIC environments. Currently, there is no agreed protocol stack for larger-scale MI networks. By organizing the existing MIC research with reference to the OSI-originated framework, we can identify the remaining issues related to MIC to establish a standard MIC protocol stack. This is crucial for Space-Air-Ground-Underground multi-network integration (SAGUIMI) for the next generation of mobile communication.

C. Contributions and Organization of This Survey

This survey reviews research on underground MICs, particularly TTE applications, covering point-to-point TTE MIC techniques and the impact of MI fast fading on existing MIC theories. To guide optimization efforts, we decompose the MI channel power gain into four components with low inter-coupling and distinct physically interpretable meanings. The survey also covers MI relay techniques, analyzing crosstalk effects in both relay and high-density networks. Moreover, we identify the remaining research tasks for a comprehensive MI network protocol in SAGUI. Based on the surveyed literature, we propose an advanced MIC framework that supports TCP/IP and Linux, addressing both the current state and future challenges of MIC. This framework enables researchers to utilize extensive Linux resources and deep learning platforms, accelerating research and implementation in SAGUI applications. The key research challenges, open issues in MICs, and promising novel techniques to address them are highlighted.

The key contributions of this survey include:

- **First Survey on MI Fast-Fading Channels:** This survey identifies that MI fast fading challenges the prevailing notion of quasi-static MI channels. We highlight that research on MI fast fading remains in its early stages due to the lack of a universal statistical model. To address this, we introduce an antenna vibration model and corresponding simulations. We also analyze the potential impacts on existing MIC theorems, a topic not yet covered in any previous surveys.
- **Comprehensive Review of MI Network Architecture:** We present a complete review of the MI network architecture across the OSI framework layers, identifying remaining issues and possible solutions. A significant finding is the absence of standardized MI protocol stacks, which represents a major barrier to achieving SAGUIMI integration in next-generation mobile communications. Existing surveys often focus on specific applications without providing a holistic and runnable framework.
- **Fine-grained Decomposition of Channel Power Gain:** We introduce a detailed conceptual modeling approach for channel power gain and provide optimization directions for MIC systems, including antenna designs, bandwidth, and MIC range improvements. This contributes to simplifying MIC optimization for future research by narrowing the scope of MI parameters to focus on relevant variables while fixing others.
- **Identification of Positive MI Crosstalk Effects:** This study uncovers the positive MI crosstalk effects, which are crucial for addressing challenges in MI waveguides

and massive MIMO systems. Previous literature primarily focused on negative crosstalk effects, while the positive crosstalk aspect has been largely overlooked.

The remainder of this survey is structured as follows (more details in Fig. 2): Section III covers MI channel modeling, including MI channel power gain and MI fast fading. Section IV summarizes P2P MIC designs, focusing on MI antenna design, bandwidth, and MIC range. Section V surveys MI relay techniques, such as MI waveguides, MI passive relay array (MPRIA), Cooperative magnetic induction communication (CMIC), and the MI crosswalk effect. Section VI reviews multi-node MIC from the perspective of the OSI framework. Section VII introduces a promising MI network framework with TCP/IP and Linux support in an attempt to address the challenges in current and future MIC studies. Section VIII explores unresolved challenges. It also discusses promising methodologies including novel MI antennas, MI communication-navigation-sensing integrated (MCNSI), massive MI MIMO, deep JSCC for MIC, heterogeneous MI network techniques, TCP/IP framework support, and Transformer-based prediction frameworks. Section IX concludes this survey.

The acronyms that appear across subsections of this survey are listed in Table I. The physical representations of mathematical symbols are listed in Tables III and II. The default values for the simulations and numerical evaluations, that we conducted in this survey, are listed in Table III.

D. Research Gap Summary

Open issues on MIC are summarized in Table VI, highlighting existing research gaps in several pivotal domains. The high-priority domains are described in detail as follows.

1) *MI fast fading for mobile MIC:* Research on MI fast fading still has significant gaps despite existing efforts. The primary gap is the absence of a universal statistical model, which severely hinders the development of upper-layer protocols for mobile UG-WSNs. To address this gap, we propose a geometric antenna vibration model that can potentially tackle this challenge using Monte Carlo methods.

2) *Significant gap in TCP/IP framework:* The TCP/IP is crucial for SAGUI networks in next-generation communications. However, when mapping the surveyed research to each OSI layer, significant gaps emerge: certain layers and key topics remain underexplored. Specifically, no literature addresses IP applicability in MI networks, and the entire Transport Layer (Ly4) lacks dedicated MI solutions. Meanwhile, the extremely low bandwidth and channel capacity of MIC may not be compatible with existing IP and Ly4 protocols, as this low performance can lead to congestion mechanism failures and retransmission storms. Additionally, excessively large headers waste scarce MI bandwidth. To address these gaps in MI TCP/IP solutions, we propose a promising MIC framework supporting TCP/IP and Linux, which systematically incorporates MI algorithms and protocols drawn from the literature and future potential solutions.

3) *Underdeveloped channel models and protocols for TTE-specific MIC:* Current studies on MIC have largely overlooked the unique challenges of the TTE scenario, including mobility, heterogeneous geological materials, and constrained antenna

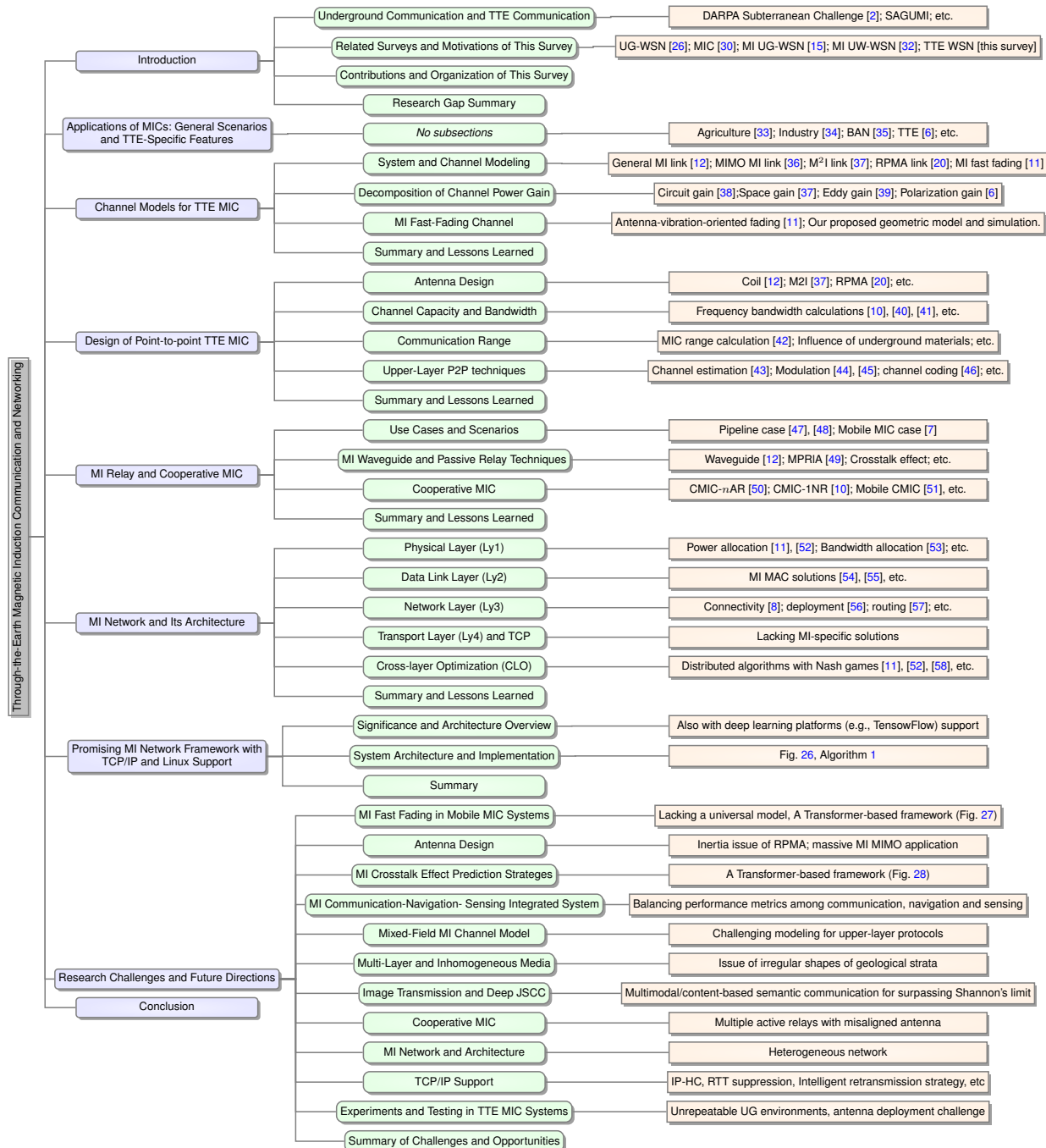


Fig. 2. The structure of this survey, where we perform fine-grained decomposition of the MI power channel gain and novel antenna vibration model for MI fast fading in Section III, MI crosstalk effect in Section V, and MI network framework with TCP/IP & Linux support in Section VII.

position and orientation (APO). Key research gaps in TTE-specific MICs are as follows: (i) The eddy gain model for heterogeneous UG materials may require correction or numerical validation; (ii) shadow fading should be considered for mobile nodes in Case (i); (iii) the existing upper-layer MI protocols lack TTE-specific design adaptations. For these gaps, the FEMs as we conducted in this survey are promising.

II. APPLICATIONS OF MICs: GENERAL SCENARIOS AND TTE-SPECIFIC FEATURES

In this section, we survey the MICs for various potential applications, as summarized in Table VII. Subsequently, we

discuss the specific challenges and considerations of applying MIC techniques to TTE scenarios.

Applications in agriculture: Soil conditions are crucial for crops, making it essential to build an MI UG-WSN for agricultural automation. This attracts some researchers. Li *et al.* [60] derived the conductivity and permittivity distribution using the Simultaneous Iterative Reconstruction Technique (SIRT) algorithm for soil moisture sensing, and obtained moisture sensing results based on an empirical model, i.e., a soil's relative permittivity function w.r.t the volumetric water content (VWC). Sensors are spaced 5 to 10 m apart. The COMSOL simulations showed that the sensing accuracy can achieve a root mean square error of 6% in VWC [60]. Agnelgo *et al.*

TABLE VI
RESEARCH GAPS AND POTENTIAL SOLUTIONS, AND THEIR MAPPINGS

OSI Layers [†]	Research gaps	Identified open issues	Potential solutions [‡]	Priority
Ly1	MI fast fading	<ul style="list-style-type: none"> Universal statistical models Related upper-layer solutions 	<ul style="list-style-type: none"> Geometric antenna vibration model (cf. Fig. 6); Monte Carlo methods (cf. Fig. 7) Expressions of ergodic performances (cf. (12), (13)) Comparison simulations for modulations and FECs (cf. Fig. 14) 	***
	MI crosstalk	<ul style="list-style-type: none"> Positive effects; spatial distribution 	<ul style="list-style-type: none"> Transformer-based prediction (cf. Fig. 28) 	**
	TTE-specific MIC	<ul style="list-style-type: none"> Closed-form expressions of MIC range; optimal carrier frequency Eddy current effects & shadow fading from heterogeneous media 	<ul style="list-style-type: none"> Derivation based on Lambert-W function properties for MIC range (cf. (20)) or FEM, as shown in Fig. 4 	***
	(Deep) JSCC	<ul style="list-style-type: none"> No relevant solutions (key: prospect of exceeding Shannon limits) 	-	**
Ly2	LLC	<ul style="list-style-type: none"> No references (optional sublayer) 	-	*
Ly3	IP	<ul style="list-style-type: none"> No references (key: VLF adaptions and large packet headers) 	<ul style="list-style-type: none"> MIC framework for TCP/IP & Linux support (cf. Fig. 26, Algorithm 1) 	***
Ly4	TCP	<ul style="list-style-type: none"> No references (key: Unstable connection and large headers) 		***

[†] OSI Layers: Ly1: physical; Ly2: data link; Ly3: network; Ly4: transport; Ly5–7: combined application layers (i.e., session, presentation, application).

[‡] Potential solutions: systematically developed approaches with specific formulations (key expressions, simulations or frameworks), distinct from generic proposals.

TABLE VII
APPLICATIONS USING MI-BASED TECHNIQUES

Applications	Predictable & stable channels [†]	Waveguide compatibility [‡]	MIC distance	Other characteristics	Impact on practical MIC systems	Involved refs.
Agriculture	Yes	Yes	Short to mid (<30m)	<ol style="list-style-type: none"> Limited free spaces Medium with high and time-variable VWC Shallow burial 	<ol style="list-style-type: none"> Restrict antenna size and deployments Variable performance due to time-variable VWC Simple hardware, complex topologies and protocol stacks designs 	[33], [59]–[62]
Industry	Yes	Yes	Short to mid (<36 m)	1) Reliant on specific applications	-	[15], [34], [63]–[70]
Underwater	No	Yes	Mid to long (1~100 m)	<ol style="list-style-type: none"> Sufficient free space Randomly misalignment coils Remarkable eddy loss 	<ol style="list-style-type: none"> Diverse antenna designs and configurations Fast fading-like phenomenon Limited P2P MIC range 	[5], [16], [20], [32], [51], [71]–[89]
BAN	No	No	Short (<5 m)	<ol style="list-style-type: none"> Low power requirements Non-magnetic dipole models 	<ol style="list-style-type: none"> Small device size Strong coupling & higher carrier frequency due to short MIC range 	[35], [90]–[101]
Military	-	-	-	1) BorderSense architecture	1) Access to EMWCs	[15], [18], [102]
Environment & disaster monitoring	Yes	Yes	Short to long (<1,000 m)	1) Lack of CSI due to disaster	1) Transmitter-side channel estimation	[31], [103]
Localization	Yes	No	Mid to Long (1~1,700 m)	1) Expecting signal difference across different positions	1) Require specific localization algorithm (e.g., ToA)	[14], [24], [64], [65], [104]–[115]
TTE	No	No	Long (60 ~1,000 m)	<ol style="list-style-type: none"> With non-uniform eddy loss Relatively limited free spaces Using VLF-LA Remarkable fast fading 	<ol style="list-style-type: none"> Shadow fading-like phenomenon High deployment costs Extremely low capacity Complex hardware and upper-layer protocols even for a simple network 	[6]–[11], [116]

[†] Predictable and stable channels in most scenarios.

[‡] Waveguide system compatibility in most scenarios.

[33] studied mid-range MI-based UG-WSNs for real-time soil moisture sensing, with a communication distance of 15–30 m. A common feature of these MI agriculture applications is that the sensors are buried near the ground surface, and the communication distance among MI nodes is shorter than 30 m. In addition, the MI waveguide has been widely applied to enhance the MIC distance.

Applications in industry: The MI-based application has broader prospects in the industrial field, including pipeline leakage detection, infrastructure monitoring, and communication within mines. For the pipeline leakage detection, many researchers focus on this area [34], [63]–[66]. Sun *et al.* [34] discussed the leakage detection and localization for the pipeline with a length of 36 m and 27 m, using the MI waveguide model. Tan's team studied the position of pipeline breakage by the MI-based method [64]. Recently, Li's team [66] developed an MI-based position system for underground pipelines by applying rotating permanent magnets. For infrastructures, monitoring their health such as residential or commercial buildings, bridges, and dams is crucial to avoiding possible disasters [15], [67], [68]. Mines provide an important application scenario. Compared to the pipeline and infrastructure scenarios, the distance between two nodes can be much

larger. Among these studies on industry applications, the MI waveguide method was widely applied to extend the distance.

Underwater Applications: Water covers over 70% of Earth's surface, offering abundant resources. MIC technology shows promise for underwater exploration. Underwater applications can be categorized into under-freshwater and under-seawater applications. As seawater has higher conductivity, the path loss in MI channels under the sea is significantly greater than that in freshwater. Li *et al.* [32] offered a comprehensive overview of existing studies on underwater applications conducted prior to 2018, including those developed in [71]–[77]. After 2018, MIC for UW-WSNs was increasingly attracting the attention of researchers. Firstly, several researchers proposed RPMA to generate modulated magnetic fields with 30 Hz~1 kHz frequencies for MIC energy saving [20], [78], [81]–[84]. Secondly, the upper-layer protocols for MI-based UW-WSNs were investigated, including MAC protocols [55], routing solutions [85], [86]. Thirdly, contrasting with UG-WSNs, the multi-antenna techniques can be applied in water tanks to ample free spaces for antenna deployment. These techniques include MI MIMO [87], antenna array [82], CMIC [51], [87], and MI waveguide. Finally, due to the sufficient free spaces, the random misalignment between the coils would generate an

unpredictable and unstable channel [89]. Notably, compared to the UG-WSNs, the acoustic (sonar) and optical techniques are optional communication methods for UW-WSNs [88].

Body Area Network (BAN): The BAN is a sensor technology used to connect small nodes with sensing abilities to collect necessary information [90]. In the cells-filled body, EMW-based in the microwave range faces high attenuation, interference, and multipath effects. MI techniques can address these issues [35], [91]–[101]. Specifically, the principle, power equations, and capacity of MI-based BANs are demonstrated in [91], [92]. Kisseleff *et al.* [94] studied a distributed beam-forming. Their simulation showed that a data rate of 3200 bits/s, at a distance of 5 m and a frequency of 13.56 MHz. Golestani *et al.* [96] derived the theoretical model of MI communication in wireless BANs, and analyzed its working frequencies of 0~50 MHz, based on the experimental MIC device at an MIC distance of 40 cm. Mishra *et al.* [99] proposed the MI waveguide for the BAN link. Compared to UG-WSNs and UW-WSNs, MI-based nodes are closer, allowing a lower power requirement and a higher working frequency, e.g., 30 MHz, as reported in [96]. Due to the coils' size being comparable to MIC distances for the wearable requirements, these designs are similar to the standard Near-Field Communication (NFC) with simulation parameters aligned with those in ISO 14443/15693.

Environment Monitoring: Environment monitoring covers public services, including pollution monitoring and disaster detection. MICs can perform chemical, biological, and pollution monitoring for river, lake, and water reservoirs [31]. Also, MIC systems can monitor transport tunnels and mining conditions, and issue early warnings from underground to relevant departments for imminent accidents. In disaster scenarios, obtaining CSI may be challenging, so Kisseleff *et al.* [103] proposed a specific channel estimation within the MI transmitter circuit without explicit feedback CSI to address this issue.

MI Localization: MI techniques are widely employed for localization in environments where EMW propagation is challenging [14], [64], [65], [104]–[114], [117]. While the signal propagation model in MI localization shares similarities with that of MIC, the underlying methods and design principles differ significantly. MIC systems prioritize uniform signal strength around the transmitter to prevent local network congestion and maintain consistent data rates. Conversely, MI localization systems benefit from amplifying signal differences to improve positional distinction and accuracy. Additionally, various advanced techniques, such as time of arrival (ToA) [14], time difference of arrival (TDoA) [14], data fusion [115], and inertial navigation [104], can be employed to further enhance localization accuracy.

TTE Applications: TTE applications typically have a vertical communication range of tens to hundreds of meters. However, due to the extremely high cost of MI-based TTE devices, most studies focused on simulations and experiments within a limited distance of several meters. Despite this challenge, several companies and research institutions have developed TTE devices. In 2011, Lockheed Martin developed the MagneLink™ MIC system, achieving a two-way communication range of 472.5 meters using an 8-meter transmit antenna [6], [118]. Vital Alert also developed MI-based TTE

TABLE VIII
COMPARISON BETWEEN TTE AND GENERAL MIC SETTINGS

Settings	TTE	General
MIC Range (m)	60~1,000 (Table VII)	<36 (Table VII)
Capacity (bps)	< 10 k	~ 1 M [15]
3-dB Bandwidth (Hz)	300~500 [11]	2 k~10 k [12], [21]
Frequency (Hz)	1 k~10 k [11]	1 M~50 M [15], [96]
Coil radius (m)	0.5~4 [7], [8]	< 0.2 [12]
Tx Power (W)	5~126 [†] [10]	< 1 [12]
MI fast fading	Yes [11]	No [32]
Propagation medium	Inhomogeneous	homogeneous
Eddy effect	Significant	Mild
Deployment cost	Extremely high	Low
Existing TCP/IP support	Challenging	Potential
Typical scenarios	Tunnel, mine, mountain	Farmland, pipeline

[†] The Tx power of 126 W stems from our Datong Coalmine TTE experiment.

devices with a claimed MIC range of over 450 m [119]. Liu's team (our team) at Tongji University developed the TTE experiment device achieving a vertical distance of 310 m in Datong Coalmine using an 8 m transmit coil [6], [8]. Based on this device, we investigated the CMIC [6], [7], [10] under the TTE environment using very low frequency (VLF) and larger antenna (VLF-LA) methods. Recently, the MI fast fading channel of TTE MIC is studied in [11]. With such fading, the MI channel becomes unpredictable and unstable. A comparison between TTE and general MIC settings is outlined in Table VIII.

While many studies (e.g., [6]–[12], [15], [116], [118], [119]) have adapted MIC technologies for underwater and general underground applications to TTE communications, they have not fully addressed the specific challenges and considerations of applying MIC techniques to TTE scenarios, including those outlined in Table VII and Table VIII.

- **Instability of channel power gain:** The uncertainty of the medium over a large space and the vibration of mobile MIC antenna cause random variations in channel power gain, ultimately leading to remarkable fast fading.
- **Extremely low bandwidth:** To extend the MIC range as much as possible, the throughput of the MI link must be greatly sacrificed, which has a significant impact on existing upper-layer solutions (e.g., centralized Q-learning-based routing [120], and TCP/IP support).
- **Eddy current in medium:** As the MIC distance increases, the eddy current is increasingly significant and complicated. Some relatively simple techniques, e.g., the MIC range/coverage [6], [8], [12], and the frequency switchable routing protocol [120], become complicated.
- **Challenging deployment:** Limited space in deep underground environments poses deployment challenges for some MIC methods, such as MI waveguide and MIMO. Moreover, we must carefully consider the energy consumption of MIC devices due to the extremely high cost of replacing their batteries.

III. CHANNEL MODELS FOR TTE MIC

In this section, we introduce the MI channel power gain and MI fast fading discovered recently. Specifically, we categorize the channel power gain of the P2P MI link into four factors with distinct physically interpretable meanings and introduce their optimization strategies. Then, we discuss the MI fast fading, including its current statistical models, limitations, derivation challenges, and our proposed antenna vibration model with a simulation for the challenges.

A. System and Channel Modeling

The block diagram of P2P MIC link S→D is shown in Fig. 3, where the channel model depends on the antenna type, medium, and orientation. Specifically, for the coil-based MIC, Sun *et al.* [12] derived the path loss expressions for both coil-based MI link and MI waveguide link, indicating that the path loss of P2P MI link scales with the sixth power of distance d_{SD} . Their findings were experimentally validated in both wet and dry soil conditions. Further, Sun *et al.* [39] examined the impact of underground materials on MI communication. Li *et al.* [36] highlighted the significant orientation sensitivity of MIC and proposed an orthogonal MIMO coil model to mitigate this effect. For the M²I link, Guo *et al.* [37] formulated the channel model using Maxwell's equations, validated through COMSOL simulations [37], and experimentally tested using a metamaterial shell composed of multiple small coils [122], [123]. In RPMA-based MIC, Rezaei *et al.* [124] analyzed the magnetic moment of a single permanent magnet, while Zhang *et al.* [20] extended this study to magnet arrays. Ma *et al.* [11] investigated fast fading in downlink vehicular MI (VMI) channels.

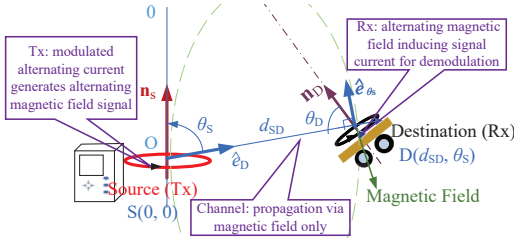


Fig. 3. P2P TTE MI communication model in polar coordinates. Here, \hat{e}_D and \hat{e}_{θ_D} are the radial and angular unit axial vectors, respectively; \mathbf{n}_S and \mathbf{n}_D are the normal vectors of the dipole and sensor, respectively.

Among these research articles, the P2P MIC modeling start with the Maxwell's equations, the magnetic intensity \mathbf{H}_D , induction intensity \mathbf{B}_D , and the flux Ψ_D received by the Rx antenna D with the polar coordinates (d_{SD}, θ_S) can be derived as $\mathbf{H}_D = \mathbf{m}_S \vec{h}_D$, $\mathbf{B}_D = \mu_u \mathbf{H}_D$ and

$$\Psi_D = \mathbf{B}_D \cdot \mathbf{n}_D = \mu_u \mathbf{m}_S (\vec{h}_D \cdot \mathbf{n}_D), \quad (1)$$

respectively, where \vec{h}_D is given by [125, Chapter 5]

$$\vec{h}_D = \frac{1}{4\pi} \frac{k_0}{2d_{SD}} e^{-jk_0 d_{SD}} \left[\cos \theta_S \left(\frac{1}{d_{SD}} \left(1 + \frac{1}{jk_0 d_{SD}} \right) \right) \hat{e}_D + \sin \theta_S \left(\frac{1}{2} \left(1 + \frac{1}{jk_0 d_{SD}} - \frac{1}{(k_0 d_{SD})^2} \right) \right) \hat{e}_{\theta_D} \right], \quad (2)$$

where $k_0 = 2\pi f \sqrt{\mu_u (\epsilon_u + j(\sigma_u / (2\pi f)))}$ [126]. Note that (2) holds only in the weak coupling and linear regime, where the distance is much greater than the antenna size. It may break down in near-resonant or highly reactive systems.

In the receive coil or magnetic sensor, the magnetic flux Ψ_D induces a current $I_D \propto \Psi_D$. The channel power gain between link S→D is given by

$$G_{SD} = \left| \frac{P_{Df}}{P_{Sf}} \right| = \frac{1}{I_S^2} \mathfrak{N}_{SD} \Psi_D^2 = \frac{|\mathbf{m}_S|^2}{I_S^2} \mathfrak{N}_{SD} \left(\mu_u (\vec{h}_D \cdot \mathbf{n}_D) \right)^2, \quad (3)$$

where the compensated variable \mathfrak{N}_{SD} significantly depends on the specific circuit and antenna type.

B. Decomposition of Channel Power Gain

Eq. (3) is a universal expression of the channel power gain both in the near field and radiation field ranges. However, this expression is challenging to analyze and formulate into a further optimization model in MIC research. Thus, in most MI UG-WSN studies, insufficient communication distance [12] or VLF-LA methods [6] lead to the assumption that $k_0 d_{SD} \ll 1$ holds. Guided by the “high cohesion and low coupling” principles in software engineering and by substituting $k_0 d_{SD} \ll 1$ into (3), we propose a decomposition of the channel power gain G_{SD} into four physically meaningful factors

$$G_{SD} = \underbrace{\frac{|\mathbf{m}_S|^2 \mathfrak{N}_{SD}}{16\pi^2 |I_S|^2}}_{\text{Circuit gain } \mathcal{C}_{SD}} \times \underbrace{\frac{|\mu_u|^2}{(d_{SD}^3)^2}}_{\text{Space gain } \mathcal{S}_{SD}} \times \underbrace{e^{-2jk_0 d_{SD}}}_{\text{Eddy gain } \mathcal{E}_{SD}} \times \underbrace{(2 \cos \theta_S \cos \theta_D + \sin \theta_S \sin \theta_D)^2}_{\text{Polarization gain } J_{SD} = \mathcal{J}_{SD}^2}, \quad (4)$$

i.e., circuit gain \mathcal{C}_{SD} , space gain \mathcal{S}_{SD} , eddy gain \mathcal{E}_{SD} , and polarization gain J_{SD} . As shown in Fig. 5, the relationships among these decomposed gains involve only three logical coupling links, conforming to the low-coupling principle. Their physically interpretable meanings are provided in the rest of this subsection. We summarize addressed issues, methods, remaining issues, and optimization directions in existing research in Table IX, as described in what follows.

1) *Circuit gain \mathcal{C}_{SD}* : The circuit gain, with two optimizable factors \mathbf{m}_S and \mathfrak{N}_{SD} , reflects energy consumption on the circuit. We observe that the studies on antenna and hardware designs, including resonance characteristics of the coil antenna [12], magnetic pole strengths of the bias and rotor magnet of RPMA [127], can be categorized as the independent considerations of the optimization of the circuit gain \mathcal{C}_{SD} . This is crucial for improving the bandwidth through the factor \mathfrak{N}_{SD} of \mathcal{C}_{SD} , and MIC range through the factor \mathbf{m}_S of \mathcal{C}_{SD} . For example, RPMA without coils can eliminate the resonance coupling (expressed in \mathfrak{N}_{SD}) [127]. However, RPMA may face an additional equivalent circuit loss due to mechanical inertia and friction (also expressed in \mathfrak{N}_{SD}). Wang *et al.* [38] used impedance matching $Z_L = R + \frac{(2\pi f M)^2}{R}$ in $\mathfrak{N}_{SD}(Z_L(f))$ to maximize the receive power, where Z_L , R , and M are the impedance and resistance of the coil, and mutual inductance, respectively. Their simulations showed that their approach produced two frequency resonant points, at 1 MHz and 5 MHz, respectively. In [128]–[130], multi-band MI techniques achieve several discontinuous 3-dB bandwidths in the frequency domain through a coil array, based on $\mathfrak{N}_{SD}(Z_L(f))$. Unfortunately, additional loss arises due to crosstalk among the coil array. The circuit gain exhibits optimal operability, as it minimizes the need to consider the MIC environment.

2) *Space gain \mathcal{S}_{SD}* : This gain represents the ideal spatial path loss due to space expansion. This gain serves as a primitive model for MIC. It is widely used in MI network studies to analyze and optimize signal transmission. When considering short to mid-range MIC systems, such as MI waveguides [13], M²I communications [37], and upper-layer protocol for MIC [52], [85], [86], researchers often choose to simplify theoretical communication models by ignoring the eddy gain \mathcal{E}_{SD} and polarization gain \mathcal{J}_{SD} . While \mathcal{E}_{SD} and \mathcal{J}_{SD} can have significant effects on signal propagation

TABLE IX
PARTITIONS OF CHANNEL POWER GAINS AND THEIR ISSUES
THE MARKER ‘●’ DESCRIBES THE METHODS; THE MARKERS ‘✓’ AND ‘✗’ DESCRIBE ADDRESSED AND REMAINING ISSUES, RESPECTIVELY.

Factors	Physical meanings	Involved Refs.	Addressed issues and methods	Remaining issues and optimization directions	Priority [†]
Circuit gain (\mathcal{C}_{SD})	Local energy consumption	[12], [38], [127]–[130]	<ul style="list-style-type: none"> ✓ Increase the magnetic moment with minimal energy ● Use RPMA to reduce \mathcal{N}_{SD} under VLF ● Impedance matching technique to maximize the receive power ● Multi-band MI technique to achieve several 3dB bandwidth 	<ul style="list-style-type: none"> ✗ Challenge to derive the capacity and energy loss of RPMA-based link due to the inertia ✗ Deviation of 3-dB bandwidth in VLF below 100 Hz 	***
Space gain (\mathcal{S}_{SD})	Field attenuation with spatial expansion	[37]	<ul style="list-style-type: none"> ✓ Mitigate the rapidly signal attenuation with spatial expansion ● M²I enhanced techniques to enhance the overall permeability between S and D 	<ul style="list-style-type: none"> ✗ Too large M²I shell occupying several times of coil volume 	**
Eddy gain (\mathcal{E}_{SD})	Loss due to eddy current of medium	[8], [130]	<ul style="list-style-type: none"> ✓ Determining the non-negligible eddy current for TTE MIC ● Derivation using magnetic potential ● Using Lambert-W function to express the MI coverage 	<ul style="list-style-type: none"> ✗ Unpredictable medium and shadow fading in the fluid scenarios or mobile MIC ✗ Eddy gain in inhomogeneous media (by FEM) 	***
Polarization gain (J_{SD})	Loss due to antenna orientation	[8], [9], [11], [36], [87], [89]	<ul style="list-style-type: none"> ✓ Stochastic misalignment coils in underwater scenarios ✓ Unpredictable MI fast fading channel in the underground/aboveground MIC ● Orthogonal MIMO coils to mitigate orientation sensitivity ● Boundary $p(x)$ distribution to model MI fast fading 	<ul style="list-style-type: none"> ✗ Challenge to deploy the MIMO antenna in the TTE scenarios ✗ Challenge to derive a universal statistical model for MI fast fading 	***
Mixed field case	Non-near-field case (not $k_0 d_{SD} \ll 1$)	[42], [78], [79], [126]	<ul style="list-style-type: none"> ✓ Channel modeling for P2P MI link ● Derivation based on Maxwell's equations 	<ul style="list-style-type: none"> ✗ Challenge in partitioning the channel power gain ✗ Challenge for antenna design and optimization due to excessive dependence on variables ✗ CMIC channel modeling ✗ Upper-layer solutions, such as MAC and routing ✗ Network deployment ✗ Frequency optimization and 3-dB bandwidth derivation 	**
Strong coupling	Coupling coefficient ≈ 1	[41]	<ul style="list-style-type: none"> ✓ Communication capacity in the strong coupling case (MIC distance much smaller than coils size) ● Non-magnetic-dipole modeling 	<ul style="list-style-type: none"> ✗ Inapplicable channel power gain expressions (3) and (4) 	*

[†] Priority: Priority level of remaining issues for exploration.

and reception, ignoring them allows for more straightforward analyses and calculations, especially during the initial stages of network design and optimization. The space gain expression $\mathcal{S}_{SD} = \frac{|\mu_u|^2}{(16\pi d_{SD}^3)^2}$ suggests that optimizing \mathcal{S}_{SD} is challenging due to the fixed permeability μ_u determined by underground material. Guo *et al.* optimized the equivalent permeability by designing a metamaterial-enhanced antenna enclosed by a metamaterial shell. This shell has a permeability of $\mu_2 = -\mu_0$ where μ_0 is the vacuum permeability [37]. This enhances the overall permeability between S and D, resulting in an improved space gain. In practice, the TTE environment is hardly modifiable, leading to limited operability of space gain.

3) *Eddy gain \mathcal{E}_{SD}* : The eddy gain is known as the Skin Effect. It is generated by induction current from the time-varying magnetic field within underground materials. In TTE communication, heterogeneous materials exhibit dynamic characteristics, especially for mobile MI networks. This makes MIC channel coefficients unpredictable. It also poses significant challenges to MIC research. For short-range MICs and early MICs research, the eddy gain can be ignored to simplify primary problems. However, for TTE MICs, the cumulative eddy current is highly remarkable. In an infinite and uniform medium, the expression of the eddy gain \mathcal{E}_{SD} is given in [130], [131] and can be approximately matched as [10]

$$\sqrt{\mathcal{E}_{SD}} \simeq \exp\left(-\frac{d_{SD}}{\delta_u}\right) = \exp\left(-d_{SD}\delta_u^{-1}\right), \quad (5)$$

with

$$\delta_u = \frac{1}{2\pi f \sqrt{\frac{\mu_u \epsilon_u}{2} \left(\sqrt{1 + \frac{\sigma_u^2}{(2\pi f)^2 \epsilon_u^2}} - 1 \right)}}, \quad (6)$$

where the permittivity ϵ_u is typically very small in most underground environments. For instance, the permittivities of dry and wet soils are $7 \times 8.854 \times 10^{-12}$ F/m and $29 \times 8.854 \times 10^{-12}$ F/m, respectively. Their conductivities σ_u are 0.01 S/m

and 0.077 S/m, respectively [39]. Hence, for the TTE MIC with VLF-LA, the condition $\sigma_u \gg 2\pi f \epsilon_u$ typically holds, allowing (6) to be further approximated as

$$\delta_u \simeq \sqrt{\frac{1}{\pi f \mu_u \sigma_u}}. \quad (7)$$

From (4) and (5), we observe that only the circuit gain \mathcal{C}_{SD} and eddy gain \mathcal{E}_{SD} depend on the carrier frequency f . This suggests a potential to enhance MIC performance through frequency optimization. For the short-range and mid-range MICs, the effect of the eddy gain is not significant. Hence, there is limited literature specifically studying the eddy gain at this moment.

Note that the eddy gain expressions in (4) and (5) apply only to near-field homogeneous media. Fig. 4 presents COMSOL simulations of magnetic flux density distributions in multilayer materials. These simulations show significant distortion in both magnetic field direction and magnitude across different media due to complex eddy effects, particularly near medium boundaries. This indicates that the eddy gain model requires correction for multilayer or inhomogeneous media.

4) *Polarization gain J_{SD}* : This gain $J_{SD} = \mathcal{J}_{SD}^2$ represents the effects of antenna orientations. From (4), J_{SD} is within $[0^2, 2^2]$. Specifically, when $\theta_S = \frac{\pi}{2}$ and $\theta_D = 0$, J_{SD} falls into 0. This poses several challenges as follows. 1) Aligning the Tx and Rx antennas may be difficult in practical scenarios, such as the autonomous underwater vehicle (AUV) scenario. To address this, the orthogonal MIMO has been introduced into the MICs. In [36], Li *et al.* deployed three orthogonal coils in each device, increasing the minimal channel power gain to $(\frac{1}{3})^2$ of the maximal one. 2) In MI UW-WSNs, antenna vibrations cause random misalignment, leading to stochastic polarization gain and channel coefficients [89]. 3) Fast fading in mobile MI UG-WSNs, such as vehicle MICs (VMICs) and

TABLE X
COMPARISON AMONG DIFFERENT MODELS OF THE FAST FADING CHANNEL IN RELATED REFERENCES

Types	Models	Compared points	Different challenges of MI fast fading	Refs.
EMWC	Rayleigh, Rician, Nakagami	1) Relatively predictable large-scale fading 2) Multi-path effect 3) Using CLT-based simplifications 4) No boundary limits	☒1) Unpredictable large-scale fading ☒2) Vibrating-oriented fading without multi-path effect ☒3) Hard to use CLT-based methods ☒4) With boundary limits	[132]–[134]
FSOC	Málaga	1) Simplified to Rayleigh, Rician, and Nakagami models 2) No boundary limits	Same as ☒1), ☒2), ☒3), ☒4)	[135]–[137]
	Geometric and misalignment loss	1) Linear propagation signals 2) No boundary limits	1) Linear propagation signals 2) Orientation sensitivity 3) With boundary limits	[138]
Acoustic communication	Rician	1) Be simplified to Rician 2) Strong LOS 3) No boundary limits	Same as ☒1), ☒2), ☒3), ☒4)	[139]
	MIMO SWA	1) With macro scattering and micro scattering 2) No boundary limits	Same as ☒1), ☒2), ☒3), ☒4)	[140]
MIC	Traditional MIC	No fast fading	With fast fading	[15], [32], [46], [141]
	Underwater	1) Antenna orientation with a uniform distribution 2) No boundary limits	1) Antenna angle with complex probability distributions 2) With boundary limits	[89]
	Vehicle MI	1) Antenna angle with a BCS distribution 2) Antenna angle with a boundary $p(x)$ distribution	1) Lacking universal solutions	[9], [11], [142]

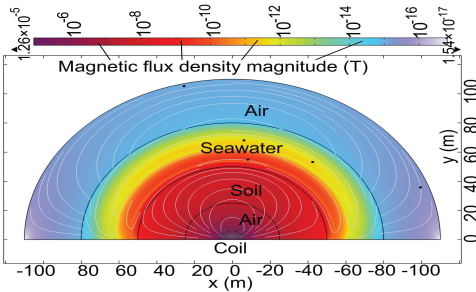


Fig. 4. FEM simulation of magnetic flux density in multilayer materials with different conductivities. Here, the conductivities of air, soil and seawater are 0, 0.01, and 4.8 S/m, respectively. The current of coil $I_S = 15 \cos(2\pi \times 10^4 t)$ (A). The coil radius is 6 m.

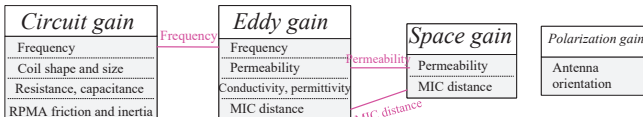


Fig. 5. Relationship among circuit, eddy, space, and polarization gains. The normal fonts with gray background represent the primary parameters.

backpack MICs, also stems from polarization gain [9], [11]. Most challengingly, in most mobile MICs, J_{SD} is a random variable with uncharacterized distribution.

In summary, the fine-grained decomposition of channel power gain into four low logical coupling gains $G_{SD} = C_{SD}S_{SD}E_{SD}J_{SD}$ allows us to simplify the optimization problem formulation by focusing on one or several specific factors, while fixing the rest of parameters. For instance, the MI antenna optimization prioritizes the circuit gain C_{SD} , while MI MIMO optimization focuses on enhancing polarization gain J_{SD} . For MIC in multi-layer medium, attention can be given to the eddy gain E_{SD} . For the long-range MIC in ultra-low-conductivity medium or the short-range MIC, focusing on space gain S_{SD} suffices.

C. MI Fast Fading Channel

In this subsection, we introduce the recently discovered MI fast fading, including its causes, distinctions from other

communications, and closed-form expressions for PDF and expectation. We highlight the derivation challenge for a more universal statistical model and propose a universal geometric model. Additionally, we perform simulations based on this geometric model. These geometric models and simulations may aid further study of this derivation challenge.

1) *MI fast fading modeling*: The concept of MI fast fading originated in 2016 [89], and was formally defined in 2020 [9]. Such fading is primarily due to the time-varying polarization gain J_{SD} [89]. The fast fading channel is a crucial concept in the field of wireless communication. Specifically, in wireless communication, a fast fading channel significantly varies over the communication time scale. In fast fading channels, the symbol time exceeds the coherence time [133, Chapter 1]. In [11], Ma *et al.* provided a detailed explanation of the different issues between MICs and other communications such as EMWC, free-space optical communication (FSOC), and acoustic communication methods, as depicted in Table X. Here, we summarize these issues as follows.

- The central limit theorem (CLT) cannot be applied to simplify the statistical channel model in MIC, making it difficult to derive a universal theoretical model
- The expectation and variance of MI fast fading are unpredictable due to the AVI. Such AVI depends on the driver's mindset.
- When vibrating, antennas may encounter boundaries, causing the PDF of MI fast fading to be discontinuous.

In traditional MIC studies, the MI channel has been assumed to be quasi-static due to reliance on near-field signals without multi-path fading. However, this assumption has been challenged in mobile MIC research [9], [11], [87], [89] since 2016. In 2016, Dumphart *et al.* [89] observed the phenomenon that the polarization gain often suffers from coil misalignment due to mobility and deployment in the underwater MIC system. They simply assumed a uniform distribution for θ_S and θ_D , and derived the PDF of J_{SD} . For example, the SISO links,

TABLE XI
COMPARISON OF TWO PDF EXPRESSIONS FOR MI FAST FADING

Refs.	Methods, Pros & Cons	Eqs.
[89]	✓ Simplified underwater model derived from uniform distribution ✗ Incapacity to represent antenna vibration ✗ Lacks universality; underwater-specific ● Derivation based on probability theory	(8)
[11], [142]	✓ Two antenna-vibration models derived from BCS distribution and boundary $p(x)$ distribution, respectively ✗ Lacks universality; base station–mobile terminal MIC link only ● Derivation and validated by Monte Carlo simulations	(9)

The markers '✓', '✗' and '●' represent pros, cons and methods, respectively.

the PDF of J_{SD} is given by

$$f_{J_{SD}}(x) = \begin{cases} \frac{\text{arsinh}\sqrt{3}}{\sqrt{3}}, & \text{if } |x| \leq \frac{1}{2}; \\ \frac{\text{arsinh}\sqrt{3} - \text{arsinh}\sqrt{4x^2-1}}{\sqrt{3}}, & \text{if } \frac{1}{2} < |x| \leq 1; \\ 0, & \text{if } |x| > 1, \end{cases} \quad (8)$$

with moments $\mathbb{E}(J_{SD}^2) = \frac{1}{6}$ and $\mathbb{E}(J_{SD}^4) = \frac{3}{50}$. This study [89] implies that the MI channel may not be quasi-static. The PDF in (8) is suitable for the underwater environment. The antenna orientation changes over time, making the MI channel unstable. Since there are many more weak vibrations than strong ones, the PDF in (8) cannot represent terrestrial/subterrestrial MI fast fading caused by the antenna vibration.

For the mobile TTE MICs using VLF-LA, previous studies have reported a Shannon's capacity range of 0.5~10 kbps at a 50-meter MIC distance [6], [7], [10]. The transmit rate achieved by TTE MIC experiment devices is significantly lower than this capacity, as mentioned in [11]. However, the frequency spectrum range of road disturbance input, causing antenna vibrations, is approximately 10 Hz~1000 Hz, as stated by ISO/TC108 and [143]. Since J_{SD} in channel power gain G_{SD} suffers rapid changes during a symbol time, MI fast fading was formally defined in [9], [11]. Due to the complexity of the antenna vibration statistical model compared to that in [89], novel mathematical concepts such as Boundary Chi-square (BCS) distribution for VMIC systems, boundary $p(x)$ distribution, and conjugate pseudo-piecewise function were proposed to derive statistical expressions [11].

However, these expressions have only been derived for specific scenarios. Specifically, for the downlink VMI channel with the same height, the PDF of J_{SD} can be simplified as

$$f_{J_{SD}}(x) = \begin{cases} \left[1 - \text{erf} \left(\sqrt{\frac{\varsigma}{2\sigma_D^2}} \right) \right] \delta_{pu}(0), & \text{if } x = 1 - \varsigma; \\ \frac{\exp \left(-\frac{1-x}{2\sigma_D^2} \right)}{\sqrt{2\pi\sigma_D^2(1-x)}}, & \text{if } 1 - \varsigma < x \leq 1; \\ 0, & \text{otherwise,} \end{cases} \quad (9)$$

where the instantaneous AVI follows the BCS distribution as proposed in [9]. From (9), the expectation of MI fast fading can be deduced as

$$\mathbb{E}(J_{SD}) = (1 - \sigma_D^2) \text{erf} \left(\sqrt{\frac{\varsigma}{2\sigma_D^2}} \right) + \frac{\sqrt{2\varsigma\sigma_D^2} \exp \left(\frac{-\varsigma}{2\sigma_D^2} \right)}{\sqrt{\pi}}. \quad (10)$$

Here, (9) and (10) represent a 2D statistical model of MI fast fading for a downlink MI link. For more universal models, it is a challenge without the support of the CLT. To address this challenge, we come up with an antenna vibration model,

as depicted in Fig. 6, where each coil angle is divided into horizontal and vertical components. Since the model is in the geodetic reference system, the horizontal and vertical components are independent, i.e., all random variables in this model are independent.

Since the theoretical statistical models for the universal MIC scenarios remain unexplored, there are no calculation lines in Row 2 (from top) in Fig. 7(b). Here, we estimate MI fast fading through Monte Carlo simulations, as shown in Fig. 7(a) and Row 2 in Fig. 7(b). This may facilitate future theoretical derivations on a more universal expectation of MI fast fading.

2) *Impact on channel power gain*: Fig. 7 exhibits the averages/expectations of MI fast fading gain. It is observed from Fig. 7(a) that most averages are below 0.9, implying a power loss of over 10% due to vibration. However, an interesting phenomenon arises: When the average AVIs of Tx and Rx reach a certain threshold, the channel power gain G_{SD} increases. This is due to the fact that $0 \leq J_{SD} \leq 4$. Thus, MI fast fading significantly influences the MIC channel.

3) *Impact on outage probability*: Outage probability is defined as the probability of instantaneous SNR below a threshold Υ_{th} [11]. In earlier MIC studies, as the MIC channel is regarded as a quasi-static channel [32], the outage probability losses its physical significance. In channels with fast fading, the outage probability is non-negligible. The closed-form expression of the outage probability p_{out}^{SD} for a P2P MI fast fading channel is given by [9]

$$p_{out}^{SD} = \mathbb{P} \left[J_{SD} < \frac{\Upsilon_{th}}{\frac{P_S}{N_o} C_{SD} S_{SD} \mathcal{E}_{SD}} \right] = \int_{-\infty}^{\frac{\Upsilon_{th}}{\frac{P_S}{N_o} C_{SD} S_{SD} \mathcal{E}_{SD}}} f_{J_{SD}}(x) dx, \quad (11)$$

In Fig. 8(a), the simulation results based on (11) indicate that even when the Tx power approaches infinity, the outage probability is over 0.1 at a relatively small AVI angle of 37° (i.e., $\sigma_D = 0.6$), thereby exerting a notable adverse effect.

4) *Impact on ergodic capacity*: Under fast fading, the ergodic capacity $EC = \mathbb{E}[\log_2(1 + \text{SNR})]$ (bits/s/Hz) is widely used for a long term average achievable rate, i.e.,

$$EC = \int_0^{\infty} \left(\log_2 \left(1 + \frac{P_S}{N_o} C_{SD} S_{SD} \mathcal{E}_{SD} x \right) \right) f_{J_{SD}}(x) dx. \quad (12)$$

In Fig. 8(b), the simulation results based on (12) show that the ergodic capacity declines by nearly one-third at an AVI angle of 37°.

5) *Impact on BER*: Recently, Chen et al. [142] established a fundamental performance limit for the BER of the MI fast fading channel under FSK modulation, as given by

$$\overline{BER} = \int_0^{\infty} Q \left(\sqrt{\frac{E_b x}{N_o}} \right) f_{J_{SD}}(x) dx \geq Q \left(\sqrt{\frac{E_b}{N_o} \mathbb{E}(J_{SD})} \right), \quad (13)$$

where $Q(\cdot)$ is the Q-function, and E_b is the energy per bit. As shown in Fig. 8(b), there is a 100-fold increase in BER at an average AVI angle of 37°. Notably, (13) indicates that the BER supremum increases with the average MI fast fading gain $\mathbb{E}(J_{SD})$, indicating that a higher $\mathbb{E}(J_{SD})$ does not guarantee better MIC performance.

Table XII summarizes the effects of MI fast fading on typical MIC performance metrics. Despite the few positive effects, MI fast fading exerts more pronounced negative impacts on

TABLE XII
IMPACT OF TYPICAL MI FAST FADING ON MIC PERFORMANCE

Performance Metrics	Refs.	Vibration input	Effect points (Compare to the MIC without fast fading)
Average channel power gain	[89]	Uniform	↘ Decrease to $\frac{1}{6}$ in a SISO system
	[11]	BCS	↘ Decrease to about 80% at an Rx average AVI of 30° ↗ More uniform around transmitter ↘ Severe variation in a poor and congested road condition
	Fig. 7(a)	BCS	↗ Increase over 5% when Tx average AVI angle = 90° and Rx average AVI angle = 90°
Outage probability	[11], Fig. 8(a)	BCS	↘ Increase over 10% when average AVI $\sigma_D > 0.6$, even if Tx Power $P_S \rightarrow \infty$
Ergodic capacity	Fig. 8(b)	BCS	↘ A decrease from 3.4 to 2.7 bps/Hz when $\sigma_D > 0.6$ (i.e., average AVI angle = 37°)
BER	[142], Fig. 8(c)	BCS	↘ A sharp increase from 10^{-3} to 10^{-1} when $\sigma_D > 0.6$

The markers ‘↗’ and ‘↘’ represent the positive and negative effects, respectively.

MIC performance through the PDF $f_{J_{SD}}(x | (\sigma_S, \sigma_D))$, which depends heavily on the AVI inputs σ_S and σ_D . In practical MIC systems, such AVI inputs frequently demonstrate substantial temporal variability, especially in the case of congested traffic conditions, leading to significant fluctuations in performance metrics over time. This characteristic markedly distinguishes MI fast fading from EMWC fast fading, as time-dependent performance variability is less pronounced in EMWC.

D. Summary and Lessons Learned

This section discusses the four decomposed gains influencing channel power gain (Table IX) and MI fast fading (Table X). Table IX suggests optimization directions for each factor, such as improving circuit gain in antenna designs.

Recent discoveries, including random coil misalignment [89] and MI fast fading [9], [11], challenge the widely accepted assumption in [32] that MIC channels are quasi-static. However, these findings address only limited aspects of non-static MI channels. In contrast to EMWCs, research on non-static MI channels is still in its early stages. Key issues include: 1) No universal statistical model exists for MI fast fading, analogous to the Rayleigh model for EMWCs, since the existing distribution models of AVI (e.g., BCS distribution) are scenario-specific; 2) The unexplored effects of MI fast fading on existing MIC theorems, such as channel estimation, CMICs, MI MIMO, and MI protocols; and 3) MI fast fading brings negative impacts on the performance of the MIC systems.

The challenges involved include: 1) The antenna vibration’s limited dependent components make it difficult to apply the CLT, a critical method for obtaining fast fading models in EMWCs; and 2) The expectation/variance of MI fast fading remains random due to its strong dependence on antenna vibration velocity. To address these challenges, we introduce a universal geometric model for antenna vibration (Fig. 6), which transforms all dependent components into independent ones. This model enables the estimation of MI fast fading gain via Monte Carlo simulation, as shown in Fig. 7.

The practical takeaways or common pitfalls include: 1) No existing MI fast fading models may hold when the near-field and weak coupling conditions are not satisfied; 2) the eddy gain requires correction in TTE practice, as TTE media are rarely homogeneous; 3) for VMICs, the ferromagnetic iron in the vehicle body can distort the magnetic field, potentially causing significant deviations in existing MI channel models; and 4) improving or uniformizing the polarization gain J_{SD} benefits MICs, whereas doing this for the average MI fast

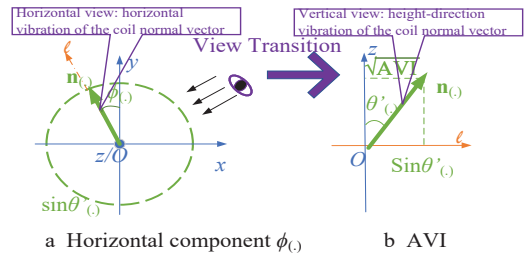


Fig. 6. Advised antenna vibration modeling in a 3-D space with independent random variables; $\mathbf{n}(\cdot)$, $\phi(\cdot)$ and $\theta'(\cdot)$ denote the normal vector, horizontal and vertical components of the antenna vibration (angle) of node (\cdot) , respectively.

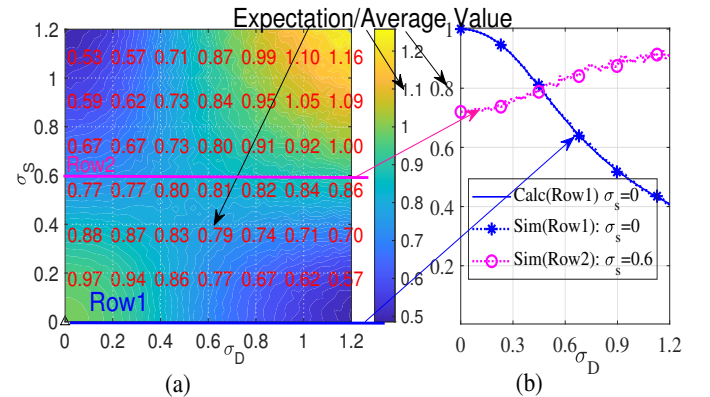


Fig. 7. Expectation of MI fast fading J_{SD} for the model in Fig. 6: (a) Ad-hoc link in 3D space; (b) Two specific links; Here, the AVIs of S and D follow BCS distributions, with a boundary $\varsigma = 0.8$ and their respective average AVIs σ_S^2 and σ_D^2 . Their horizontal components ϕ_S and ϕ_D follow the uniform distribution within $[0, 2\pi]$. The dotted lines of Row 1 and Row 2 in Fig. 7(b) are obtained through Monte Carlo simulations (sim), and the solid line of Row 1 in Fig. 7(b) is the calculation (calc) from (10). Here, the overlap between the calculated curve of Row 1 and its simulated counterpart validates (10). The calculation curve for Row 2 cannot be presented due to the lack of a universal expression.

fading gain $\mathbb{E}[J_{SD}]$ may be detrimental due to increased outage probability and BER.

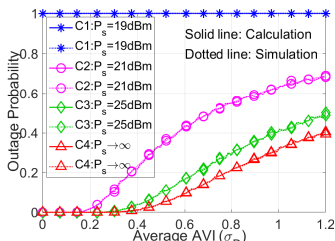
IV. DESIGN OF POINT-TO-POINT TTE MIC

This section introduces the MI antenna designs, and compares the advantages and disadvantages of four MI antenna types, including the RPMA design as a recent research hotspot in MI antennas. Subsequently, we discuss the key performance metrics of point-to-point (P2P) MI links, with a particular focus on the challenging derivations of the 3-dB MI bandwidth and MIC range for a TTE MI link. Moreover, we discuss the upper-layer P2P MI techniques, such as channel estimation,

TABLE XIII
OVERVIEW OF RELATED RESEARCH ON P2P MIC TECHNIQUES
THE MARKER ‘●’ DESCRIBE THE METHODS; THE MARKERS ‘✓’ AND ‘✗’ REPRESENT PROS AND CONS, RESPECTIVELY.

Aspects	Refs.	Addressed issues & methods	Remaining issues (& Proposed approaches)	Priority [†]
Channel modeling	[11], [12], [37], [78]	✓ Two typical MI fast fading models ✓ See Table IX in Section III	✗ More universal MI fast fading modeling ✗ See Table IX in Section III	***
Antenna design	[11], [78], [122]	✓ Coil, orthogonal MIMO, RPMA, M ² I ✓ See Table XIV	✗ Orientation sensitivity; Practical deployment issues ✗ See Table XIV	**
Capacity	[37], [39]	✓ Expressions of capacity for coil based and M ² I MICs	✗ Expressions of capacity for RPMA-based MICs	**
Bandwidth	[10], [41]	✓ Expressions (16), (17), and (18) (see Table XV)	✗ Bandwidth of RPMA-based MICs	***
MIC Range	[42]	✓ Expression for short MIC range (see (19))	✗ Expressions for TTE MIC with significant eddy gain	***
Channel estimation	[144]	✓ Lacking in sufficient CSI ● Transmitter-side estimation without explicit training sequence	✗ Insufficient feedback for the dyadic backscatter MI channel estimation	*
	[145]	✓ Unknown propagation environment (e.g., medium conductivity) ● Environment-aware method using Kernel function to learn the positive/negative factors in the environment	✗ Unclear in the case of VLF TTE MICs and MIC with fast fading	*
	[43]	✓ For inter-media MI backscatter channel ● Joint channel estimation and data transmissions, and stratified medium model for high penetration	✗ Lacking the analysis for VLF and long-distance MIC	*
Modulation	[45]	✓ Basic MI Modulation schemes and filter design ● Frequency-division multiplexing (FDM) with multiple sub-bands	✗ Incompatibility with RPMA systems ✗ Shortage similar to FDM in EMWCs	**
	[20], [44], [124], [146]	✓ Basic modulation for RPMA-based MICs ● Amplitude shift keying, on-off keying, frequency-shift keying, Chirp-rate shift keying	✗ Requiring additional GTSs and energy for overcoming inertia	**
Channel coding	[52]	✓ FEC with higher channel estimation requirement ● EMW-based multilevel cyclic BCH coding	✗ Ignoring non-static MI channel cases ✗ FEC's resistance characteristics to MI fast fading	*
	[46]	✓ Polar code for variable attenuating MI channel ● Bhattacharyya parameter estimation algorithm	✗ Higher channel estimation requirements with low capacity ✗ Ignoring \mathcal{E}_{SD} and J_{SD} in their algorithm. ✗ FEC's resistance characteristics to MI fast fading	***

[†]Priority: Priority level of remaining issues and proposed approaches for exploration. Here, low priority (*) indicates that: 1) the remaining issues have been explored in subsequent MIC literature; 2) the existing EMWC schemes are compatible with MIC for these issues; or 3) exploring these issues is optional.



(a) Outage probability

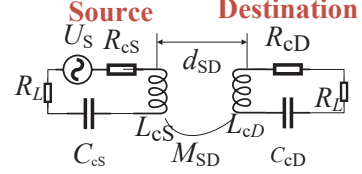


Fig. 9. Equivalent circuit model for the coils-based link S→D, where U_S denotes the instantaneous voltage in the Tx antenna, and d_{SD} denotes the distance between source S and destination D. Additionally, R_{cS} , R_{cD} , L_{cS} , L_{cD} , R_L , R_{cS} and R_{cD} are described in Table II, respectively.

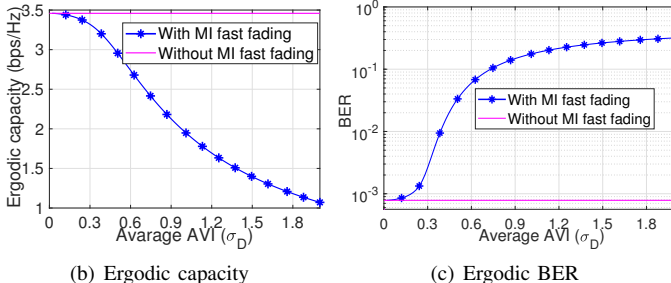


Fig. 8. Impact of MI fast fading on MIC performance: (a) Outage probability v.s. Rx average AVI (σ_D); (b) Ergodic capacity v.s. Rx average AVI (σ_D) under the SNR of 10; and (c) BER v.s. Rx average AVI (σ_D) with $\frac{E_b}{N_0} = 10$ [142]. The solid lines in Figs. 8(a), 8(b) and 8(c) are calculated from (11), (12) and (13), respectively. The dotted lines in Fig. 8(a) are obtained through Monte Carlo simulations.

modulation, and FEC. Recent challenges and approaches about these techniques are briefly summarized in Table IV.

A. Antenna Design

In this subsection, we introduce four MI antenna designs, with the RPMA design. Table XIV summarizes their key features. Detailed studies are presented below.

1) *Coil Tx/Rx Antenna*: The coil is the most widely used antenna in the field of MICs [15], [32] owing to its high

receive sensitivity, ease of implementation, and deployment. It is very suitable for TTE applications with limited free space. The utilization of coils dates back to research on NFCs, a short-range MIC that commonly employs a 13.56 MHz carrier frequency according to ISO/IEC 18092 standards. The MIC link is established through mutually inductive coupling between the Tx coil and the Rx coil (see Fig. 9). However, unlike standard NFC, MICs for UG-WSNs and UW-WSNs exhibit weak coupling due to longer communication distances. The Tx coil is typically modeled as a magnetic dipole, and the bandwidth of such MIC is much smaller than the standard NFC, especially for the TTE MIC applications. Due to this weak coupling, the Tx coil with current I_S generates the magnetic moment with a norm $|\mathbf{m}_S| = \pi^2 a_{cS}^2 a_{cD}^2 N_S N_D I_S$ and current loss compensating coefficient $\mathfrak{N}_{SD} = \left| \frac{(2\pi f)^2 R_L}{Z_S Z_D^2} \right|$. Such \mathfrak{N}_{SD} determines predominantly the frequency bandwidth of an MI link. The overall circuit impedances of the Tx and Rx coils are denoted by $Z_S = j2\pi f L_{cS} + \frac{1}{j2\pi f C_{cS}} + R_{cS}$ and $Z_D = j2\pi f L_{cD} + \frac{1}{j2\pi f C_{cD}} + R_{cD} + R_L$, respectively. The channel power gain G_{SD} of coils-based link S→D has the specific circuit gain \mathcal{C}_{SD} which can be expressed by

$$\mathcal{C}_{SD} = \frac{|\mathbf{m}_S|^2 \mathfrak{N}_{SD}}{|I_S|^2} = (\pi a_{cS}^2 a_{cD}^2 N_S N_D)^2 \left| \frac{(2\pi f)^2 R_L}{Z_S Z_D^2} \right|. \quad (14)$$

TABLE XIV
COMPARISON AMONG DIFFERENT ANTENNA TYPES

Antenna types	Direction	Focuses on G_{SD}	Advantages	Disadvantages	Refs.
Coil	Rx/Tx	J_{SD}, \mathcal{C}_{SD}	1) Low system complexity 2) Easy deployment 3) Lower costs	1) Strong orientation sensitivity 2) Low bandwidth and energy efficiency 3) Remarkable fast fading in mobile MICs	[6], [11], [12]
Orthogonal MIMO coils	Rx/Tx	\mathcal{J}_{SD}	1) Low orientation sensitivity 2) High receive sensitivity 3) Higher capacity and bandwidth	1) Challenging deployment in vehicle and TTE environments 2) Complex circuit and protocol designs	[8], [51]
RPMA	Tx	\mathcal{C}_{SD}	1) Low energy consumption under VLF 2) Smaller antenna size for TTE and mobile MICs 3) Lower cross-talk effects	1) Only for Tx antennas 2) High maintenance costs 3) Limited \mathbf{m}_S by permanent magnets 4) Longer GTS requirement due to inertia	[20], [44], [66], [78], [82], [124], [146]–[152]
M^2I	Rx/Tx	\mathcal{S}_{SD}	1) Extremely high receive sensitivity 2) Higher capacity and bandwidth	1) High costs 2) Larger radius (e.g., $\frac{50\text{mm}}{15\text{mm}}$ times) than coil	[37], [122], [123], [153]–[155]

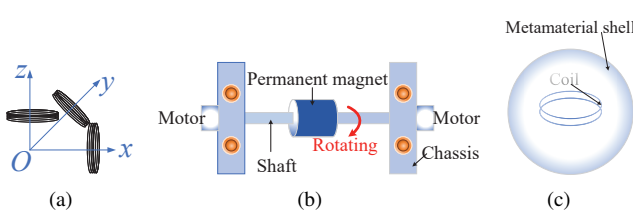


Fig. 10. Non-conventional MI antenna types: (a) Orthogonal MIMO coils [8]; (b) A typical RPMA [124]; (c) M^2I antenna [37].

From (4) and (14), the circuit gain \mathcal{C}_{SD} in G_{SD} increases with frequency f . Meanwhile, the eddy gain \mathcal{E}_{SD} in G_{SD} also increases with f . When f is sufficiently large, the condition $\sigma_u \gg 2\pi f \epsilon_u$ no longer holds. The effect of circuit gain $\mathcal{C}_{SD}(f)$ becomes significant. Consequently, coils-based MIC systems with a higher frequency achieve higher performance compared to RPMA. Also, the expressions for Z_S and Z_D indicate that the coil resonance makes the MI channel frequency-selective. This results in a narrow 3-dB bandwidth and a negative impact on the design of upper-layer protocols.

2) *Orthogonal MIMO coils*: SISO coil-based MIC systems exhibit antenna orientation sensitivity due to polarization gain J_{SD} . This can cause remarkable fast fading in mobile MIC applications. To address this, Lin *et al.* developed the orthogonal MIMO coil antennas [52], consisting of three orthogonal coils, as shown in Fig. 10(a). This antenna reduces the orientation sensitivity and enhances the MIC channel capacity through spatial diversity. Their directional pattern showed that the minimal mutual inductance increased from 0 to $\frac{1}{3}$ of maximal mutual inductance. However, for the TTE applications using VLF-LA [6], [10], deployment of such an antenna faces challenges due to limited free space and crosstalk among coils.

3) *RPMA*: The RPMA is a mechanical antenna (see Fig. 10(b)) that can generate a magnetic field of 960 Hz [147] and achieves a transmission bit rate of over 12.5 bits/s [20], [148]. Bickford *et al.* have been designing RPMA since 2017 [156]. Recently, the RPMA was used for cross-medium communication in [150], [151], where the research [150] focused on omnidirectional communication and the research [151] applied the bionic methodology.

Apart from the channel modeling, researchers also studied modulation for RPMA-based systems such as amplitude shift keying (ASK) [124], on-off keying (OOK) [20], frequency-shift keying (FSK) [146] and Chirp-rate shift keying (CSK) [44]. When using a single magnet as an RPMA, circuit gain \mathcal{C}_{SD} changes, while the other gains in (4) remain

unchanged. According to [78], the moment generated by a single magnet can be calculated by $|\mathbf{m}_S| = \frac{V_m}{I_S \mu_0}$, where V_m denotes the volume of the RPMA. The factor $\frac{1}{I_S}$ represents the remanence (denoted by \mathcal{B}_{rm}) of RPMA. Thus, the circuit gain can be calculated by

$$\mathcal{C}_{SD} = \frac{|\mathbf{m}_S|^2 \mathcal{N}_{SD}}{16\pi^2 |I_S|^2} = \left(\frac{\mathcal{B}_{rm} V_m}{4\pi \mu_0} \right)^2 \mathcal{N}_S(f) \mathcal{N}_D(f), \quad (15)$$

where μ_0 is the vacuum permeability; $\frac{1}{\mathcal{N}_S(f)}$ and $\frac{1}{\mathcal{N}_D(f)}$ are the friction loss of RPMA and the circuit loss of the receiving device, respectively. Here, $\frac{1}{\mathcal{N}_S(f)}$ increases as the frequency f increases. In contrast, $\frac{1}{\mathcal{N}_D(f)}$ decreases as the frequency increases since the Rx antenna is a general coil-based MIC device. According to [142], for a link with a Tx RPMA (as shown in Fig. 10(b)) and an Rx coil, the circuit loss can be expressed as $\frac{1}{\mathcal{N}_D(f)} = \frac{2Z_D}{\pi^2 f a_{cD}}$. The experiment in the sea near Sanya city [78] indicated that the RPMA Rx node received a magnetic field of 25 nT at a distance of 10 m.

Mechanical constraints, such as inertia and energy loss, may limit frequency agility or energy efficiency. For the RPMA shown in Fig. 10(b), the instantaneous input power is $P_S^{\text{RPMA}} = (\tau_{fr} + \tau_{nr}) 2\pi f / \eta$ [78], where η denotes the energy conversion efficiency, and τ_{fr} denotes the friction loss. The inertia constraint $\tau_{nr} = \frac{I_{nr} 2\pi f}{dts}$ depends linearly on the frequency f , indicating a higher energy proportion of τ_{nr} in high-frequency systems. The moment of inertia $I_{nr} \approx 3.75 \times 10^{-4} \text{ kg}\cdot\text{m}^2$ leads to a rated angular acceleration of approximately 539 Hz/s [78].

Some issues were not considered in previous studies. By comparing (15) with (14), it can be found that RPMA-based system can achieve higher performance under VLF conditions and lower performance under high-frequency conditions. This phenomenon can be attributed to the increase in friction and inertia associated with higher rotating speeds. Additionally, the lifespan of an RPMA-based MIC device may be shorter than that of a coil-based one due to friction. Particularly, the RPMA-based MIC requires an additional guaranteed time slot (GTS) to overcome inertia, resulting in additional data rate loss and a variable data rate under the same packet length. Most importantly, permanent magnets on Earth are unable to generate ultra-strong magnetic moments sufficient to support MIC over ultra-long distances (e.g., 1,500 m). Thus, the massive RPMA MIMO can be promising due to negligible crosstalk among RPMA.

4) *M^2I antenna*: From (4), we observe that space gain $\mathcal{S}_{SD} \propto \frac{1}{d_{SD}^6}$, indicating that the magnetic field attenuates

very fast along the signal path. To improve the magnetic fields around the MI receivers, Guo *et al.* [37] proposed the M²I enhanced technique by enclosing MI antennas with metamaterial shells (see Fig. 10(c)). Unlike natural inductors, metamaterial is an artificial material with arbitrary permeability and permittivity. It compensates antenna-generated reactive power and converts the reactive power into real power that extends the MIC range. They also proposed an easily implementable M²I antenna with a shell made of many small coils for practical use in [122], [153]. Subsequently, Li *et al.* [123] designed an active and reconfigurable M²I antenna under given meta-sphere size and power constraints. Although the simulations in [37] indicated that the MIC distance increased from 20 m to 60 m under a capacity of 1 bit/s, deploying M²I may be challenging due to the large space occupied by the metamaterial shell. For example, the meta-sphere shell in [37] has a radius six times that of a coil, i.e., a volume about 8,649 times larger. This creates a critical trade-off between performance and deployability. In the scenarios similar to deep mining, this volume penalty is justifiable. However, in narrow boreholes or mobile applications, conventional coils or RPMAAs remain preferable.

B. Channel Capacity and Bandwidth

As early as 2013, Sun *et al.* [130] suggested that the capacity C_{SD} for plat MIC channel can be derived from Shannon's equation $C_{SD} = B_w \log_2(1 + \frac{P_{Sf}}{N_{of}} G_{SD})$. For P2P MIC, the MI bandwidth is important to enhance channel capacity, especially when the Tx and noise power spectral densities (PSDs) are predetermined and cannot be altered, respectively.

The bandwidth widely refers to the 3-dB bandwidth, which is defined as the frequency range where signal power halves. There are primarily two methods (see Table XV) that can evaluate the 3-dB bandwidth of the MI links. When the noise PSD is fixed, the bandwidth can be obtained by solving the inequality with respect to f , i.e.,

$$\left| \frac{G_{SD}(f)P_{Sf}(f)}{N_{of}} \right| \geq \frac{1}{2} \left| \frac{G_{SD}(f_0)P_{Sf}(f_0)}{N_{of}} \right|, \quad (16)$$

which is referred to as the inequality calculation. For the TTE MICs, the Tx coil is treated as a magnetic dipole. Assuming identical Tx and Rx coils, the study [10] obtained the solution for the bandwidth of a P2P coil-based MIC link $B_{w,SD}^{\text{dipole}} = B_w \left(\frac{1}{8} (R_{cD} + R_L)^3 \right)$, where $B_w(\cdot)$ is

$$\begin{aligned} B_w(\mathcal{Z}_C) &\simeq \sqrt{\varpi_w(\mathcal{Z}_C) + \varrho_w(\mathcal{Z}_C)} - \sqrt{\varpi_w(\mathcal{Z}_C) - \varrho_w(\mathcal{Z}_C)}, \\ \varpi_w(\mathcal{Z}_C) &= f_0^2 + 2\pi^2 C_{cD}^2 f_0^4 \left[\mathcal{Z}_C^{-\frac{2}{3}} - (R_{cD} + R_L)^2 \right], \\ \varrho_w(\mathcal{Z}_C) &= \sqrt{\left\{ f_0^2 + 2\pi^2 C_{cD}^2 f_0^4 \left[\mathcal{Z}_C^{-\frac{2}{3}} - (R_{cD} + R_L)^2 \right] \right\}^2 - f_0^4}. \end{aligned} \quad (17)$$

However, (17) involved the assumptions of VLF-LA ($\frac{1}{2\pi f_0^2 C_{cD}} \gg 2\pi M_{SD}$) and $a_{cS} = a_{cD}$. If these assumptions are not met, the bandwidth $B_{w,SD}^{\text{dipole}}$ can be obtained through numerical methods. This inequality calculation can be extended to the non-coil-based MIC, but it may not yield closed-form analytical expressions.

Also, studies have considered MICs with shorter communication ranges, particularly in BAN applications. In these

TABLE XV
COMPARISON OF TWO BANDWIDTH CALCULATIONS

Refs.	Advantage	Limitations	Typical Eqs.
[10]	Possibility for non-coils MIC	Closed-form solution with homogeneous VLF-LA limit	(16),(17)
[40], [41]	Not limited by homogeneous coils	Only for coil-based MIC	(18)

scenarios, the Tx coil is not treated as a magnetic dipole [40], [41]. The bandwidth and channel capacity become more complex. To put it simply, since the loosely coupled coils generate the boundary conditions based on the coupling coefficient $k_c = \frac{M_{SD}}{\sqrt{L_{cS}L_{cD}}}$, both the bandwidth and channel capacity are piecewise functions of Q_S and Q_D . Here, $Q_S = \frac{2\pi f_0 L_{cS}}{R_{cS} + R_L}$ and $Q_D = \frac{2\pi f_0 L_{cD}}{R_{cD} + R_L}$ are the loop quality factors of Tx and Rx devices, respectively. In [41], the bandwidth of this model is estimated as

$$B_{w,SD}^{\text{coupling}} = \begin{cases} \frac{f_0}{Q_S}, & \text{if } Q_S > Q_D; \\ \frac{f_0}{Q_D}, & \text{if } Q_S < Q_D. \end{cases} \quad (18)$$

Obviously, (18) cannot be used to obtain the non-coils-based MIC, such as RPMA-based MI links.

As $f_0 = \frac{1}{2\pi\sqrt{L_{cS}C_{cS}}}$ holds, two calculation methods (17) and (18) imply that the P2P MIC bandwidth under VLF is roughly independent of the resonance frequency f_0 . Under the simulation parameters of Table III, the bandwidth is around 450 Hz when $1 \text{ kHz} \leq f_0 \leq 1 \text{ MHz}$, which is evaluated based on (16).

Subsequently, we focus on the MI channel capacity. Fig. 11 shows that higher frequencies boost MIC capacity in shorter ranges, and also enhance capacity over long distances in air media. In these cases, the trend of capacity decreasing with frequency is determined by the space gain S_{SD} , while the eddy gain \mathcal{E}_{SD} is negligible. However, for TTE and undersea MICs, the capacity drops sharply with increasing frequency and distance. This is due to the fact that the eddy gain \mathcal{E}_{SD} becomes the key determinant of the channel power gain G_{SD} . The frequency characteristics of MIC bandwidth and capacity motivate researchers and engineers to adopt VLF-LA methods in TTE MIC networks, evident from [6]–[11], [119]. Even at the VLF of 1 kHz, the MIC capacity in low-conductivity media (0.01 S/m, e.g., soil) is over 320-fold greater than in high-conductivity media (4.8 S/m, e.g., seawater) at 45 m MIC distance. Fig. 11 also shows that MIC channel capacity drops below 10 kbit/s beyond a distance of 60 m.

C. Communication Range

The communication range refers to the distance between the transmitter and receiver for correct data reception. It is the key performance metric for TTE communications. For the MICs, many studies focus on this metric. For example, Sun *et al.* conducted simulations and experiments for communication range and proposed the MI waveguide to extend the communication range [12]. Guo *et al.* [37] proposed the M²I enhanced communication to increase the communication range. Zhang *et al.* used a relay to extend the MIC range [6].

For MICs, most studies (e.g., [12], [85], [108], [116]) have simplified the channel model by omitting polarization and

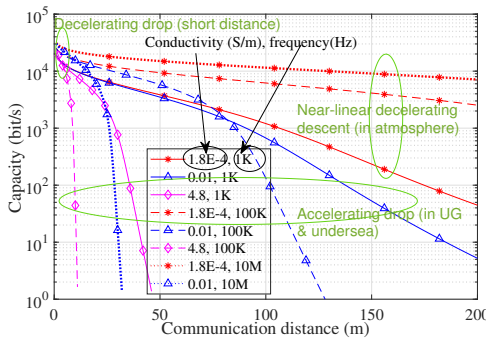


Fig. 11. MATLAB simulation of MIC channel capacity v.s. distance under different environments. All simulation parameters are listed in Table III, except for the frequency f (shown in the legend) and the MIC distance d_{SD} (as the simulated independent variable). This simulation is based on $\mathcal{C}_{SD} = B_w \log_2 \left(1 + \frac{P_{Sf}}{N_{of}} G_{SD} \right)$; see (4) and (17).

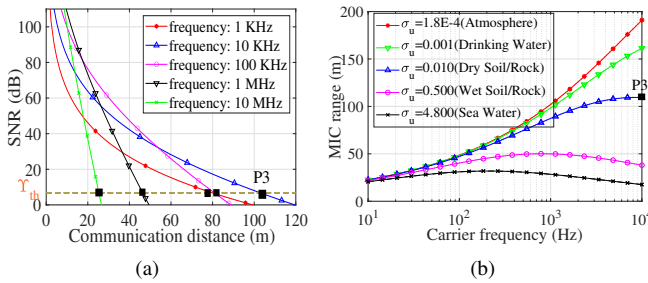


Fig. 12. MIC range simulations: (a) Description of the MIC range; (b) MIC range v.s. carrier frequency under different UG materials. The values of the horizontal coordinates of the solid rectangles represent the MIC ranges in which the SNRs are sufficiently strong to receive correct data. All MATLAB simulation parameters are listed in Table III, and the SNRs are obtained from the left side of (20).

eddy gains to address their respective concerns, and evaluated their concern performance metrics (e.g., path loss [12] and capacity [13]) w.r.t. distance via simulations or experiments. Obtaining closed-form expression of the MIC range may initially seem straightforward. For example, Zhou *et al.* [42] derived the MIC range d_{SD}^* as

$$(d_{SD}^*)^3 = \frac{\mu |\mathbf{m}_S|}{4\pi S_{\min}} |3(\mathbf{m}_S \cdot \mathbf{r}_0)|\mathbf{r}_0| - \mathbf{m}_S|, \quad (19)$$

where denotes \mathbf{r}_0 unit vector of S→D, S_{\min} denotes the minimum detectable signal strength. Obviously, (19) does not consider the eddy gain \mathcal{E}_{SD} . In TTE applications, the significant eddy current produced by large-scale underground materials cannot be ignored, as illustrated by comparing “Decelerating descent” with “Accelerating descent” in Fig. 11.

Assuming a required SNR threshold Υ_{th} for correct data reception (see Fig. 12), the MIC range d_{SD}^* of MI link S→D can be obtained by solving $\frac{P_S G_{SD} (d_{SD}^*)}{N_o} = \Upsilon_{th}$ w.r.t. d_{SD}^* , i.e.

$$\frac{P_S S_{SD} \mu_u^2}{N_o} \frac{1}{d_{SD}^*} e^{-\frac{d_{SD}^*}{\sigma_u}} J_{SD} = \Upsilon_{th}. \quad (20)$$

Fig. 12(a) describes the MIC range for TTE scenarios via MATLAB simulation. The simulation shows that the MIC system has the largest range at 10 kHz, while this frequency is neither the highest nor the lowest in this simulation. Further, the maximal MIC range exceeds 100 m but remains below

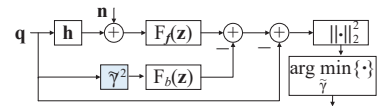


Fig. 13. Detection of changes in mutual inductance M for MI channel estimation [144]. $\tilde{\gamma}$ is the estimated positive coefficient and $M = \tilde{\gamma} M_0$, where M_0 denotes the initial value of the mutual inductance. \mathbf{q} denotes a training sequence. \mathbf{h} stands for the discrete-time channel impulse response. \mathbf{n} denotes the noise. \mathbf{z} is the equalized received signal. The transfer functions $F_f(\cdot)$ and $F_b(\cdot)$ are discrete-time feedforward and feedback filters, respectively.

50 m in wet soil, as shown in Fig. 12(b). Fig. 12(b) illustrates the relationship between carrier frequency and the MIC range across UG media with varying conductivities: for high-conductivity media, the range shows a non-monotonic trend with increasing frequency, while for low-conductivity media, it exhibits a more consistent increase. On the other hand, in the lower-conductivity materials, further optimization of the MIC range is possible once the solution to (20) is obtained.

D. Upper-Layer P2P Techniques

This subsection discusses the upper-layer P2P techniques, including channel estimation, modulation, and FEC schemes. Compared to EMWC, applying these schemes to TTE MIC faces issues of inefficient bandwidth and channel capacity. Chen *et al.* [46] proposed a Polar coding scheme with code lengths of 256 and 1024, the capacity of the TTE MIC channel may not accommodate such a large frame.

1) *Channel estimation*: Compared to EMWC, while the MI channel estimation faces inefficient bandwidth for CSI exchanging, the assumption of larger MI channel coherence time helps improve channel estimation performance. For this feature, the transmitter-side channel estimation method (see Fig. 13) was proposed in [144]. Such a method does not require an explicit training sequence. However, insufficient feedback challenges the dyadic backscatter channel (DBC) estimation. Guo *et al.* [43] designed a system for joint channel estimation and data transmissions. They considered the effects of UG material conductivity and sensor depth, which may not be the focus in the EMWC field.

2) *Modulation*: The modulation scheme encounters the issues caused by low bandwidth and frequency-selectivity, which allows a higher-order modulation scheme. Kisseleff *et al.* [45] proposed a modulation approach like frequency-division multiplexing (FDM) for MI links. Like EMWCs, the FDM scheme faces inter-subcarrier interference. It may not be suitable for RPMA systems. Hence, researchers applied amplitude shift keying [124], frequency shift keying [20], [146], chirp-rate shift keying [44], and on-off keying [20] to MIC systems. Due to the inertia of RPMA, additional delays should be considered when converting the mechanical states.

3) *Channel coding*: Channel coding is important in the physical layer. Lin *et al.* [52] used the BCH code for the FEC enhancing the MI link transmission reliability. However, the BCH code-based design did not consider the underground MI channel which is not quasi-static. To tackle this, Chen *et al.* [46] proposed a Polar code construction scheme with Bhattacharyya parameters specially optimized for MI UG-WSNs. Here, one of the inputs is SNR w.r.t circuit gain \mathcal{S}_{SD} and the space gain \mathcal{S}_{SD} ; in other words, the authors did

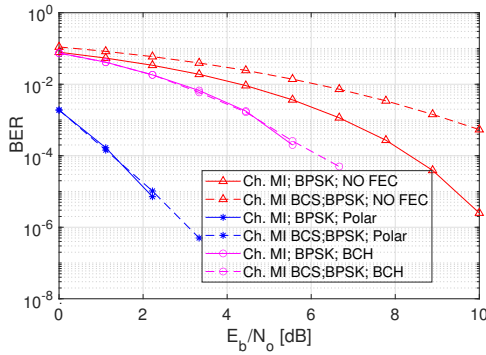


Fig. 14. BER simulations of BPSK Modulation & FECs for MI channel and MI fast fading channel, where the AVI follows the BCS distribution (MI BCS): ($\sigma_D^2=0.5^2$, $\varsigma=0.8$); FECs: BCH ($n=15$, $k=11$), Polar coding ($n=128$, $k=66$). The FECs exhibit an anti-fast fading characteristic.

not consider the eddy gain \mathcal{E}_{SD} and polarization gain J_{SD} . Compared to traditional coding, this work considered multiple distributions within a codeword from underground conductors. However, this method requires frequent CSI exchange, which may pose a challenge for the VLF-LA MIC.

By reviewing the literature, e.g., [46], [52], on modulation and FEC in a P2P MI channel and considering MI fast fading effects, we conduct comparative simulations in Fig. 14. It is noticed that an appropriate FEC strategy can significantly reduce BER, with Polar coding offering far greater advantages than BCH. On the other hand, the FEC mitigates the adverse impact of MI fast fading on BER at low SNRs. As shown in Fig. 14, with FEC employed, the dashed and solid lines nearly coincide. Although we minimize the physical layer frame length for simulating current modulation and FEC schemes, it remains excessive for TTE MIC channels, indicating room for improvement in these schemes provided by the existing MIC literature, as listed in Table IV.

E. Summary and Lessons Learned

This section discusses the addressed and remaining challenges in MI antenna designs and MIC performance metrics (such as 3-dB bandwidth [10], [41], channel capacity [13], and MIC range) in TTE scenarios. We introduce four antenna designs, each with its respective advantages and disadvantages (see Table XIV).

Notably, RPMA has emerged as a key area of research due to its minimal crosstalk among Txs. Future work could explore the application of massive MIMO and beamforming techniques, though these are difficult to implement in coil-based systems because of crosstalk. RPMA, however, faces challenges related to additional delay and energy consumption required to overcome inertia. For other antenna types, the design focus should be on optimizing \mathcal{C}_{SD} and J_{SD} . Moreover, advancements in sensor and quantum technologies, such as high-sensitivity TMR sensors, could significantly reduce antenna size and crosstalk, making it easier to apply massive MIMO and beamforming techniques in MICs. Additionally, we discuss channel estimation, modulation, and FEC strategies for MIC, validate their effectiveness through simulations, and demonstrate their role in mitigating MI fast fading-induced BER degradation.

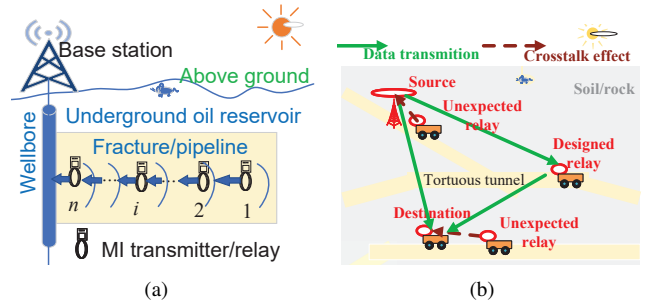


Fig. 15. Use cases of relay and CMIC: (a) Pipeline case [47], [48]; (b) Mobile MIC case. In Fig. 15(a), MI waveguide, CMIC-nAR and hybrid relay techniques can be used; in Fig. 15(b), the CMIC-1NR technique can be used.

Regarding MIC performance metrics, two key aspects remain underexplored: the closed-form expressions for the 3-dB bandwidth and the MIC range in TTE scenarios (as detailed in Table XV). While numerical methods can approximate both metrics, they are time-consuming. Furthermore, significant potential exists to improve the MIC range once its expression is fully developed, as suggested by (20).

The practical takeaways or common pitfalls include: 1) The GTSs in physical layer protocol designs for RPMA inertia have been substantially overlooked, and so has the lifespan of the RPMA; 2) the spatial inhomogeneity of TTE materials may act as a dominant source of systematic errors, causing inconsistencies between theoretical P2P MIC predictions and experimental observations; and 3) the P2P upper-layer solution tends to overlook the eddy gain and polarization gain.

V. MI RELAY AND COOPERATIVE MIC

Improving the communication range and achievable rate are the two key goals of MI studies for TTE applications. Existing research has demonstrated that these two performance metrics can be increased by one or several orders of magnitude through the use of MI relays. Most MI relay techniques require sufficient space for relay deployment. This section categorizes the MI relay into the passive MI relay (including MI waveguide) and active MI relay (called CMIC). Furthermore, we consider the advances in these two relay techniques, particularly highlighting their respective limitations. Additionally, we theoretically analyze the crosstalk effect phenomenon among MI relays through our derivations and simulations, which are overlooked in the existing studies. Table XVI outlines the challenges and methodologies of the MI relay techniques.

A. Use Cases and Scenarios

For the TTE scenarios, there are two typical use cases, as shown in Figs. 15(a) and 15(b).

In the first use case, such as oil reservoirs, straight tunnels and pipelines provide sufficient space and a clear path for signal propagation. In these scenarios, MI coils can be aligned and deployed as a stable linear topology along these pathways, ensuring reliable communication between MI Txs/relays and the base station above ground. For example, Guo and Abdallah proposed the framework of a linear pipeline/oil sensor network topology with dense nodes in [34], [47]. In this framework, most MI nodes do not require an independent power supply. As shown in Fig. 15(a), the energy of MI modes is induced

TABLE XVI
OVERVIEW OF RELATED RESEARCH ON MI RELAY TECHNIQUES
THE MARKER '●' DESCRIBE THE METHODS; THE MARKERS '✓' AND '✗' REPRESENT PROS AND CONS, RESPECTIVELY.

Types	Aspects	Refs.	Addressed issues & methods	Remaining issues (& Proposed approaches)	Priority [†]
Passive relay	MI waveguide	[12], [13]	✓ Increase the channel power gain [12] and capacity [13] by several orders of magnitude ● Channel modeling [12]; waveguide capacity analysis [13]	✗ Challenge in aligning and deploying coils to ensure the same mutual inductance between adjacent relays	**
		[157]	✓ Allowing slight misalignment of coils and being robust to node failure ● MST and TC algorithms to reduce the number of relays	✗ Crosstalk effect in misaligned coils	*
	MPRIA	[49]	✓ Bandwidth increased by over 15% compared to a quadrilateral array ● Hexagonal MPRIA using KVL equations	✗ Challenge of coil alignment	*
Crosstalk effect	[32]	✓ Existence of crosstalk effect	✗ Lack theoretical analysis; overlook positive crosstalk effect ✗ Crosstalk among local high-density nodes in a network ● Proposed Transformer based framework (Fig. 28)	***	
Active relay	Stationary CMIC-nAR	[121]	✓ Capacity increasing by an order of magnitude ● CMIC-nAR modeling and capacity analysis using AF, DF and FF schemes	✗ Approximate coil alignment required; higher energy consumption and protocol complexity than the MI waveguide	**
		[50]	✓ The number of relay reduced by about $\frac{2}{3}$ ● Formulating optimum relay placement problems using RCP based approach	✗ Strict coil alignment required	*
	Stationary CMIC-1NR	[6]	✓ OCMI yielding over 20% increase in CMIC range. ● Fixed-coil-based CMIC-1NR; optimal angle CMI (OCMI) for larger ranges	✗ Limited application scenarios due to fixed relay position	*
		[10]	✓ Potentially capacity increasing over 50% ● Non-fixed coil-based CMIC-1NR; AF schemes; CMI bandwidth derivation	✗ Space constraint of tunnels ✗ Bandwidth expression restricted to isomorphic coils	*
		[7]	✓ Excellent global optimal search ability and convergence ● Geometric approximation and random-search approaches	✗ Validation of multi-relay CMIC systems with arbitrary APOs	**
	Mobile underwater CMIC	[51]	✓ Obtain the PDF of CMI channel for underwater scenarios ● Derivation based on uniform distribution antenna angle input	✗ Uniform-based PDF not applicable to mobile underground CMI channels	**
Hybrid relay	Stationary CMIC	[32]	● Place passive relays between two adjacent active relays ✓ Energy saving	✗ Challenging antenna deployment for TTE and mobile applications	**

[†] Priority: Priority level of remaining issues and proposed approaches for exploration. Here, low priority (*) indicates that: 1) the remaining issues have been explored in subsequent MIC literature; 2) the existing EMWC schemes are compatible with MIC for these issues; or 3) exploring these issues is optional.

by the EMW generated by a large dipole. The required power to transmit data from a sensor to its neighbor sensor 3 m apart is about -50 dBm. Thus, the passive relay techniques can be used to achieve high data rate and energy performance.

In the second use case, the CMIC with one non-aligned relay (CMIC-1NR) topology [7] is designed for more dynamic and less predictable environments. For example, in underground Internet of Vehicles (IoV) systems, the mobile nodes cannot form a stable linear topology. In such scenarios, nodes are typically sparsely and randomly distributed, with each requiring a power supply to generate signals. Thus, the CMIC topology is suited for these conditions. However, randomly distributed nodes might form locally dense clusters, as shown in Fig. 15(b). Within these clusters, certain nodes inadvertently act as unexpected passive relays, inducing a crosstalk effect. In what follows, we discuss the MI passive relay, CMIC techniques, and MI crosstalk effect in detail.

B. MI Waveguide and Passive Relay Techniques

The MI passive relay passes signals through without requiring an active power source for amplification or processing. In this subsection, we introduce two MI passive relay techniques i.e., MI waveguide and MPRIA. We highlight their advantages and disadvantages for TTE applications. We also discuss the previously unstudied MI crosstalk effect, with a simulation to validate this effect.

1) *MI Waveguide*: Research on passive relays began with the introduction of the MI waveguide approach in [158], [159]. In TTE environments, the overall cost of the relay deployment, including price, time, and risks, is enormous. However, for the

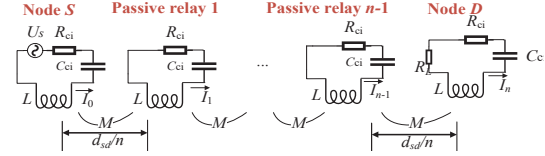


Fig. 16. MI waveguide channel model. Here, M , L , and C_{ci} denote the mutual inductance between two adjacent relays, inductivity, and matching capacitor for $f_0 = \frac{1}{2\pi\sqrt{LC_{ci}}}$, respectively.

non-emergency and non-mobile TTE MIC applications, the MI waveguide can be considered due to its excellent performance.

In [12], [13], Sun's and Kisseleff's teams increased the MIC range and channel capacity several times through the waveguide techniques. The typical structure of the MI waveguide is shown in Fig. 16 where identical passive relays are placed at equal intervals between S and D. The channel power gain of the MI waveguide link was derived as [12], [13]:

$$G_{wg} = \frac{R_L}{\text{Sn}(Z_M, Z_L, n)\text{Sn}(Z_M, Z_L, n+1)},$$

$$\text{Sn}(Z_M, Z_L, k) = \text{Fn}(Z_M, k) + Z_L \cdot \text{Fn}(Z_M, k-1),$$

$$\text{Fn}(Z_M, k) = \frac{\left(\frac{(Z_M + \sqrt{Z_M^2 - 4})}{2}\right)^{k+1} - \left(\frac{(Z_M - \sqrt{Z_M^2 - 4})}{2}\right)^{k+1}}{\sqrt{Z_M^2 - 4}}, \quad (21)$$

through Kirchhoff's voltage law (KVL), where $Z_M = \frac{Z_{LC} + R_{ci}}{j2\pi f M}$, and $Z_L = \frac{R_L}{j2\pi f M}$. The experiment in [12] indicated that the channel power gain increased by several orders of magnitude when using MI waveguide. Later, the MI waveguide networks were investigated. However, the number of MI

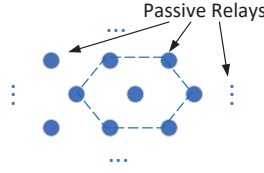


Fig. 17. Regular hexagonal MPRIA. Here, identical passive relays are uniformly placed in a 2D plane, and each relay serves as the center of a hexagon whose vertices are its nearest neighboring relays.

passive relays determines the complexity of the MI waveguide system. To reduce the number of passive relays, Sun *et al.* proposed the minimal spanning tree (MST) algorithm and TC algorithm coils [157], [160]. Their simulations indicated that the number of relays decreased from about 2,500 to 1,300 when using the MST algorithm at a sensor density of 10^{-3} nodes/m². These studies indicate that the MI waveguide techniques are constrained by the challenge of coil alignment in the TTE environment, even in the UW-WSNs.

2) *MPRIA*: The MPRIA is categorized as a 2D/3D MI waveguide [161] or non-linear MI waveguide [32], as exemplified in [49], [162]. Ma et al. [49] proposed a topology for a regular hexagonal MPRIA (see Fig. 17). The passive relays transmit propagation energy to adjacent coils and return reflection energy. They modeled the channel of this regular hexagonal MPRIA using the KVL and found that the bandwidth of the regular hexagonal MPRIA increased by over 15% compared to a quadrilateral array. However, the MPRIA techniques also face the challenge of coil alignment.

3) *Crosstalk effect of short-range passive relays*: In [32], Li *et al.* briefly mentioned the existence of crosstalk among the aligned relays. Consider the crosstalk effect caused by an arbitrarily placed unexpected passive relays, including the randomly moving Rx or idle coils belonging to other networks. Consider an MI link S→D with an unexpected passive relay R within the MIC range of S. The locations of S, R, and D are shown in Fig. 18. According to KVL, we have

$$\begin{aligned} I_S Z_{LC} + I_D \cdot j2\pi f M_{SD} + I_R \cdot j2\pi f M_{SR} &= U_S \\ I_S \cdot j2\pi f M_{SD} + I_R \cdot j2\pi f M_{RD} &= -I_D Z_{LC} \\ I_S \cdot j2\pi f M_{SR} + I_D \cdot j2\pi f M_{RD} &= -I_R Z_{LC}, \end{aligned} \quad (22)$$

where $Z_{LC} = j2\pi f L_{cS} + \frac{1}{j2\pi f C_{cS}} + R_{cS} + R_L$. Let $Z_{SR} = j2\pi f M_{SR}$, $Z_{RD} = j2\pi f M_{RD}$ and $Z_{RD} = j2\pi f M_{RD}$. Solving these equations, we obtain the current in coil D:

$$I_D = -\frac{U_S (Z_{SD} Z_{LC}^2 - Z_{pa1}(S, D, R))}{Z_{LC}^4 + Z_{pa2}(S, D, R)}, \quad (23a)$$

$$Z_{pa1}(S, D, R) = Z_{RD} Z_{SR} Z_{LC}, \quad (23b)$$

$$\begin{aligned} Z_{pa2}(S, D, R) &= 2Z_{RD} Z_{SD} Z_{SR} Z_{LC} - Z_{RD}^2 Z_{LC}^2 \\ &\quad - Z_{SD}^2 Z_{LC}^2 - Z_{SR}^2 Z_{LC}^2, \end{aligned} \quad (23c)$$

where we call $Z_{pa1}(S, D, R)$ and $Z_{pa2}(S, D, R)$ the *crosstalk impedances* of link S→D. Thus, we can define the *crosstalk effect* as the phenomenon occurring when a link has at least one non-zero crosstalk impedance. Also, using KVL equations as (22), we can derive the more complex expressions of crosstalk impedances $Z_{pa1}(S, D, R, \dots)$ and $Z_{pa2}(S, D, R, \dots)$ when a link has more than two passive relays.

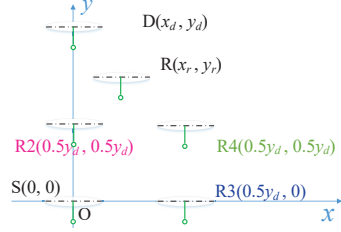


Fig. 18. Example of Crosstalk effect from an unexpected passive relay. Suppose that a passive relay R moves (sufficiently slowly to avoid MI fast fading) along the path R→R2→R3→R4.

It is noticed in (23) that the MI crosstalk effect directly impacts the performance of the MIC network through the crosstalk impedances $Z_{pa1}(S, D, R, \dots)$ and $Z_{pa2}(S, D, R, \dots)$. For example, when $Z_{pa1}(S, D, R, \dots) > 0$ and $Z_{pa2}(S, D, R, \dots) > 0$, the received current I_D decreases, thereby inducing the negative crosstalk effect. This effect may reduce the MIC range and increase the BER. Conversely, the negative impedances $Z_{pa1}(S, D, R, \dots)$ and $Z_{pa2}(S, D, R, \dots)$ can result in positive crosstalk effects, which may improve the MIC range and capacity. The MI waveguide conforms to this case. For long-range MIC using VLF-LA with low f , where M_{SD} , M_{SR} and M_{RD} are sufficiently small to satisfy $Z_{LC} \gg j2\pi f M_{SD}$, $Z_{LC} \gg j2\pi f M_{SR}$ and $Z_{LC} \gg j2\pi f M_{RD}$, the crosstalk impedances can be ignored.

This is verified by our simulation results as shown in Fig. 19. This simulation also shows that the short-range or higher-frequency MI links encounter a significantly more pronounced crosstalk effect. When the ratio $\frac{G_{SD, R}}{G_{SD}}$ exceeds 1, the passive relay serves as part of the MI waveguide and has a positive effect on MIC. For long-range MIC, all curves in Fig. 19 converge to 1, indicating the elimination of crosstalk. It is worth noting that the CMIC and large-scale MI network also have the crosstalk effect issue according to KVL equations.

From (23) and $M_{ij} = \frac{\pi a_{ci}^2 a_{cj}^2 N_i N_j \mu_u}{2d_{ij}^3} \mathcal{J}_{ij} \sqrt{\mathcal{E}_{ij}}$ with $i, j \in \{S, D, \dots\}$, it can be concluded that both $Z_{pa1}(S, D, \dots)$ and $Z_{pa2}(S, D, \dots)$ are multimodal functions. Determining their signs is challenging. To address this, future studies are needed on the spatial distribution of positive crosstalk effects. We also propose a deep learning framework to predict the signs of $Z_{pa1}(S, D, \dots)$ and $Z_{pa2}(S, D, \dots)$, as will be described in Section VIII-C.

C. Cooperative MIC (CMIC)

In this subsection, we delineate two active relay techniques, i.e., CMIC with multiple aligned relays (CMIC-nAR) and CMIC-1NR. We also summarize distinct challenges associated with cooperative communication between MIC and EMWC.

The MI waveguide enhances channel capacity and range but requires numerous underground relays. For several decades, cooperative communication has been a focus in the EMWC, FSOC, and acoustic communication [163]–[167]. These communication channels experience significant small-scale fading. Cooperative relays use spatial and time diversity to mitigate these fading effects, which significantly reduces outage probability and enhances achievable rates. Various cooperative

TABLE XVII
COMPARISON OF COOPERATIVE EMW AND CMI COMMUNICATIONS

Comparison	EMW	Refs.	CMI	Refs.
Channel characteristic	Small-scale fading	[163]	Quasi-static fading [†]	[6], [7], [121]
Key issue	Reducing outage probability	[163]	Enhancing Rx signal strength	[6], [7], [121]
Methods	AF, DF, Compress-and-forward	[163]	AF, DF, FF	[7], [32], [121]
Benefits	Universal	[163]	Limited by coil locations and orientations	[6], [7], [10]

[†] With Advances in MI fast fading research, limited literature on the CMI channel with non-quasi-static fading (e.g., [51]) has been released.

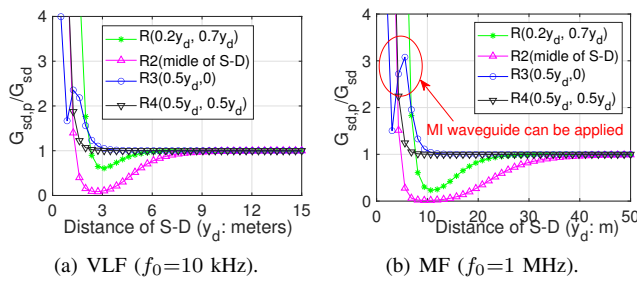


Fig. 19. Ratio $\frac{G_{SDP}}{G_{SD}}$ for crosstalk effect as shown in Fig. 18, where G_{SDP} represents the power gain of the MI link S→D when a passive relay is used, i.e., $G_{SDP} = \frac{I_D^2 R_L}{I_S U_S}$, where I_S and I_D are obtained from (22) and (23), respectively. This ratio quantifies how much the power gain improves (or deteriorates, if < 1) with the introduction of a passive relay. The simulation parameters are listed in Table III, except for $a_{cD} = a_{cr} = 0.6$ m, and $N_{cD} = N_{cr} = 15$.

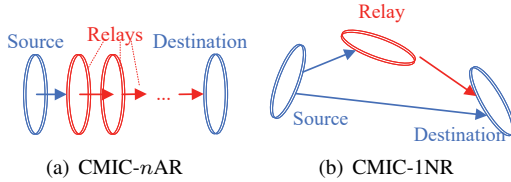


Fig. 20. Two types of the CMIC. The topology of CMIC-nAR is similar to the MI waveguide, and signals are transmitted one by one. The coils exhibit a near-perfect alignment. In CMIC-1NR, the coil of the relay does not need to be aligned, and a diversity combining method should be used to combine the relay and source signals.

communication schemes were proposed, such as amplified-and-forward (AF), decode-and-forward (DF), and filter-and-forward (FF) schemes [32], [163].

However, the traditional MIC channel model is quasi-static without small-scale fading. Such quasi-static property renders outage probability physically meaningless. Spatial and time diversity offer limited benefits for mitigating small-scale fading in traditional MICs. Fortunately, researchers discovered that active relays can enhance signal strength at the Rx coil under certain conditions. The CMIC can be categorized into two types: CMIC-nAR [32], [50], [121], [159] and CMIC-1NR [6], [7], [10]. The typologies of the CMIC-nAR and CMIC-1NR are as shown in Figs. 20(a) and 20(b), respectively.

The topology of CMIC-nAR is similar to that of MI waveguide [121]. The simulations indicated that the data rate increased from 10^4 to over 10^5 at the distance of 70 m when using a DF or FF relay. To reduce energy consumption, Li *et al.* [32] proposed a hybrid relay structure that combines the waveguide and active relay. Their simulation showed that the energy consumption decreased from 1 J to 0.3 J at the distance of 96 m. In 2021, Ishtiaq *et al.* [159] developed a mathematical model for evaluating the performance of the multi-hop MI link, including the hop state. Also, the multi-relay optimiza-

tion has caught researchers' attention. In [50], Khalil *et al.* proposed a CMI system similar to an MI waveguide without S, achieving the maximum throughput and reducing the number of relays. The transmission rate must be positive, leading to the constraint inequalities shaped as convex functions with negative values [50]. Therefore, reverse convex programming (RCP) was introduced as a solution. However, similar to the MI waveguide, the CMIC-nAR is suitable for underwater and limited underground scenarios.

Due to the disadvantage of CMIC-nAR for TTE MICs, some researchers explored the CMIC-1NR by optimizing J_{SD} . Zhang *et al.* [6] proposed the CMIC-1NR. Later, Ma *et al.* [7], [10] further investigated CMIC-1NR systems to boost MIC achievable rates. In [10], they studied the achievable rate of AF-based CMIC with an arbitrary relay APO. Specifically, they derived the closed-form expressions for CMIC bandwidth. The bandwidth of the CMI link varies with the APO and is smaller than that of the Direct magnetic induction (DMI) link (see Fig. 21). Even with the smaller bandwidth, an active relay may enhance the achievable rate of the MI link (see Fig. 22), especially for weak signals. Unlike the DMI link, this improvement is APO-dependent. This complicates TTE applications due to underground space constraints. In Fig. 22, despite maximal CMIC achievable rate gain (CMG) at the RA center, the relay cannot be placed there due to tunnel constraints. Ma *et al.* [7] addressed this with a geometric modeling approach and a random-search algorithm to find the optimal APO for relay deployment in tunnels. Their simulations showed that compared to the Gradient Descent Algorithm, the number of iterations for their algorithm decreased from 600 to 100, and the number of local optima decreased from 11 to 1. However, despite the contributions of CMIC-1NR, it can be summarized that all the CMIC-1NR techniques mentioned in this survey are significantly subjected to the APOs. Also, the CMG of CMIC-1NR is much smaller than that of CMIC-nAR.

With advances in MI fast fading research, researchers have focused on the CMI channel with random polarization gain J_{SD} . In 2024, Zhang *et al.* [51] investigated the CMIC systems with an unidirectional coil and a tri-directional active relay, respectively. Assuming that norm directions of coils S, R, and D follow the uniform distributions, they derived closed-form expressions for the PDFs of received SNRs. Their simulations indicated that the ergodic rate increased from 6 bps/Hz to 16 bps/Hz at a distance of 20 m and a Tx power of 20 dBw, even using an AF relay. However, for the terrestrial mobile MIC, it is obvious that the probability of a weak antenna vibration $\theta'_D \simeq 0$ is much greater than that of a strong one $\theta'_D \simeq 90^\circ$. Thus, the uniform distribution-based model deviates significantly from the feature of non-underwater mobile MICs.

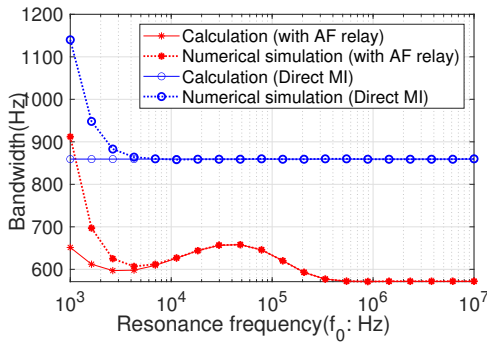


Fig. 21. Comparison of the bandwidth between AF-based CMI and DMI links. The simulation parameters are listed in Table III, except for $\theta_D = 30^\circ$. Here, solid lines are calculated from $B_{w,SD}^{\text{dipole}} = B_w \left(\frac{1}{8} (R_{cD} + R_L)^3 \right)$ and $B_w^{\text{AF}} = B_w(\mathcal{Z}_{C, \text{AF}})$, respectively. The function $B_w^{\text{AF}}(\cdot)$ is given by (17) in this paper. The impedance $\mathcal{Z}_{C, \text{AF}}$ is given by Equation (14) in [10].

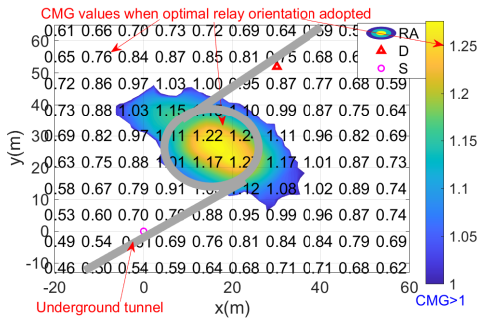


Fig. 22. Effects of relay positions on the CMI performance, and an example of tunnel constraints. The simulation parameters are listed in Table III, except for $\theta_D = 30^\circ$. Here, CMG (defined in [10]) is the ratio of capacities of the CMI link to the DMI link, and the area where $\text{CMG} > 1$ is called the relay area (RA). The thick gray curve represents an arbitrary underground tunnel in which S, R, and D are constrained to reside.

D. Summary and Lessons Learned

Table XVI summarizes the key issues, methods, and remaining challenges in MI relay research, covering MI passive relay [157], MI active relay (CMIC) [51], and hybrid relay techniques [32]. These studies show that both passive relay and CMIC techniques can significantly enhance channel capacity and extend the MIC range, sometimes by orders of magnitude.

The passive relay technique is energy-efficient with simple protocol complexity, but it faces deployment challenges, particularly in antenna alignment due to the negative crosstalk effect. A potential solution involves the use of an iron core coil to collect MI signals, although careful attention is needed to mitigate the effects of the eddy current. Additionally, implementing passive relays in RPMA-based systems is challenging due to minimal crosstalk effects. Moreover, passive relay and CMIC-nAR techniques are unsuitable for mobile MICs due to their dynamic topology, which prevents the formation of stable systems with positive crosstalk effects (see (23) and Fig. 19). In contrast, CMIC significantly reduces the number of required relays. The CMIC-1NR solution, which eliminates the need for coil alignment, can be applied to RPMA-based systems and mobile MICs. We introduce the unexpected passive relay phenomenon, specifically the crosstalk effect in relays, and highlight its role in MI waveguides as a special case.

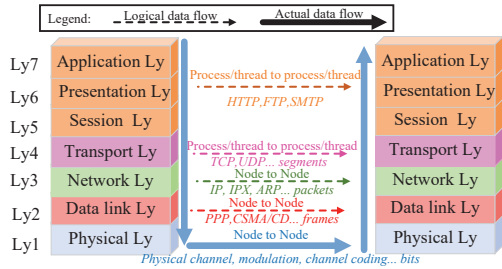


Fig. 23. The OSI framework, which has seven layers.

The practical takeaways or common pitfalls include: 1) A primary practical challenge in MI relay is antenna alignment. Thus, the MI waveguide for TTE suits only scenarios like straight tunnels, which is infeasible for mobile MICs; 2) increasing active relays does not guarantee throughput improvement; and 3) a high-density multi-node MI network exhibits the crosstalk. However, determining the spatial distribution of positive crosstalk remains challenging, complicating the passive relay deployment.

VI. MI NETWORK AND ITS ARCHITECTURE

In wireless communications, key focal points include improving network throughput, increasing access to users, and reducing energy consumption. However, recent techniques in EMWC using signal reflection and refraction [170]–[172] are challenging to apply to MIC signals due to their lack of reflection and refraction. Consequently, the role of MI network architecture becomes more important than that of the EMWC network. In this section, we categorize recent literature on multi-node MIC with reference to the widely used OSI framework. The OSI framework (see Fig. 23) originated from the International Organization for Standardization (ISO) in 1984. It serves as a conceptual framework for designing network communication protocols and facilitating communication between different systems. The research on the MI network and differences from other communication networks are summarized in Tables XVIII and XIX, respectively, with more details provided below.

A. Physical Layer (Ly1)

Most research on MIC focused on the physical layer issues, including channel modeling, performance, estimation, modulation, coding, and resources allocations. We have discussed the issues of physical layer schemes on P2P and MI relay-based system, i.e., channel modeling, key performance metrics, channel estimation, modulation, and channel coding in Sections IV and V. For the MI physical layer with multiple nodes, the focus has been primarily on the resource allocations, including power allocation [11], [52], [53], as well as frequency and bandwidth allocations [53].

1) *Power control*: From the network's perspective, power control aims to optimize signals, reduce interference, and enhance efficiency. Lin et al. [52] pioneered the study of power optimization formulation from the entire multi-hop network. To formulate the power control problem, they used the Nash

TABLE XVIII
OVERVIEW OF RELATED RESEARCH ON MIC IN LINE WITH THE OSI FRAMEWORK
THE MARKER '●' DESCRIBES THE METHODS; THE MARKERS '✓' AND '✗' DESCRIBE ADDRESSED AND REMAINING ISSUES, RESPECTIVELY

OSI Lys	Aspects	Refs.	Methods and addressed issues	Remaining issues	Priority
Ly1	P2P & relay-based MICs	[10], [12], [45], [46], [144]	✓ Channel modeling, channel capacity, MIC range, channel estimation, channel coding and modulation (see Sections III, IV, and V) ● Detailed in Tables IX, IV, and XVI	✗ A universal MI fast fading model; TTE MIC range; RPMA channel capacity; MI crosstalk effects; CMIC with MI fast fading ✗ Detailed in Tables IX, IV, and XVI	-
	Power allocation	[52], [58]	✓ Power allocation issue for a stationary MI channel ● Nash game	✗ Not suitable for time-varying channel over a longer time span ✗ Quantization-induced precision loss	*
		[11]	✓ Power allocation issue for an MI fast fading channel ● Nash game-based multiagent RL with Bellman iteration	✗ Slow convergence due to lack of information exchange; ✗ Sacrifice precision for faster convergence	**
	Frequency allocation	[53]	✓ For lower system delays (> 40% decrease) for cluster-based UW-WSN ● Multi-variable alternating iterative resource allocation algorithm	✗ No considerations of network throughput and energy consumption	**
Ly2	MAC	[54], [168]	✓ Low-cost (\$100); low energy (Currents: Rx/Tx=0.49/253 mA) ● Designing three packet types (reservation, acknowledge, data)	✗ Lacking analysis for SISO case for VLF-LA	*
		[55]	✓ Considering both energy (Rx/Tx: 0.49mA/0.74mA) and throughput (46-144 bytes/cycle) ● Contention-based protocol using hybridizing three configurations of the orthogonal MIMO coils	✗ Low energy efficiency for SISO-coil; low EPR; high collision probability ✗ Too large MAC headers for a VLF-LA system	***
	LLC	No refs.	-	✗ Adaptive retransmission strategy for unnecessary packets ✗ Compatibility of existing solutions for MIC	*
Ly3	Connectivity	[169]	✓ Dynamic connectivity for a 2D model ● Designing framework of connectivity probability bounds	✗ Only applicable to the 2D model ✗ Disregarding attenuation differences with directions	*
		[72]	✓ k -connectivity for an underwater grid network ● Derivation based on power and BER	✗ Disregarding attenuation differences with directions	*
		[8], [116]	✓ Randomly deployed in a 3D space, and considering attenuation differences with directions . ● Probability theorem; gradient descent method; homogeneous Poisson Point Process	✗ Violating homogeneous condition in heterogeneous networks or mobile MIC.	**
	Data collection and node deployment	[56]	✓ Optimal data collection and network lifetime (21.2%~38.3% higher) with low energy consumption (0.2~0.34 J) ● HENPC algorithm and ant colony optimization	✗ Large delay caused by ant colony algorithm	**
		[80]	✓ May increasing the network lifespan (by $\frac{1}{31} \sim \frac{5}{18}$). ● AANSFR algorithm	✗ Non-guaranteed optimality due to the constraint of [80, Eq. 10(a)]	*
	Routing	[85], [86]	✓ Balancing the network latency (reduced by 18% in [86]), and energy efficiency (increasing by 16% in [86]) ● Q-learning based energy-delay routing (QL-EDR) [85] and Balanced routing protocol based on Q-learning [86] algorithms	✗ Overlooking the frequency features ✗ Slow convergence of Q-learning	**
		[57], [120]	✓ Frequency-selective property in a dynamic multilayer MI UG-WSN ● Distributed Q-learning-based algorithm; formulating frequency-switchable routing decision problem	✗ Slow convergence for Q-learning ✗ Poor efficiency of routing tables exchange in narrow-band MI channels	***
	Topology	[169]	● Ad-hoc (high self-organizing capability; limited scalability)	-	-
		[47]	● Linear topology (simple protocol; single point of failure)	-	-
		[11]	● Cellular topology (frequency reuse; local network congestion)	✗ Basic resource allocation/reuse schemes ✗ A basic MI cellular network protocol stack	***
	IP	No refs.	-	✗ Low efficiency in TTE MIC due to the large IP header (over 20 bytes) and limited channel capacity (IP-IC scheme required) ✗ Compatibility of existing solutions for MIC	***
Ly4	TCP	No refs.	-	✗ Fairness issue; RTT suppression issue; congestion control scheme for TCP connections w.r.t. the SNR in Rx MI nodes ✗ Compatibility of existing solutions for MIC	***
Ly5-7	Applications	cf. Table VII	-	✗ MCNSI, TTE infrared image transmission; TTE IoV applications; DARPA Subterranean Challenge	**
CLO	-	[52]	✓ Statistical QoS guarantee and obtaining both optimal energy savings and throughput gain concurrently ● DEAP framework jointing Ly1, Ly2, and Ly3	✗ Not suitable for the mobile MIC in an MI fast fading channel due to its drastically fluctuating average AVI	**
		[58]	✓ Optimal energy efficiency and low computational complexity, with higher throughput than EDAP; ● Distributed Energy-throughput efficient Cross-Layer solution using Naked Mole Rat algorithm (DECN)	✗ Not suitable for the mobile MIC in an MI fast fading channel due to its dramatically fluctuating average AVI	**

[†] Priority: Priority level of remaining issues and proposed approaches for exploration. Here, low priority (*) indicates that: 1) the remaining issues have been explored in subsequent MIC literature; 2) the existing EMWC schemes are compatible with MIC for these issues; or 3) exploring these issues is optional.

game with the utility function as shown in Table XX. The study presented in [52] did not consider mobile MI networks with the unpredictable AVI inputs. To address this, Ma *et al.* [11] proposed a power allocation algorithm for cellular VMI networks. They used the Nash game-based RL (Q-learning) with the utility function, as shown in Table XX. The RL solution from [11] addresses the problem of the unpredictable AVI inputs in MIC systems.

Due to the convergence limit, it can be difficult for the RL algorithm to obtain a high-precision power allocation policy. Moreover, since this power allocation algorithm requires no information exchange among the nodes, it is feasible for low-capacity channels. By contrast, the expectation of EMW fast fading is predictable in most cases; in this sense, RL may not

be needed for an EMW cellular network.

2) *Frequency and bandwidth allocation*: Effective frequency/bandwidth allocation can enhance capacity, QoS, and cut the network energy consumption. Due to the narrow MI bandwidth and limited research on MI cellular topology, frequency/bandwidth allocation has garnered limited attention. Nonetheless, Li *et al.* [53] studied bandwidth allocation involved schemes, applied to the AUVs and cluster-based UW-WSNs. A joint optimization was proposed to obtain allocations of Tx power, bandwidth, and computational resources. The key goal (see Table XX) was to minimize total system delay T . The authors developed a centralized multi-variable alternating iterative resource allocation algorithm. The core of the algorithm lies in its two-stage iterative process within a

TABLE XIX
COMPARISON OF WAVE-BASED AND MI COMMUNICATIONS BASED ON THE OSI FRAMEWORK
THE MARKERS ‘’, ‘’ AND ‘’ DESCRIBE EMWC, ACOUSTIC COMMUNICATION AND MIC, RESPECTIVELY

OSI Lys	Aspects	Typical refs.	Other communications compared to MIC	MICs
Ly1	Channel estimation	[144]	→ Estimation not based mutual inductance → Overlooking the medium conductivity	○ Estimation based mutual inductance ○ Significantly influenced by medium conductivity
	Modulation	[45]	→ Negligible frequency dependent eddy currents effect → Larger frequency bandwidth	○ Non-Negligible frequency dependent eddy currents effect ○ Much smaller frequency bandwidth
	Channel coding	[46]	→ Negligible conductor on the propagation path	○ Variable codeword duration from underground conductors
	Resource allocation	[11]	→ Sufficient bandwidth for allocation table exchange	○ Insufficient bandwidth for allocation table exchange
Ly2	MAC	[55]	→ Often ignoring the directional nature of EMW	○ Requiring further bit-level compression for MAC headers ○ With directional nature of magnetic fields
	LLC	[173] [†]	○ Acoustic channel quality based retransmission scheme	○ MI channel quality based retransmission scheme [†]
Ly3	Connectivity	[8]	→ Negligible attenuation differences with directions	○ Attenuation differences with directions
	Deployment	[157], [174]	→ Higher protocol complexity → Less APO dependent	○ Full utilization of MI waveguide advantages ○ Higher APO dependent
	Routing	[57]	→ Less frequency-selective and APO-selective	○ Significant frequency-selective and APO-selective
	IP	[175] [†]	○ IP-HC scheme using acoustic network information	○ IP-HC scheme depending on MI channel [†]
Ly4	TCP	[176] [†]	→ Less RTT suppression	○ Significant RTT suppression [†]
CLO	-	[11], [52]	→ $G_{SD} \propto d_{SD}^{-2}$ → Stable and determined moments of fast fading gain	○ $G_{SD} \propto d_{SD}^{-6} e^{-d_{SD}/\delta u}$ ○ Random moments of MI fast fading gain

The superscript [†] indicates the issue lacking relevant literature on MIC-related research and MIC solutions, to the best of our knowledge, to date.

TABLE XX
COMPARISON OF THREE RESOURCES ALLOCATION METHODS ON MIC RESEARCH

Refs.	Goal function / utility function	Explanations	Methods
[52]	$u_i(p_i, p_{-i}) = C_i(p_i, p_{-i}) - w\mathfrak{E}_i(p_i, p_{-i})$	Power allocation for stationary MICs: C = data rate, \mathfrak{E} = total power, i =this user, $-i$ =competing users, p =power allocations, w =weight	Nash game
[11]	$u_i(p_i, p_{-i}) = \mathbb{E}[C_i(p_i, p_{-i}) \sigma_i^{(t)}]$	Power allocation for mobile MICs: $\mathbb{E}[C]$ =ergodic data rate, i =this user, $-i$ =competing users, p =power allocations, $\sigma_i^{(t)}$ =average AVI during time slot t	Joint Nash game and RL algorithm
[53]	$\min_{P_{UA}, P_{CH}, B, F} T$	Bandwidth allocation for MICs: T =system delay, P =power allocations, B =bandwidth allocations, F =computational resources, UA =acoustic node, CH =MI cluster header	Centralized optimization

single loop, including obtaining power allocations with fixed bandwidth, and obtaining bandwidth allocations with fixed power. Although this study greatly reduces the system delay by up to 40%, it does not account for frequency allocation for the performance improvement of the capacity, QoS, and network energy consumption.

Table XX compares the three resource allocation schemes discussed above. The first two methods suit low-speed channels, minimize inter-user information exchange but converge slowly, where the second, though better for dynamic channels, converges extremely slowly. The third, with fast convergence, fits higher-speed networks (e.g., hybrid MIC).

B. Data Link Layer (Ly2)

The data link layer is responsible for ensuring reliable data transfer between adjacent network nodes through functions such as error detection, error correction, and flow control. It is divided into the MAC and logical link control (LLC) sub-layers. While only the MAC sub-layer is channel-dependent.

1) *MAC*: The low bandwidth of an MIC link presents challenges for real-time MAC protocol implementation. Also, many EMWC MAC solutions cannot be directly applied to MI UG-WSN due to the directional nature of magnetic fields [54]. Ahmed *et al.* [54] provided valuable insights into energy-efficient MI-based MAC protocols. They designed three packet types, i.e., reservation, acknowledge, and data packets, and a general state transition machine for the MAC packets exchanging. They also designed an MI device with this MAC protocol that achieves less than \$100 in cost, 60 μ A in the sleep mode, 0.49 mA in the Rx mode and 253 mA in the Tx

mode. However, this work did not consider the throughput. Recently, in [55], they proposed an improved MAC protocol and algorithm that considers detailed MI channel parameters. This work balanced the energy and throughput performance metrics by hybridizing three configurations of the orthogonal MIMO coils, each corresponding to a different packet type (as detailed in Fig. 24). They applied the CSMA-based scheme, and pointed out that their MI MAC protocol exhibits low energy efficiency under the SISO-coil-based MIC. That is, it may encounter problems with the MIC that employs VLF-LA. Furthermore, the large MAC header (8 bytes) can be further compressed at the bit-level for the VLF-LA channel.

2) *LLC*: The LLC sub-layer is often only a thin adaptation sub-layer that provides the reliability of communication, e.g., through data transfer, flow control, and error control. Since the LLC sub-layer is designed to be independent of the physical layer and media in the OSI model, it has received limited attention in MIC research. Only a few studies have explored LLC protocols for other communication channels (e.g., acoustic communication channel [173], [177] and quantum communication [178]). Specifically, Daladier *et al.* [173], [177] proposed the SW-MER protocol to enhance throughput and reliability by employing an adaptive retransmission strategy that takes advantage of acoustic channel quality to minimize redundant packet transmissions. This approach can serve as a reference LLC for MIC, as both acoustic and MIC channels share low data rate characteristics.

C. Network Layer (Ly3)

The network layer routes data packets efficiently to their destinations. In this subsection, we introduce the studies on the

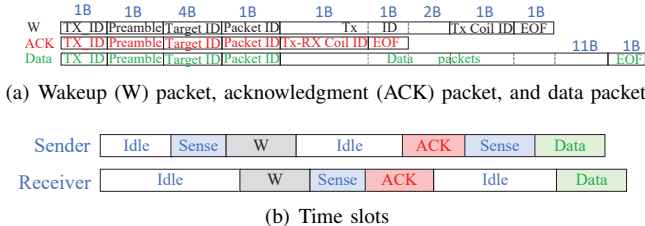


Fig. 24. A typical MI MAC solutions in [55]. (a) The packets are designed into three types. (b) Complete communication cycle between a Tx and Rx, where the Tx node starts with a W packet; the Rx node, after successfully receiving the W packet, acknowledges with an ACK packet; upon receiving the ACK packet, the Tx node then sends out the whole data packet [55]. However, for TTE MICs, the packet size should be further compressed.

functionality of the MI network, including connectivity, data collection, node deployment, and MIC routing. Here, routing in MIC has recently represented a new research aspect.

1) *Connectivity*: Connectivity is a cornerstone of networks and is crucial for designing network layer protocols, including routing algorithms, traffic control, and quality of service (QoS). It has been widely studied in EMWC research. For n network nodes uniformly distributed within a circular area of πR^2 , Gupta *et al.* [179] derived $\mathcal{R}(n) = \sqrt{\frac{\log(n) + c(n)}{\pi n}}$, where $c(n)$ is a correction function. They proved that these nodes are connected with probability one if $\lim_{n \rightarrow \infty} c(n) \rightarrow \infty$. The connectivity analysis differs fundamentally between MIC and EMWC. As the MIC is immune to shadowing, the geometric disk/sphere models used in EMWC network studies [179]–[182] are inadequate for the MIC channel.

Since 2011, there has been little literature on the connectivity in the MIC field. Sun *et al.* [169] conducted a 2-D connectivity analysis of UG-WSN using probability derivation, yet overlooked attenuation differences. Gulbahar and Akan [72] performed a k -connectivity analysis on an underwater MI grid network with Tx coils at the fixed positions and directional angles. Zhang *et al.* [8] performed a connectivity analysis of TTE MI UG-WSN and proposed an optimization algorithm to address the connectivity adaptability of frequent frequency-switching w.r.t. APO-switching. For the mobile MIC, the MI fast fading results in an irregular shape of the MI coverage space. In heterogeneous MI UG-WSNs, the nodes are not homogeneous. These features violate their assumptions in the connectivity model (e.g., Poisson point process) and represent open issues.

2) *Deployment strategic and data collection*: The strategic deployment and data collection of MI sensors are also essential for effective local network design. Fig. 3 and Eq. (3) show that the APOs significantly impact the polarization gain J_{SD} . Optimizing APO is a distinct issue from EMWC [6], [7], [10], [174]. Specifically, Kisseleff *et al.* [174] optimized the antenna deployment to avoid channel interference from other nodes. Recently, focus has been placed on node deployment for efficient data collection and routing protocols. For a 3D-UW-WSN, Wang *et al.* designed an optimal deployment strategy and a clustering algorithm to prolong the network lifetime by 38.3% and 21.2% compared to the EELEACH-C algorithm [56]. This algorithm is also compatible with the 3D-UG-WSN. Wei *et al.* [80] studied the power-efficient AUV data collection schemes in an MI and acoustic hybrid sensor.

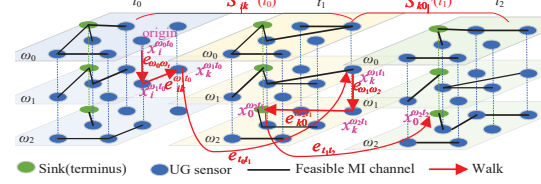


Fig. 25. Schematic of a walk (arrow trajectories) for the frequency-selective MI links (from sensor i , through sensor k , to the sink 0) [57]. In this figure, ω denotes the operating frequency; t denotes the time; x denotes the node state; $S(\cdot)$ denotes a step. The objective of the optimization problem is to maximize the total capacity of related walks.

They proposed the alternating anchor nodes selection and flow routing (AANSFR) for AUV data collection, where the 3dB MI bandwidth is considered. Using AANSFR, the lifespan could increase from 14 hours to 18 hours.

3) *Routing*: Although routing design is a kernel function model in the network layer, studies on routing in MI UW-WSNs and UG-WSNs are limited. From (3), it is observed that circuit gain $\mathcal{C}_{SD}(f)$ and eddy gain $\mathcal{E}_{SD}(f)$ are the functions of carrier frequency f . These gains represent the frequency-selective property. Compared to traditional routing strategies, this property makes the MI UG-WSN appear to have entirely different topological structures at different operating frequencies [57]. Likewise, as the MIC based on VLF-LA is orientation sensitivity (called APO-selective property), the mobile MI-UG-WSN can also encounter different topological structures due to the unpredictable moment of MI fast fading gain J_{SD} .

For the frequency-selective property, Liu *et al.* [57], [120] proposed the frequency-switchable strategies for routing decisions, using a distributed Q-learning-based algorithm. Specifically, in [120], they mapped the frequency-switchable MI UG-WSN to a multilayer network and proposed a distributed Q-learning-based algorithm to provide a description on its routing decision. They also evaluated the convergence of the algorithm and network lifetime. As Q-learning is time-consuming, in [57], they redefine the routing decision problem with frequency switchability in dynamic MI-WUSNs (see Fig. 25). Their simulations showed that the throughput increased from 40 to over 45 when the connectivity is 1.

Improving network lifetime and reducing the transmission delay are two conflicting goals in routing studies. To balance these goals, Wang *et al.* [85] proposed two algorithms based on RL, *i.e.*, the QL-EDR algorithm, and the path selection strategy algorithm. Alsalmam *et al.* [86] proposed a balance routing protocol based on machine learning (BRP-ML) to reduce network latency and energy consumption. In these studies [57], [85], [86], [120], the eddy gain \mathcal{E}_{SD} and polarization gain J_{SD} are ignored. Moreover, their centralized-based multiagent RL algorithms require the exchange of band tables among nodes. This poses a practical challenge due to the low data rate in the MIC with VLF-LA.

4) *Internet Protocol (IP)*: In the TCP/IP framework, the IP, including IPv4 [183] and IPv6 [184], was originally designed to be channel-independent. To the best of our knowledge, there has been no literature specifically addressing the issues related to IP in the field of the MIC. However, the most significant challenge is IP's low efficiency in TTE MIC due

to the large IP header (over 20 bytes) and the limited channel capacity of TTE MI links. In the fields of other communication techniques, such as bandwidth-constrained EMWC [185] and acoustic communication [175], this challenge was mitigated or addressed via IP header compression schemes. Specifically, Parrein *et al.* [175] proposed an acoustic protocol based on the static context header compression (SCHC) protocol to reach the header compression ratio of 99.74% using lower-layers' information. This also can be applied to the MIC.

D. Transport Layer (Ly4) and TCP

The transport layer, akin to the LLC sub-layer and including TCP [186], ensures end-to-end communication with reliable data transfer, flow control, and error recovery. It was originally designed to be channel-agnostic. There is limited literature on MI transport layer research. Particularly for TCP, fairness and congestion control issues pose a challenge and can be potentially optimized utilizing the characteristics of the specific channel. For example, TCP connections with shorter round-trip times (RTTs) often hinder the throughput of those with longer RTTs (i.e., RTT suppression issue). In the EMWC field, these issues have received some attention, e.g., [176], [187]. In [176], the congestion window was modeled as a function of the SNR of the EMW link, suggesting that one can formulate the corresponding optimization problem of the RTT for TCP w.r.t. the MI channel power gain G_{SD} .

Besides the TCP schemes, in the Internet of Things (IoT), constrained devices proliferate under strict power/bandwidth limits, motivating researchers to develop IoT-specific protocols with transport layer adaptations, such as the Constrained Application Protocol (CoAP) [188], Delay-Tolerant Networking (DTN) [189], and ROBust Header Compression [190]. The lightweight design of CoAP and its support for unreliable transport (established on UDP) align with the low-power requirements of TTE MIC devices. The bundle protocol of DTN can mitigate challenges posed by intermittent connectivity arising from low bandwidth and data rate. These protocols and mechanisms, validated through established RFC standards, offer potential directions for adapting transport-layer or cross-layer functionalities in TTE MIC networks.

E. Cross-layer Optimization (CLO)

The OSI framework promotes modularity and standardization with high cohesion and low coupling. However, it faces efficiency challenges in MI networks due to strict bandwidth, energy, and latency constraints. In this scenario, the lower layer may call upper-layer parameters or algorithms to improve the network performance. Notably, for UG-WSNs, the solution for optimizing energy consumption in Ly1 may require the routing decision results in Ly3.

Lin *et al.* [52] developed a distributed environment-aware protocol (DEAP) based on the Nash game to satisfy the statistical quality of service (QoS) requirement. This protocol achieved both optimal energy savings and throughput gain concurrently in 2015. The DEAP considers the interactions of different layer functionalities, such as power control, modulation and FEC in Ly1, the distributed MAC schemes in Ly2 and geographical routing algorithm in Ly3.

In 2021, Singh *et al.* [58] developed a Distributed Energy-Throughput Efficient Cross-layer solution using the Naked Module Rat algorithm (NMRA), also called the DECN approach. While this approach is similar to DEAP one, the DECN approach can apply to direct and waveguide MI links. Their simulations showed that when using the DECN approach with 50 nodes, the energy consumption decreased from 160~390 J/packet to 100 J/packet, whereas the normalized throughput increased from 2~6 packets to 11 packets/s. Compared to wave-based communication (e.g., EMWCs), the DEAP and DECN approaches fully consider the fact that the received power diminishes linearly to the distance d_{SD}^6 in an MIC channel, which diminishes much faster than in the EMW channel (in the order of d_{SD}^2).

Compared to EMWC, it can be concluded that all MI CLO solutions use distributed algorithms. This is due to the fact that the capacity and bandwidth of an MI channel are much lower than those of an EMW channel. This lack of information exchange can cause slow convergence of algorithms.

F. Summary and Lessons Learned

Table XVIII summarizes the issues addressed, their corresponding methods, and the remaining issues of research on the multi-node MI network under the OSI-originated framework, including the physical, data link, network, transport, and application layers. It can be summarized that the issues of the MI network primarily stem from the coil resonance feature, i.e., low MI bandwidth and significant frequency-selectivity.

Apart from MI fast fading, many remaining issues need to be addressed: 1) The physical layer support for RPMA-based MICs is inadequate, even lacking a universal expression for channel capacity, with key challenges stemming from mechanical inertia and friction. Despite the packets having the same length, the RPMA MI channel may lead to variable data rates; 2) the high collision probability of existing MI MAC solutions [54], [55], [168] has not been addressed due to the coil resonance feature; 3) most solutions in Ly3, especially the routing solutions [57], [85], [86], have overlooked the gain factors \mathcal{E}_{SD} and J_{SD} . These solutions in Ly3 have limited support for MI UG-WSNs and UW-WSNs with longer ranges; 4) the channel-independent OSI-based solutions, particularly TCP and IP, need to be validated due to issues, such as excessively large frame headers and RTT suppression. These are crucial for the SAGUMI; and 5) all solutions using RL [11], [85], [86], especially those using distributed RL with the Nash game, may face low convergence and precision.

Regarding these five challenges 1) – 5), our proposed framework, the status quo, potential solutions, and research gaps are elaborated on in the subsequent sections. Table XXI summarizes the reviewed techniques mapped to each OSI layer and their respective technical readiness levels (TRLs), revealing that most existing MI techniques lack experimental evidence, particularly for multi-node solutions.

The practical takeaways or common pitfalls include: 1) Most multi-node MI protocol studies have assumed near-field and weak coupling conditions, which are more prone to breakdown in TTE environments than in general MIC environments; 2) existing MI upper-layer protocols tend to overlook the eddy gain and polarization gain; 3) TCP/IP stack application to TTE

TABLE XXI
TECHNICAL READINESS OF MI TECHNIQUES MAPPED TO OSI LAYERS

OSI Lys	Technology	TRL [†]	Future research directions	Priority
Ly1	MI fast fading	★	A universal statistical modeling	★★★
	Channel modeling	★★★★	Mixed-field & multilayer medium cases	★★
	Antenna design	★★★★	TMR Rx antenna; deployment	★★
	Channel estimation	★	For VLF-LA and MI fast fading cases	★★
	Modulation	★★★★ [‡]	For RPMA-based links	★
	Channel coding	★★	Deep JSCC	★★
	Passive relays	★★★	Positive MI crosstalk	★★
	Active relays / CMIC	★	Arbitrarily deployed multi-relays	★★
Ly2	Resource allocation	★	Bandwidth and frequency allocations; balancing precision and convergence	★★★
	MI MAC	★★	Header compression; conflict reduction	★★★
	LLC	☆ (0)	Optimization for VLF-LA case	★
Ly3	Connectivity	★	Heterogeneous or mobile MI networks	★★
	Data collection and node deployment	★	Algorithm convergence	★
	Routing	★	Minimizing information exchange among nodes	★★
Ly4	IP	☆ (0)	IP-HC	★★★
	TCP	☆ (0)	Fairness, congestion control, connection issues due to extremely low bandwidth	★★★

[†] ★: Technology Readiness Level (TRL) (cf. [191]) 1–3 (basic research); ★★: TRL 4–5 (lab validation); ★★★: TRL 6–7 (system-level testing); ★★★★: TRL 8–9 (industrial application); ☆: No MI-specific references available for this TRL level.

[‡] The TTE MIC products have entered the market [119], and modulation is an essential integrated technical module.

MICs may suffer from the congestion mechanism failures and retransmission storms; 4) existing MI upper-layer protocols overlook that the MI channel bandwidth may be insufficient to support the exchange of their large control data, such as routing and Q tables; and 5) the frequent variation in average AVIs may render many existing MI solutions from Ly1 to Ly7 for both P2P and multi-node networks inapplicable.

VII. PROMISING MI NETWORK FRAMEWORK WITH TCP/IP AND LINUX SUPPORT

This section proposes a Linux-and-TCP/IP-supported MI network framework to implement most existing MIC protocols and algorithms, including those in Sections IV, V, and VI.

A. Significance and Architecture Overview

1) *Significance*: While MIC techniques have been applied in various underground applications, few studies explore their compatibility with standard protocols, particularly the TCP/IP framework, due to the limited bandwidth of MIC systems. With ongoing advancements in MIC performance and the expansion of SAGUMI applications, integrating MIC with the TCP/IP framework is becoming an inevitable and essential trend. While deep learning has proven effective in addressing EMWC challenges [192], [193], its application to MIC remains largely unexplored due to the difficulties of using robust neural network platforms in embedded systems.

On the other hand, Linux excels in large-scale wireless applications, such as mobile ad-hoc networks (MANETs) and Android (built on the Linux kernel) smartphones, enabling dynamic routing and offering scalability via its modular kernel and TCP/IP stack. Moreover, Linux offers a wealth of open-source resources across diverse research domains, particularly in wireless network protocol stacks (e.g., IEEE 802.15) and neural network platforms (e.g., TensorFlow, PyTorch, and RKNN). These resources facilitate rapid development by providing robust tools and platforms for research.

As illustrated in Fig. 26, we propose a Linux-based MIC framework. This framework tackles multi-hop MIC challenges by integrating TCP/IP, Linux kernel modules, and the MI solutions discussed in the preceding section, balancing protocol compatibility with UG-WSN requirements.

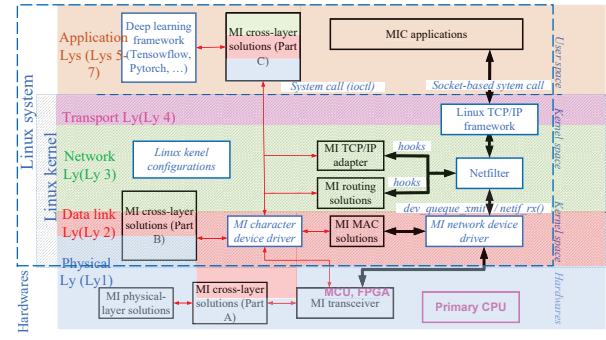


Fig. 26. Proposed framework for TCP/IP & Linux support. The thick arrow line represents effective Tx/Rx data, and the thin red arrow line represents control data for the MI network protocol stack. The box with a white background and italic text represents the interface between Linux system and MI protocol. The box with a white background represents the Linux model.

2) *Linux wireless network device driver-inspired architecture*: Building on the support schemes for TCP/IP and Linux in EMWCs, such as the Linux driver designs [194] for WiFi and Bluetooth, we come up with a Linux-based MIC framework. This framework, as illustrated in Fig. 26, draws parallels with EMWC solutions. It incorporates MI cross-layer solutions (Part A) and MI transceivers, which are hardware and firmware-based models designed for protocols and algorithms that rely on analog signals, high parallel computation, or high-accuracy real-time processing, such as channel modeling and estimation. The MI character device (MCD) driver and MI network device (MND) driver are designed to handle the retrieval and storage of MIC data. The MCD driver forwards control data, such as CSI, while the MND driver handles effective data streams, enabling MIC applications to directly access the full TCP/IP protocol through the `socket()` interface.

3) *MI-specific models*: In this framework, several models differ from conventional Linux wireless drivers:

- *MI TCP/IP adapter*: This model adapts the native Linux TCP/IP framework with MI-specific TCP/IP optimization schemes proposed by researchers, such as TCP/IP header compression and RTT optimization for the MIC.
- *MI routing solutions model*: This model can implement and help evaluate specific MI routing algorithms proposed by researchers. These algorithms can be invoked similar

to the MI TCP/IP adapter.

- *Cross-layer solutions model (Part C)*: This model supports deep learning-based solutions, such as deep JS SCC. However, as it resides in the user space of the operating system, it may not be suitable for algorithms with stringent real-time requirements.
- *Cross-layer solutions model (Part B)*: To reduce device size and energy consumption, Some MI modulation and channel coding can be incorporated into the MI cross-layer solutions (Part B) model rather than in FPGA or MI cross-layer solutions (Part A) model. The TTE MIC system uses the VLF-LA technique, which allows the primary CPU sufficient time to process, enabling the removal of FPGA and MI cross-layer (Part A) models in some simpler MI nodes.

B. System Architecture and Implementation

Fig. 26 describes the system implementation of the Linux-based MIC framework, focusing on the interface between Linux TCP/IP stack and MI solutions models.

1) *Linux MCD and MND drivers*: The MCD and MND drivers models mirror EMWC driver architectures, facilitating hardware-Linux data exchange and laying a foundation for MI-specific models. The MCD driver operates as follows.

- Register a character device associated with several Linux file operations, whose members include `open`, `close`, `read`, `write`, and `ioctl` callbacks, to the kernel;
- Invoke MI-specific models (MI cross-layer solutions Parts A and B) via hardware interrupts and Linux/user APIs;
- The `write` and `ioctl` callbacks can manage downlink control streams (from application layer to physical layer);
- The `read` and `ioctl` callbacks can manage uplink control streams (from physical layer to application layer).

The MND driver operates as follows.

- Register a Linux MND with integrating its netfilter hooks with the MI TCP/IP adapter and MI routing models. Linux can invoke models via these hooks automatically;
- Invoke MI MAC solutions via the callbacks of the MND;
- Manage routing and downlink data streams (from application layer to physical layer) via the MND callbacks (e.g., `ndo_start_xmit`);
- Manage routing and uplink data streams (from physical layer to application layer) via the MND callbacks (e.g., `netif_rx`).

2) *MI physical-layer solutions and MI cross-layer solutions (Part A)*: In line with the most EMWC solutions that employ hardware-centric implementation in PHY/MAC in dedicated chips, the models of MI physical-layer solutions and MI cross-layer solutions (Part A) reside in MCUs or FPGAs (not Linux). Given that a few MI solutions exhibit strong dependency on analog signal processing and impose stringent timing constraints, these requirements exceed the performance capabilities of the Linux kernel. For this reason, these models handle modulation/coding and cross-layer logic (e.g., interference mitigation) using FPGA/MCU cores. These models interface with Linux system via custom bus protocols, e.g., serial peripheral interface (SPI), or memory-mapped I/O.

Algorithm 1: Example of a TCP/IP transmit process.

```

/* Conventions: The italic text represents a Linux API, and
   Model_name.Function_name(Input_data) represents a
   function of a model with parameter Input_data */
/*
 * Boot/initialization stages of Linux
 */
1 Register MCD and MND;
/* IP-HC in TCP/IP adapter called after routing */
2 Register a netfilter hook named MI_adapter with
   hooknum=NF_IP_POST_ROUTING, hook=MI_IPHC,
   priority≥100;
3 Register a netfilter hook named MI_routing with
   hooknum=NF_IP_LOCAL_OUT,
   hook=frequency_switchable_routing (cf. [57]), priority≤400;
/* Runtime stage of Linux */
4 for Loop do
5   Call MI_Channel_Estimation in Algorithm 2 which generates
      MI_CSI;
6   User calls sendto(Destination_IP, Destination_port, MI_packet)
      which generates MI_IP_packet;
7   Linux TCP/IP calls the hook
      MI_routing.frequency_switchable_routing(MI_IP_packet) to
      complete routing based on [57], see Fig. 25;
8   Linux TCP/IP calls the hook
      MI_adapter.MI_IPHC(MI_IP_packet) and generates
      MI_IPHC_packet;
9   Obtain MI_IPHC_packet via callback MND.ndo_start_xmit();
10  MND.ndo_start_xmit() calls MI_MAC.Mac_based_on_
      [54](MI_IPHC_packet, MI_CSI) to complete MAC and
      generates MI_MAC_packet;
11  MND.ndo_start_xmit() calls
      MI_cross_layer_Part_B.BPSK_Polar_based_on_
      [46](MI_MAC_packet, MI_CSI) and generates
      MI_BPSK_packet and control bytes;
12  This BPSK and Polar encoder function downloads the
      MI_BPSK_packet and control bytes to the MI transceiver's
      corresponding buffer and hardware registers, respectively;
13 end
14 Unregister all devices and netfilter hooks

```

Algorithm 2: MI_Channel_Estimation() based on deep learning framework.

```

1 MCD calls MI_crosslayer_Part_B.MI_estimation_based_on_ [144]
   (MI_CSI);
2 MCD calls MI_crosslayer_Part_B.MI_fast_fading() to require
   MI_crosslayer_Part_C.MI_fast_fading() via Linux callback read();
3 MI_crosslayer_Part_C.MI_fast_fading() completes the MI fast fading
   estimation based on Fig. 27 and Pytorch framework;
4 MI_crosslayer_Part_C.MI_fast_fading() responds the updated
   MI_CSI to the MI_crosslayer_Part_B via Linux callback write();
5 return updated MI_CSI

```

3) *MI cross-Layer solutions (Part B)*: For the VLF within the Linux kernel's capabilities, this model can directly implement most physical and MAC layer solutions.

- Perform MI channel estimations without deep learning (e.g., [144]) in the Linux Interrupt Service Routine registered by the MCD driver upon receiving the control stream from the MI transceiver;
- Perform modulations (e.g., BPSK) and FECs (e.g., Polar codec [46]) upon MAC frame/packet arrival at the MND driver, as shown in Algorithm 1 (Lines 11 and 12);
- Forward the control stream to MI cross-Layer solutions (Part C) via `read`, `write` and `ioctl`.

4) *MI cross-layer solutions (Part C)*: This model facilitates access to the interfaces of deep learning platforms (e.g., PyTorch), as these interfaces and platforms can only run in user space. Following are the details (cf. Algorithm 2):

- MI cross-layer solutions (Part B) forward required data

to Part C via `read` callback;

- Part C executes algorithms using the interfaces of the deep learning platform in the user space;
- Part C responds the results to Part B via `write` callback.

5) MI TCP/IP adapter and MI routing solutions:

The MI TCP/IP adapter and routing solutions integrate with the Linux TCP/IP framework primarily through netfilter hook points [195], which correspond to distinct stages in the local machine's internal routing process, i.e., `NF_XX_PRE_ROUTING` (prior to routing decisions), `NF_XX_LOCAL_IN` (before packets destined for the local system enter the protocol stack), `NF_XX_FORWARD` (for packets being forwarded), `NF_XX_LOCAL_OUT` (before packets originated from the local system exit the protocol stack), and `NF_XX_POST_ROUTING` (after the routing decision has been made but before the packets are transmitted on the network interface). Here, `xx` denotes the protocol type (e.g., IPv4, IPv6, or bridge protocol).

Upon Linux startup, the NMD driver registers netfilters for MI TCP/IP adapter and routing solutions. The MI routing netfilter should be set to the highest priority to prevent other routing schemes. MI-specific routing functions attach to hook points `NF_XX_LOCAL_OUT` and `NF_XX_PRE_ROUTING`, as shown in Algorithm 1 (Line 2). MI TCP/IP adapter (especially IP-HC) is set to low priority to avoid kernel packet modification. Then, the functions of the MI TCP/IP adapter are associated to `NF_XX_POST_ROUTING`, as shown in Algorithm 1 (Line 3). These netfilters are automatically invoked by the Linux TCP/IP framework.

6) MI MAC solutions: This model packages the MAC header (see Fig. 24(a)) and maintains the state machine as the one in [54]. MI MAC functions for uplink streams are triggered by MI transceiver interrupts; those for downlink streams are invoked via the `ndo_start_xmit` callback of the MND (see Algorithm 1, Line 11).

7) Example: Consider an MI protocol stack integrated into the Linux TCP/IP framework. This stack includes physical-layer solutions, such as channel estimation, MI fast fading prediction (see Fig. 27), BPSK modulation, and Polar coding (as in [46]). It also incorporates the MAC solution from [54] and the routing solution from [57]. The TCP/IP transmit process is described in Algorithm 1. When an application sends a packet via the Linux Socket API `sendto`, the packet passes through the Linux TCP/IP framework, including netfilters associated with MI routing and IPHC schemes, and arrives at the MND. The MND invokes the MI MAC algorithm, BPSK modulation, and Polar encoding to generate a physical-layer frame, which is then downloaded to the MI transceiver.

C. Summary

The proposed framework enables researchers to leverage the abundant Linux resources available for communication networks and deep learning, such as OpenZigbee [196], TensorFlow, and RKNN [197]. As a result, it can accelerate MIC research and development.

The proposed framework manages control flow across OSI layers using Linux interrupt service routines and MCD callbacks `read/write`. It handles data flow and protocol encapsulation across OSI layers via interrupt service routines, MND

callbacks `ndo_start_xmit/netif_rx`, and socket APIs. MI-specific network layer protocols are managed through Linux netfilter hooks.

The following sections provide further insights into related MI techniques, which can also be supported by this framework.

VIII. RESEARCH CHALLENGES AND FUTURE DIRECTIONS

Sections III–VI have provided a comprehensive overview, encompassing a wide range of MIC topics of state-of-the-art methodologies and theoretical frameworks, including the MI channel modeling, P2P MIC, MI relay, and MI network architecture. Many algorithms and solutions discussed within this comprehensive review can be implemented and/or evaluated through the MI framework proposed in Section VII; see Table XXIII. For instance, the channel modeling and estimation solutions in [11], [12], [144] require processing analog signals and can be implemented in the MI transceiver model.

In this section, we summarize the potential challenging issues that were not addressed in the literature. We also introduce new promising techniques (e.g., deep JSCC, MCNSI, etc.) for future research. Table XXII outlines the remaining issues, their potential solutions, and novel techniques for MIC.

A. MI Fast Fading in Mobile MIC Systems

Until 2020, no concept of an MI fast fading channel was formally introduced. The research on MI fast fading is still in its early stages (see Table X). In this subsection, we discuss the challenges and remaining tasks for channel statistical characteristics, and elucidate the potential ramifications on established MIC (from Ly1 to Ly3), including outage probability, channel estimation, MI MIMO, and CMIC. Table XXIV summarizes the typical issues arising from the introduction of MI fast fading into MI channels.

1) Statistical modeling when the CLT does not apply:

Previous literature has derived closed-form expressions of the CDF/PDF and expectation of the MI fast fading. These expressions are only applicable in typical scenarios, such as underwater [51], [89], 2D TTE [9] and 3D TTE using MI cellular network [11]. Firstly, unlike EMWCs, MI fast fading is not caused by signal propagation. As illustrated in Fig. 6, we modeled MI fast fading using four independent random variables $(\phi_S, \theta'_S, \phi_D, \theta'_D)$ with distinct distributions. These four random variables are not suitable for applying CLT since CLT requires a large number of independent random variables. Thus, deriving a universally used CDF/PDF, such as the Rayleigh model, becomes challenging. We utilize Monte Carlo simulations to obtain universal models for MIC links (e.g., Fig. 7). However, these models have high time complexity for network algorithms and protocols. Secondly, antenna design, antenna carrier, and its mechanical degrees of freedom affect the MI fast fading. For example, the antennas composed of orthogonal MIMO coils, RPMA, M²I, and magnetoresistance exhibit different CDFs of MI fast fading. The vibration model of the backpack antenna may not follow the boundary $p(x)$ distribution. The mechanical degrees of freedom of the vehicle influence the distributions of horizontal components of antenna vibration ϕ_S and ϕ_D . These interdisciplinary issues also pose the challenge to derivation of a universal statistical model.

TABLE XXII
FUTURE ISSUES, PROMISING WORK AND ADVISED METHODOLOGIES FOR TTE MICs

Types	Research aspects	OSI layer	Future issues & works	Advised methodologies
P2P MICs	MI fast fading	Ly1	1) A universal statistical model 2) A velocity-dependent expectation/variance 3) See Table XXIV	1) Maxwell-equations-based derivation and FEMs 2) Probability-theorem-based derivation 3) Deep JSCC 4) Transformers model or LLM to predict average AVI
	Antenna design	Ly1	1) Inertia issue of a mechanical antenna 2) Using high-sensitivity and small-size magnetic sensor	-
	MCNSI	Ly1-Ly3, Ly7	1) Balancing between MI, navigation and sensing 2) Chaotic RSSIs	1) GAN techniques and DWE algorithm 2) Formulating a joint optimization problem
	Mixed-field channel model	Ly1	1) Difficulties in sub-modeling of channel power gain G_{SD}	1) Maxwell-equations-based derivation
	Inhomogeneous medium	Ly1	1) Boundary conditions for multi-layer materials 2) Boundary conditions between the near-field region and radiation field region 3) Statistical characteristic of dynamic medium	1) Maxwell-equations-based derivation 2) Geometrical approximation by jointing regular shapes 3) Data fusion and attention mechanism
	JSCC	Ly1, Ly7	1) Image, audio & video data transmissions 2) Content-based communication 3) High-dimensional data communication	1) Deep JSCC 2) Multimodal semantic communication 3) Offline distilled LLM
MI Relay	CMIC	Ly1	1) Spatial distribution of Cross-talk effects 2) Multiple active relays with misaligned antenna	1) KVL equations
MI network	Heterogeneous MI Network	Ly1-Ly7	1) Channel licensing and spectrum sensing 2) Connectivity issues 3) Power and throughput optimization	1) Percolation theory 2) Multiagent RL
	MI MAC	Ly2	1) The SISO Antenna case 2) Balancing the frame error ratio and EPR 3) Power and throughput optimization 4) Communication security issues	1) Machine learning for CSMA-CA issue 2) Using antenna orientation information for frame error ratio & EPR issue 3) Bit-level compression for the MAC header
	MI routing	Ly3	1) Effects of \mathcal{E}_{SD} and J_{SD}	-
	MI TCP/IP	Ly1-Ly4	1) Large TCP/IP packet header unsuitable for ultra-narrow-band MI channel 2) Significant RTT suppression for TCP connections 3) Excessive duration for connection establishment	1) Header compression techniques 2) RTT optimization based on MI channel conditions 3) Optimizing data chunking and aggregation 4) Intelligent retransmission strategy 5) Machine learning solution under MI fast fading
Implementations	MI network framework	Ly1-Ly7	1) Experiments and testing for TTE MIC systems 2) TCP/IP support	Fig. 26

TABLE XXIII
OUR PROPOSED PROTOTYPE FOR MI NETWORK IMPLEMENTATION TO SUPPORT EXISTING AND FUTURE STUDIES

Models in Fig. 26	Recommended solutions [†]	Typical refs.
MI transceiver	Channel modelings and estimations	[10]-[12], [36], [37], [144]
MI cross-layer solutions (Part A)	Modulations; Polar coding; JSCC; high real-time CSMA-CA	[45], [46]
MI MAC solutions	Contention based MI MAC protocols	[54], [55], [168]
MI cross-layer solutions (Part B)	Modulations, FEC; Polar coding; data collection	[11], [45], [46], [52], [80]
MI routing solutions	MI connectivity and routing solutions	[8], [57], [85], [86], [120]
MI TCP/IP adapter	IP-HC, RTT optimization, intelligence retransmission, etc.	Future research
MI cross-layer solutions (Part C)	Deep JSCC; algorithms with deep RL	Future research
MI character device driver	Reading/writing protocol control data from/to the MI transceiver	[194]
MI network driver	Reading/writing effective data from/to the MI transceiver	[194]

[†] In this table, we prioritize the solutions of the MIC under the VLF-LA case

TABLE XXIV
POTENTIAL FURTHER ISSUES IF MI FAST FADING CHANNELS ARE INTRODUCED

OSI layers	Research aspects	Involved refs.	Typical issues with introduction of MI fast fading
Physical layer	Channel modeling	[89], [9], [11]	For more universal scenarios
	Achievable rate	[7], [10], [51], [130]	Random outage probability in most cases
	Channel estimation	[144]	Unpredictable CSI; Spectrum obtaining
	Channel coding	[46]	Unpredictable average AVI
	Power control	[11]	Frequent disruptions of Nash equilibrium due to unstable average AVIs
Data link layer	MIMO & CMI	[7], [10], [36], [51]	Spatial diversity; Outage probability reducing
	MAC	[54], [55]	CSMA-related time / time-slot
Network layer	Connectivity	[8], [169]	Irregular shape of MI coverage space
	Routing	[46]	Variable latency and energy consumption
Cross-layer	Cross-layer protocols	[52], [58]	Unpredictable average AVI; QoS requirement
	Networking	-	Variable network topology

It is noticed that the practical relevance of existing MI fast fading models remains untested. Monte Carlo simulations have validated three such models, each with AVIs distributed as uniform, BCS, and boundary $p(x)$. Despite the validation, the practical applicability of these models is yet to be confirmed. Future research can give priority to experimental validation using measured disturbance profiles across diverse environments to enhance their practical applicability.

2) *Outage probability with velocity-dependent AVIs*: MI fast fading influences the achievable rate through the expectation $\mathbb{E}(J_{SD})$ and outage probability. For mobile MIC, the expectation $\mathbb{E}(J_{SD})$ is determined by the average AVIs σ_S and σ_D . These AVIs are velocity-dependent, making the AVIs statistically unpredictable due to their dependence on the driver's mindset. Additionally, unlike the traditional MIC, the outage probability regains its physical meaning due to fast

fading. Both the unpredictability of $\mathbb{E}(J_{SD})$ and the outage probability of a mobile MIC link have a significant impact on the existing solutions for MIC networks. Unlike the EMWC, such an outage probability is still random in most cases. However, as the vehicle velocity exhibits a human activity, the attention-based deep learning (e.g., Transformer and BERT models) and large language models (LLMs) can be considered to address the challenges caused by unpredictable $\mathbb{E}(J_{SD})$.

3) *Lack of frequency spectrum for channel estimation*: For the study of MIC channel estimations [144], an MIC channel is assumed to be quasi-static. For mobile MIC with a fast fading channel and a given time t , the mutual inductance $M_{SD} = M_{SD}(\phi_S(t), \theta'_S(t), \phi_D(t), \theta'_D(t)) = M_{SD}(t)$ changes faster during the coherence time T_c . An mobile MIC channel exhibits time-selective fading. Let $T_c = \mathcal{N}_t T_t$, where \mathcal{N}_t is the number of symbols between two pilot signals and T_t is the duration of a symbol. The receive signal is \tilde{y} with the CDF $F_{J(\phi_S(t), \theta'_S(t), \phi_D(t), \theta'_D(t))}(y)$. For time-selective fading, one of the widely used methods is interpolation between symbols 1 and \mathcal{N}_t . Hence, the frequency spectrum of $J(\phi_S(t), \theta'_S(t), \phi_D(t), \theta'_D(t))$ is crucial. As the CDF of J_{SD} helps obtain this frequency spectrum, it is an open issue for MIC channel estimation. Additionally, the statistically unpredictable expectation $\mathbb{E}(G_{SD})$ makes it hard to obtain accurate CSI, which is also an issue for channel estimation.

4) *Unpredictable bandwidth for Spatial diversity for MIMO and CMICs*: For traditional MIC links with quasi-static channels, MIMO and CMI techniques enhance signal strength at the Rx node. The received SNR determines the feasibility of MIMO and CMI in these scenarios. For MIC with fast fading MI, outage probability must also be considered. For example, in Fig.22, CMIC is feasible in RA with $\Upsilon_{AF} > \Upsilon_{SD}$, where Υ_{AF} and Υ_{SD} are the received SNRs of CMI and DMI links at D, respectively. For mobile MIC, not all points in RA are suitable for a CMI relay due to the presence of outage probability conditions. Similarly, some points outside RA may be suitable for a CMI relay.

In addition, the achievable rate of an AF-relay CMI system can be expressed as [10]

$$\mathfrak{C}_{AF} = \frac{1}{2} \int_{f_0 - \frac{1}{2} B_{AF}(\mathbf{v})}^{f_0 + \frac{1}{2} B_{AF}(\mathbf{v})} \log_2(1 + \Upsilon_{AF}(f)) df, \quad (24)$$

where the bandwidth B_{AF} is a function of the APO \mathbf{v} and, in turn, a function of MI fast fading gains J_{SD} , J_{SR} and J_{RD} . This poses a challenge to the ergodic rate calculation of mobile CMI links.

5) *Non-uniform and irregular MI coverage*: For a stationary MI SISO link, the polarization gain satisfies $J_{SD} = 1 + 3 \cos^2 \theta_{SD}$, where θ_{SD} is the angle between the norm vector of the coil and line SD, implying that MI coverage space has petal shape. However, it is observed in Fig. 7 that the shape of MI coverage space may become irregular in the presence of MI fast fading. This is a challenging issue for MI connectivity modeling. On the other hand, the MI fast fading may increase the channel power gain, as shown in Fig. 7, presenting an exciting opportunity for network optimization.

6) *Proposed framework for average AVI prediction*: The average AVI relies significantly on a vehicle's velocity, which depends on driver intent and is hard to predict using conventional methods (e.g., Kalman Filter). Attention-based deep

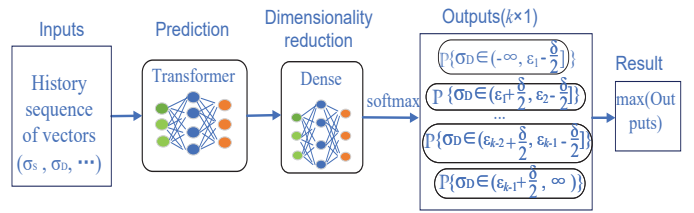


Fig. 27. Proposed framework of Rx average AVI σ_D prediction. This framework is a k -class classification supervised deep learning framework where predicted AVI σ_D (output) is discretized into k levels, and δ is the boundary margin. Inputs include average AVIs of Tx and Rx (σ_S, σ_D), road/traffic conditions, and vehicle velocity, and are assumed to be pre-denoised.

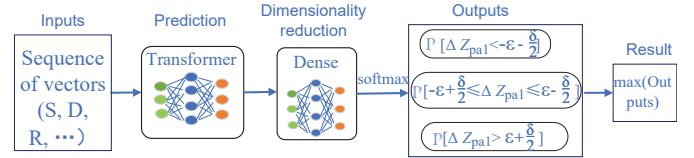


Fig. 28. Proposed framework of MI crosstalk impedances prediction. Here, the classifications $\mathbb{P}[\Delta Z_{pa1} < -\varepsilon - \frac{\delta}{2}]$, $\mathbb{P}[-\varepsilon + \frac{\delta}{2} \leq \Delta Z_{pa1} \leq -\varepsilon + \frac{\delta}{2}]$ and $\mathbb{P}[\Delta Z_{pa1} > \varepsilon + \frac{\delta}{2}]$ represent a decrease, no change, and an increase in impedance Z_{pa1} , respectively, where ε is a boundary threshold and δ is the boundary margin. Inputs are assumed to be pre-denoised.

learning can be an alternative to obtaining average AVIs. We propose a Transformer-based supervised deep learning framework to obtain a discretized/classified average AVI, as shown in Fig. 27. In this framework, historical sequence vectors act as inputs, pass through a Transformer for prediction, and then go through dimensionality reduction via a Dense layer. Final outputs are normalized by the softmax function. The result is obtained by taking the index of the maximum in the outputs tensor. The boundaries $\varepsilon_1, \varepsilon_2, \dots, \varepsilon_{k-1}$ are determined by analyzing historical average AVI distributions (including mean, variance, and extreme values), and aligning with practical operational requirement, based on the pre-designed k classes.

Assume a standard Transformer configuration with the number of attention heads $h=8$, multi-head attention blocks $b=12$, and hidden dimension $d=64$. The sequence lengths are constrained to $n=128$ due to on-device memory limits. The computational complexities of the Transformer block and subsequent Dense layer are $\mathcal{O}(bn^2d + 8nd^2)$ and $\mathcal{O}(dk)$, respectively, with a total of 16,818,176 FLOPs when $k=5$. This workload is executable on a low-speed MCU (100 MHz ARM Cortex-M4) with an inference latency of up to 75 ms.

The remaining issues are listed in Table XXIV.

B. Antenna Design

Due to lower circuit gain \mathcal{C}_{SD} , coil-based antennas are larger, especially in VLF-LA systems for TTE applications. In deep underground environments, the large size makes it difficult to use MIMO techniques. Several non-coil antenna types can be considered for future long-distance MICs:

1) *Mechanical antenna*: A mechanical antenna has a smaller size for mid-range and mobile MICs [198]–[200]. Such an antenna presents challenges stemming from inertia.

- Additional latency: The MIC protocols (e.g., modulations) need additional preset time slots between different symbols to overcome antenna inertia.
- Additional energy consumption: Changing the mechanical state requires additional energy to overcome inertia. Specifically, transmitting ‘010101’ (5 state switches) requires more energy than ‘111000’ (1 state switch).
- Variable data rate under the same packet length: For packets of the same length, transmitting ‘010101’ takes 5 GTSs, while ‘111000’ takes only 1 GTS, meaning ‘010101’ transmits slower than ‘111000’.

2) *Magnetic sensor*: Mechanical antennas are often used in the Tx nodes, while magnetic sensors can be utilized at the Rx nodes. There are high-sensitivity magnetic sensors, such as TMR and quantum magnetic sensors. These sensors have potential applications in underground MICs. Due to the limitations of current magnetic sensor techniques, the receiver sensitivity of a magnetic sensor is much lower than that of a coil. Few studies investigate magnetic sensor-based MICs for underground applications. Nevertheless, magnetic sensors have two advantages.

- Small antenna size: The size of a magnetic sensor is much smaller than that of a coil. For example, a TMR sensor with a small outline package 8 (SOP8) has dimensions of 6 mm \times 5 mm \times 1.5 mm. These dimensions are several orders of magnitude smaller than coils.
- Low crosstalk effect: The crosstalk effect among the magnetic sensors can be greatly reduced. Techniques such as massive MIMO and intelligent reflective surfaces can be introduced into MICs.

Given these advantages and the advancement of magnetic sensor techniques, magnetic sensors emerge as a highly promising option for MIC antenna design.

3) *MI beamforming and massive MI MIMO*: The massive MIMO technology plays a pivotal role in the fifth-generation (5G) mobile communication systems and beyond. The MI MIMO and beamforming techniques are also widely employed for wireless power transfer [201]–[205] and short-range MIC [94], [206]. However, these techniques exhibit extremely low performance for mid-range and long-range MICs due to the MI crosstalk effects among coils. There is no literature on massive MI MIMO. With the advancements of RPMA techniques and magnetic sensor technology, MI beamforming and massive MIMO techniques hold promise, as RPMA and magnetic sensors generate minimal MI crosstalk effects among coils. For a coil-based MI system, avoiding crosstalk is crucial for the application of massive MIMO. Our simulation in Fig. 19 may assist in addressing this challenge.

C. MI Crosstalk Effect Prediction Strategies

It is observed in (23) that the crosstalk impedances $Z_{pa1}(S, D, R, \dots)$ and $Z_{pa2}(S, D, R, \dots)$ are crucial for the crosstalk effect mitigation. Unfortunately, the expressions of crosstalk impedances are complex multimodal functions, posing a challenge for predicting $Z_{pa1}(S, D, R, \dots)$ and $Z_{pa2}(S, D, R, \dots)$ using conventional methods. We propose a Transformer-based framework (see Fig. 28) for crosstalk impedance predictions for crosstalk effect mitigation. This framework is similar to that of average AVI prediction (see

Fig. 27) with $k=3$. Its computational complexity is 16,801,792 FLOPs with the number of attention heads $h=8$, multi-head attention blocks $b=12$, and hidden dimension $d=64$. The sequence length is $n=128$. The latency remains under 75 ms on the 100 MHz Cortex-M4.

D. MI Communication-Navigation-Sensing Integrated System

The MCNSI system aims to achieve high intelligence, supporting high-quality localization and sensing services while achieving high-quality communication. As summarized in Table XXV, MIC studies have been focused on the stability of signals among different positions in traditional research. By contrast, the MI localization/navigation focuses on signal differences among different positions, while MI sensing emphasizes sensitivity to the direction and strength of magnetic fields, both of which are highly susceptible to interference and noise.

Recently, there have been some studies on joint localization and communication in 5G/6G technologies using intelligent reflecting surfaces [209], [210]. These signal-reflection-based techniques may not be suitable for MICs. There are key issues listed below according to these challenges and Table XXV.

- Small MI signal difference: Since the space gain S_{SD} in MI channel decays with the 6th power of distance (see (4)), the difference in MI signal strength between two points is much smaller than that of an EMW signal in a long-distance communication environment.
- Chaotic received signal strength indicator (RSSI): For mobile MICs, velocity-dependent MI fast fading channels cause the MI RSSI around the MI base station to be chaotic.
- Balance between communication and navigation: In the MCNSI system, since small differences in MI signals are beneficial for MICs but detrimental to MI localization and navigation, the localization accuracy and achievable communication rate often cannot reach their optima. We need to balance these two performance metrics.
- Interference and noise: As both MIC and MI navigation subsystems are expected to generate sufficiently strong signals, these signals can interfere with MI sensing. The carrier frequency of TTE MIC using VLF-LA is closer to that of MI sensing, making interference suppression techniques (e.g., frequency band isolation) more challenging for the MI sensing subsystems.

For the first issue, we can use dynamic weighted evolution/learning (DWE) from [115]. Furthermore, we consider generative adversarial networks (GANs) to obtain a super-resolution model of MI signal fingerprints. For the second issue, RL techniques can be used for stochastically changing communication environments. For the third issue, the key method is to obtain closed-form expressions for the ratio of time slot allocation between communication and navigation, and formulate a joint optimization problem of communication and navigation. For the fourth issue, the joint time-space-frequency isolation method can be adopted for appropriate electromagnetic compatibility design.

TABLE XXV
COMPARISON OF MIC, MI LOCALIZATION/NAVIGATION AND MI SENSING

Aspects	MIC	MI localization / navigation (cf. [24], [207])	MI sensing (cf. [208])
Key	Alternating magnetic fields	Magnetic fields differences	Sensitivity to magnetic fields' direction & strength
Techniques.	Modulation, channel coding, MAC, routing	Magnetic fingerprint, ToA, inertial navigation	Interference & noise suppression
Signals	Active sources	Active sources	Passive sources
Components	Coil, RPMA, M ² I	Coil, RPMA, Inertial measurement unit	TMR, Giant Magnetoresistance, Hall sensor, Coil
Applications	UG-WSN, UW-WSN, UG robot communication	AUV, Indoor position, UG Robot navigation	Oxygen content detect, current measurement

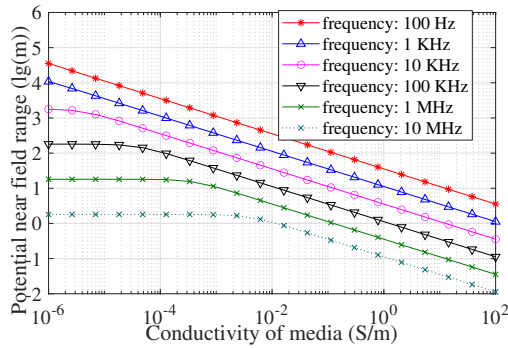


Fig. 29. Near-field ranges. The simulation parameters are listed in Table III, except for the media conductivity σ_u and frequency f .

E. Mixed-Field MI Channel Model

The MIC channel is modeled within the near-field range ($k_0 d_{SD} \ll 1$) in the vast majority of MIC research. There are a few works, such as [78], [79], [126], that focus on MIC in the non-near-field range (called mixed-field MIC) using (1), (2), and (3), where $k_0 d_{SD} \ll 1$ does not hold.

Under the mixed-field conditions, the channel power gain G_{SD} is difficult to be sub-modeled as C_{SD} , S_{SD} , \mathcal{E}_{SD} and J_{SD} . This makes the MIC channel model difficult to analyze since more effects of device components and environmental factors must be considered. For example, for the near-field model (4), the antenna-vibration-based MI fast fading is primarily related to MI polarization gain J_{SD} , which represents the APOs. For the mixed-field, more device and environment parameters (μ_u , ϵ_u , σ_u) also determine the antenna-vibration-based MI fast fading, according to (2) and (3).

In scenarios with a high conductivity medium, the near-field range is very small. As shown in Fig. 29, when the media conductivity is $\sigma_u \approx 0.01$ S/m, the near-field range is less than 10 m under $f_0 = 100$ kHz. For TTE MIC channels with higher frequency and media conductivity, the radiation field cannot be disregarded. Studies on existing upper-layer MIC protocols relying on a near-field model may encounter issues.

F. Multi-Layer and Inhomogeneous Media

For TTE scenarios, the underground medium is unlikely to be homogeneous and isotropic. There are three scenarios:

- Multi-layered medium: The medium near mineral deposits is often multi-layered. In these layers, the mineral layer may have a high conductivity and even high permeability. This may invalidate existing works.
- Inhomogeneous medium with arbitrary geometric shapes: Such scenario appears more frequently than that with a multi-layered medium, such as underground tunnels like the gray thick line in Fig. 22, urban subway systems, and subterranean business districts.

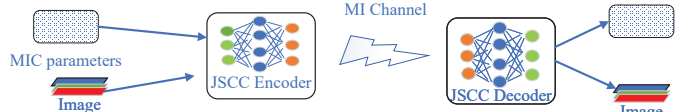


Fig. 30. Block diagram of P2P MIC based on deep JSCC.

- Dynamic medium: This scenario typically appears in oil fields, underground rivers, and mobile MICs. In this scenario, MIC channel exhibits MI fast fading, despite its longer coherence time than symbol duration.

For the first scenario, the boundary conditions between different layers and the boundary between the near-field region and radiation field region need to be considered. For the second scenario, a geometrical approximation (see [7]) can be used to transform geometric shapes. Methods based on Maxwell equations (see [48], [126]) and finite element methods (FEM) (see Fig. 4) can analyze the MIC channel model. For the third scenario, the statistical characteristics of dynamic medium are a key issue. While the derivation based on classical probability theorems can be used, the attention mechanism can be applied to obtain crucial channel information.

G. Image Transmission and Deep JSCC

Image and video transmission remains an intriguing yet unattainable function for TTE communications. It necessitates a higher achievable rate, potentially beyond Shannon's capacity for MICs utilizing VLF-LA. Using separate source-channel coding (SSCC), such as BCH and Polar coding, for further enhancing MI performance increases complexity with minimal gains, hindering sustainable development. In the EMWC area, the JSCC technique [211] has been explored to tackle this issue. Meanwhile, deep learning has been widely used to address issues on the physical layer of communication systems [192]. Deep JSCC [212]–[214] is a JSCC technique using deep learning. The source code on deep JSCC is available on Github [215]. It is a highly efficient approach for transmitting high-dimensional data.

Employing deep JSCC techniques, one can compress the high-dimensional data, including the underground environment information, through multimodal semantic or other goal-oriented analyses. If the deep JSCC technique is successfully applied to MICs (see Fig. 30), the MIC achievable rate may exceed Shannon's capacity limit. Such a technique may make the transmission of images and even videos feasible.

According to [216], the deep JSCC framework can be formulated as

$$\mathbf{x} = \mathbb{C}_\alpha(\mathbb{S}_\beta(\mathbf{s})), \quad (25)$$

where \mathbf{x} is the encoded symbol; \mathbf{s} is the input signal; $\mathbb{C}_\alpha(\cdot)$ is the neural network of the channel encoder with the parameter set α , including the MI device parameters and the underground

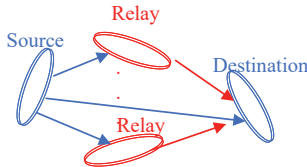


Fig. 31. The topology of the CMIC with multiple active relays featuring misaligned coils.

environments; $\mathbb{S}_\beta(\cdot)$ is the neutral network of the source encoder with the parameter set β .

For text message transmission applications, deep semantic communication techniques [216], [217], which optimize text transmission rather than symbols transmission, can be employed to compress the overall effective data stream. Transfer learning (e.g., [216]) can be employed to reduce the number of pre-trained models required across different channel environments sharing the same statistical model. This is particularly relevant for MI fast fading channels in ad-hoc links, as the PDF is difficult to derive.

H. Cooperative MIC

As depicted in Table XVII, researchers have applied either CMIC-1NR [6], [7], [10], [51] or CMIC-nAR [32], [121]. Consequently, some open issues arise, as follows.

- Crosstalk effect of CMI system: The crosstalk effect in CMI systems is typically small and often ignored in long-distance CMIC investigations (see Fig. 19). For high node-density networks, the key issue is the spatial distribution of negative crosstalk effects. Inevitably, large-scale UG-WSNs with high-density nodes generate many sufficiently close node pairs. Obtaining this spatial distribution can help upper-layer protocols, such as MAC and routing, avoid the crosstalk effect.
- Multiple active relays with misaligned coils: It has been witnessed that both CMIC-nAR and CMIC-1NR can improve MIC performance. However, the improvement from multiple active relays with misaligned antennas (see Fig. 31) is less clear due to spatial diversity limitations.

For the first issue, we can use the KVL and fundamental matrix operations to obtain a closed-form expression of the MI crosstalk effect. However, it is still a challenge to find its spatial distribution.

I. MI Network and Architecture

Table XVIII shows that existing studies can form a basic protocol stack for a large-scale, runnable TTE network. Some open issues remain for further study.

1) *Heterogeneous MI Network*: In TTE environments, free space for antenna deployment varies widely. It ranges from large spaces, such as subway stations and malls, to extremely small spaces, such as collapsed tunnels and mine shafts. We can deploy large antenna devices that constitute the backbone of a UG-WSN in large spaces and small antenna devices that constitute various levels of branch UG-WSNs in small spaces. Together, the backbone UG-WSN and the various levels of branch UG-WSNs form a heterogeneous MI UG-WSN (see Fig. 32), including cognitive MI and femtocell networks. The

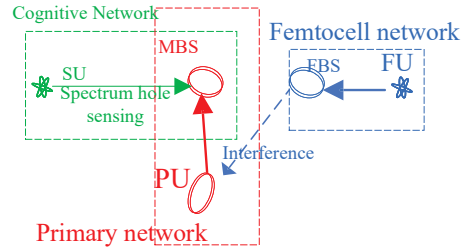


Fig. 32. Examples of heterogeneous MI UG-WSN. Here, primary users (PUs) and a macro base station (MBS) constitute the primary network. Secondary users (SUs) and an MBS can function as a part of the cognitive network. Femtocell users (FUs) and a femtocell base station (FBS) constitute the femtocell network.

cognitive network addresses the issue of spectrum scarcity, while the femtocell network improves coverage and capacity in specific areas. Recent upper-layer protocol advancements highlight the significant potential of heterogeneous MI UG-WSNs on the following key aspects.

- Channel licensing and spectrum sensing: The bandwidth of an MI channel is extremely narrow (see Fig. 21). Perceiving and utilizing spectrum holes is a fundamental task for spectrum reuse in a heterogeneous MI network. Parameters like the relationship between the resonance frequency f_0 and working frequency f are crucial for channel licensing, spectrum sensing, and their optimization solution (e.g., dynamic frequency selection).
- Connectivity: Existing investigations on MI connectivity are under the assumption of uniform MI coverage. However, heterogeneous MI UG-WSN has different antennas, such as SISO coil, RPMA, M²C antenna, and Orthogonal MIMO coils. These MI antennas can generate MI coverage spaces with varying shapes and ranges. This significantly impacts the existing statistical model of MI connectivity, such as the CDF of isolated MI nodes.
- Power and throughput optimization: Multiagent deep RL methods are widely used to address the joint power and throughput optimization problem under an unpredictable channel [218]–[220]. The key issue is insufficient bandwidth for exchanging cooperative packets among agents/players. This issue led to the abandonment of cooperative multiagent RL method with high convergence performance.

2) *MI MAC Solutions*: The IEEE 802 standards divide the data link layer into the logical link control and MAC sub-layers. The logical link control sub-layer is responsible for non-media access-related functions. The functions seem to be compatible with the MI network, but not validated. For the MAC sub-layer, although the studies [54], [55], [168] have proposed MAC solutions, there are several open issues:

- High orientation-sensitivity SISO: For the TTE scenarios, an SISO coil is a frequently used MI antenna. However, its orientation sensitivity may affect the existing MAC solutions, such as channel sensing and packet design.
- CSMA-CA: Reducing the probability of collision is an important indicator for low-bandwidth channels. The methods, such as supervised machine learning, send window optimization, and time slot optimization, can be introduced into collision avoidance (CA) schemes to

minimize the search range in the time domain.

- Frame error ratio (FER) and effective payload ratio (EPR): Lowering the FER and increasing the EPR can improve the effective data rate. However, these two ratios often cannot be optimized simultaneously. Besides multi-objective and multiagent optimization methods, antenna orientation information can be utilized as the frame header, secret key, and even the beacon sent from the MI coordinator. Additionally, the MI MAC headers in [55] require bit-level compression.
- Communication security: As MIC has low bandwidth and a frequency near resonance, it is more susceptible to interference than EMWC. Existing security schemes in EMW-based MAC layers, e.g., those in the IEEE 802.15.4 standard, are insufficient to address this issue.

3) *MI Routing Solutions*: Routing is an important function in the network layer for a large-scale network. Since 2019, there have been many studies on MI routing issues, such as issues of lifetime, transmission delay, and routing decision algorithms. However, the channel models in studies on MI routing issues are air-based MIC channels, where the eddy gain \mathcal{E}_{SD} and polarization gain J_{SD} in TTE scenarios are ignored. Air-based MIC channels are similar to EMWC. Whether $\mathcal{E}_{SD}(f)$ and J_{SD} affect the MI routing solutions, e.g., the frequency switch scheme, remains an open issue.

4) *MI Network Architecture*: Most studies on MIC focus on the physical layer, such as MI channel modeling, channel estimation, and energy and capacity optimization. In recent years, researchers have increasingly dedicated efforts to upper-layer protocols like MAC and routing protocols (see Table XVIII). The OSI-originated network framework adheres to the principle of high cohesion and low coupling in the field of software engineering, e.g., standard OSI, TCP/IP, and IEEE 802 frameworks. This principle can bring high communication performance, robustness, security, standardization, and compatibility to MI networks. Although most solutions of OSI-originated network frameworks are compatible with the MI networks, some issues can be considered for future studies and implementations.

- High cohesion and low coupling: High cohesion and low coupling in a network framework benefit system stability and compatibility. To achieve higher MIC performance, cross-layer optimization methods have been proposed in the literature (see Table XVIII). These methods, to some extent, increase the coupling among different layers. Improving MIC performance while maintaining the functionality of the mature network architecture is also a consideration in future research on MI optimization. In our framework for future research and implementation (see Fig. 26), we take this point into account.
- Standardization for MIC: As research on MIC network optimization temporarily boosts performance but disrupts the design principle of “low coupling and high cohesion”, the standards for MIC are lacking. While NFC has standards [221] (e.g., ISO 18092, NFCIP-1), its short-range and fixed-frequency design does not align with the need of UG-WSN for wide coverage and heterogeneous network integration, hindering access of large-scale TTE MIC in SAGUMI networks.

7B	1B	14B	20-60B	20-60B	4B
Preamble	0xAB	MAC Header	IP Header	TCP Header	Payload

Fig. 33. A typical TCP frame being propagated in a physical channel. In this figure, FCS denotes the Frame Check Sequence. Italicized text indicates the frame header, needing further compression for the VLF-LA channel.

J. TCP/IP Support

MIC device with TCP/IP support has broad application prospects. As most modules of TCP/IP were originally designed to be channel-agnostic, the research of TCP/IP specific supporting for MI network has been largely overlooked. However, the general TCP/IP stack is not fully compatible with an ultra-narrow-band network due to its large packet header (i.e., low EPR). As shown below, some techniques can be applied for MIC-specific TCP/IP.

1) *Header Compression (HC)*: The TCP/IP packet header, including the MAC frame header, IP header, and TCP/UDP header, is quite large. For example, the traditional IPv4 header and TCP header are both over 20 bytes in size (see Fig. 33), causing 74% overhead [185]. Such large headers total over 320 bits, taking over 3 seconds to transmit on a 100 bits/s TTE MI channel. Using header compression methods, we can achieve a potential compression ratio of over 99%. Besides channel-agnostic solutions (e.g., [190]) proposed in EMWC, dynamic SNR-dependent header size w.r.t frequency f and MI polarization gain $J_{SD}(\theta_S, \theta_D)$ can be considered to achieve further compression.

2) *RTT Optimization (RTTO)*: In the TCP/IP framework, several schemes have been used to ensure multiple applications operate over a link through various connection schemes, such as TCP, HTTP, and LLC connections. Most of these connection schemes would face fairness challenges due to RTT suppression in MI channels with a low capacity. Since RTT suppression depends heavily on the transmission channel, we can potentially formulate the corresponding optimization problem w.r.t. the SNR $\Upsilon_{SD}(f, J_{SD}(\theta_S, \theta_D))$ of the MI links, which can be further transformed into the frequency and APO optimization problem. Meanwhile, the dynamic congestion window scheme based on RTT and SNR can be adopted.

3) *Optimizing Data Chunking and Aggregation (ODCA)*: Appropriate data chunking and aggregation help reduce the number of retransmissions. For example, the TTE MIC with a 100 bit/s data rate can use 15-byte data chunks much smaller than a typical maximum transmission unit size (1500 bytes). The receiver sends an aggregated ACK after accumulating multiple chunks. This strategy can be dynamic, adapting to the CSI of the MI channel determined by f and $J_{SD}(\theta_S, \theta_D)$.

4) *Intelligent Retransmission Strategy (IRS)*: Priority retransmission involves immediate retransmissions of critical data (e.g., control commands) and delayed batch retransmissions of non-critical data (e.g., sensor readings). Context-aware packet loss detection dynamically adjusts retransmission timeouts based on MI channel quality predictions (e.g., SNR) to avoid unnecessary retransmissions.

5) *Machine-learning-based solution (ML-TCP/IP)*: For the specific MI channel, the aforementioned methods (i.e., HC, RTTO, ODCA, and IRS) can be further optimized by machine learning tools. Since the MI fast fading depends on driver's velocity, we can use attention-based deep learning (e.g., Fig. 27)

TABLE XXVI
COMPARISON OF POTENTIAL TCP/IP SCHEMES FOR TTE MICS

Schemes	Primary objective	Key mechanism	Complexity	MIC optimization directions
HC	Reduce payload overhead	Robust HC tunnel with CID negotiation [185]	Low	SNR-dependent header size
RTTO	Improve fairness; minimize round-trip time	Optimize transmission/retransmission timing	Medium	RTT-SNR problem formulation
ODCA	Reduce retransmissions	Multiple small chunks with an aggregated ACK	Medium	CSI-aware optimization
IRS	Reduce retransmissions	Priority retransmission scheme	Low	SNR-aware retransmission
ML-TCP/IP	Adapt protocol to dynamics	AVI-driven scheme	High	Attention-based for AVI predictions

or LLMs to predict the average AVIs σ_S and σ_D , dynamically adjusting the parameters of the methods w.r.t. the expectation of channel power gain ($\mathbb{E}[G_{SD}(\sigma_S, \sigma_D)]$) of the MI link.

Table XXVI compares potential TCP/IP schemes (i.e., HC, RTTO, ODCA, IRS, and ML-TCP/IP) for TTE MIC systems, indicating that MI-specific optimizations can potentially establish relationships between their primary objectives and SNR-related parameters (e.g., APO and frequency).

K. Experiments and Testing in TTE MIC Systems

Some researchers have developed MIC testbeds for both general UG scenario [222] and TTE scenario [8]. Even though TTE MIC products have entered the market [119], a lack of robust experimental validation remains a key challenge in TTE MIC research.

1) *Unrepeatable and unrepresentative UG environments*: The TTE environment is highly heterogeneous. Materials' conductivity, permittivity, and moisture content can vary significantly, even within a small area. Such unrepresentative environments may invalidate theoretical assumptions, introducing measurement noise that researchers struggle to eliminate. Moreover, VLF signals in TTE MIC are highly vulnerable to geomagnetic fluctuations and industrial interference. High-precision equipment, essential for capturing weak MI signals, is costly and scarce in academic labs. To address this challenge, a cross-scale channel model spanning centimeter-level particles to kilometer-scale strata can be developed to match the validation requirements of target theories. A data-driven method similar to the one depicted in Fig. 27 can be considered to predict the environment.

2) *Antenna deployment challenge*: In deep subsurface environments, TTE MIC antennas (0.5~4 m) often exceed the space in narrow underground areas like mine tunnels. Flexible cables distort coil shapes from standard circles, especially on mobile vehicles, causing signal deviations from theoretical expectations. For future MI fast fading validation, high-permeability metallic components (e.g., vehicle bodies and tire bearings) act as unintended magnetic reflectors/absorbers, distorting field propagation and compromising the reliability of fading model (see Fig. 6) validation. Mitigation can focus on compact rigidizable antenna designs (e.g., shape-memory structures), magnetic shielding for vehicle-mounted systems, and calibration protocols accounting for metallic interference. In addition, RPMA arrays are promising to replace Tx coils for testing due to their smaller sizes.

L. Summary of Challenges and Opportunities

Table XXII outlines the key future challenges, tasks, and recommended approaches for advancing MIC research, specifically in TTE applications. These future directions cover

critical areas, such as P2P MIC communication, MI relay techniques, and overall MI network development.

One of the most pressing challenges is the development of a universal statistical model for MI fast fading. The lack of CLT support, combined with the complexity of antenna carrier configurations, has made this task particularly difficult. Furthermore, the impact of fast fading on existing MIC theorems is significant. Unlike traditional EMWC, the randomness and unpredictability of MI fast fading's expectation and variance, which are velocity-dependent, presents unique challenges that must be addressed.

There are several other challenges related to performance metrics, antenna designs, MI MAC and routing protocols, channel modeling in inhomogeneous media, CMIC techniques, TTE MI experiment and testing. A comprehensive understanding and resolution of these challenges is key to advancing MIC technology. There are also promising research directions and novel techniques that will significantly enhance MIC performance and broaden its applications. These include MC-NSI, MI massive MIMO, deep JSCC for MIC, heterogeneous MI network techniques, and support for TCP/IP frameworks. Despite their potential, there is currently a scarcity of published research on these topics. In this paper, we propose an attention-based deep learning framework that is not limited to the prediction of the average AVI. As described in Section VII, our MI network framework carefully considers the unresolved challenges and promising future research directions highlighted above.

IX. CONCLUSION

Since 2020, research on MIC studies for TTE applications, including MI fast fading and CMIC, has increased significantly. Research in MIC continues to advance across all network layers. This survey provides a comprehensive overview of the latest developments in MIC technology within the TTE environment, covering aspects such as channel modeling in deep-penetration environments, MI fast fading channels, CMIC, and MI network architecture. Specifically, we reviewed the MI channel modeling and P2P MIC techniques, proposed a fine-grained decomposition of MI channel power gain into four key factors, and outlined optimization directions based on these factors. We discussed the challenges and impacts of MI fast fading on MIC systems. We reviewed MI relay techniques, including the MI waveguide and CMIC, analyzed their performance in TTE environments, and explored theoretically MI cross-talk effects. Moreover, we summarized advancements in multi-node MIC and large-scale MI networks by using the OSI-originated framework as a guide, and identified outstanding issues, including channel estimation, modulation, and coding in physical layer functions, MAC protocols in link layer functions, and connectivity, data collection, and routing in network layer functions.

Notably, we conceived a new and promising MI network framework with TCP/IP and Linux support, which enables researchers to leverage abundant research and development resources, accelerating MIC studies. We also summarized its challenges and open issues from the OSI-originated perspective, focusing on accessing SAGUMI in future network systems, and delineated the potential novel technical solutions, such as MCNSI, MI massive MIMO, deep JSCC for MIC, and heterogeneous MI network techniques.

REFERENCES

- [1] M. Abdollahi, W. Ni, M. Abolhasan, *et al.*, “Software-defined networking-based adaptive routing for multi-hop multi-frequency wireless mesh,” *IEEE Trans. Veh. Technol.*, vol. 70, no. 12, pp. 13 073–13 086, 2021.
- [2] V. L. Orehov and T. H. Chung, “The DARPA subterranean challenge: Synopsis of the circuits stage,” *Field Robot*, vol. 2, pp. 735–747, 2022.
- [3] Q. Cui, X. You, W. Ni, *et al.*, “Overview of AI and communication for 6G network: Fundamentals, challenges, and future research opportunities,” *Science China Information Science*, vol. 68, no. 7, p. 171301, 2025.
- [4] C. Wrigley, “Going deep: Excavation, collaboration and imagination at the Kola Superdeep Borehole,” *Environment and Planning D: Society and Space*, vol. 41, no. 3, pp. 549–567, 2023.
- [5] I. I. Shovon and S. Shin, “Survey on multi-path routing protocols of underwater wireless sensor networks: Advancement and applications,” *Electronics*, vol. 11, no. 21, p. 3467, 2022.
- [6] Z. Zhang, E. Liu, X. Zheng, *et al.*, “Cooperative magnetic induction based through-the-earth communication,” in *IEEE/CIC ICCC*, Shanghai, China, Oct. 2014, pp. 653–657.
- [7] H. Ma, E. Liu, R. Wang, *et al.*, “Antenna optimization for decode-and-forward relay in magnetic induction communications,” *IEEE Trans. Veh. Technol.*, vol. 69, no. 3, pp. 3449–3453, 2019.
- [8] Z. Zhang, E. Liu, X. Qu, *et al.*, “Connectivity of magnetic induction-based Ad Hoc networks,” *IEEE Trans. Wireless Commun.*, vol. 16, no. 7, pp. 4181–4191, Apr. 2017.
- [9] H. Ma, E. Liu, R. Wang, *et al.*, “Channel characteristics for vehicle magnetic induction communication with road disturbance,” *IEEE Commun. Lett.*, vol. 24, no. 7, pp. 1363–1367, 2020.
- [10] H. Ma, E. Liu, R. Wang, *et al.*, “Effect of antenna deployment on achievable rate in cooperative magnetic induction communication,” *IEEE Commun. Lett.*, vol. 23, no. 10, pp. 1748–1752, Oct. 2019.
- [11] H. Ma, E. Liu, Z. Fang, *et al.*, “Fast-fading channel and power optimization of the magnetic inductive cellular network,” *IEEE Trans. Wireless Commun.*, vol. 23, no. 10, pp. 15 096–15 111, 2024.
- [12] Z. Sun and I. F. Akyildiz, “Magnetic induction communications for wireless underground sensor networks,” *IEEE Trans. Antennas Propag.*, vol. 58, no. 7, pp. 2426–2435, Jul. 2010.
- [13] S. Kisseleff, W. Gerstacker, R. Schober, *et al.*, “Channel capacity of magnetic induction based wireless underground sensor networks under practical constraints,” in *IEEE WCNC*, Shanghai, China, Apr. 2013, pp. 2603–2608.
- [14] M. Zeeshan, M. Chavda, K. M. Ehsan, *et al.*, “A review on Non-RF underground positioning techniques for mining applications,” *IEEE Trans. Instrum. Meas.*, vol. 72, pp. 1–17, 2023.
- [15] S. Kisseleff, I. F. Akyildiz, and W. H. Gerstacker, “Survey on advances in magnetic induction-based wireless underground sensor networks,” *IEEE Internet Things J.*, vol. 5, no. 6, pp. 4843–4856, Dec. 2018.
- [16] M. Muzzammil, N. Ahmed, G. Qiao, *et al.*, “Fundamentals and advancements of magnetic-field communication for underwater wireless sensor networks,” *IEEE Trans. Antennas Propag.*, vol. 68, no. 11, pp. 7555–7570, 2020.
- [17] P. N. Wrathall and J. Sojdehei, “Magneto-inductive communications,” in *Info. Syst. Navy Divers & AUVs in Shallow Water*, J. L. Wood-Putnam, Ed., vol. 3711, International Society for Optics and Photonics, SPIE, 1999, pp. 229 – 236.
- [18] I. F. Akyildiz and E. P. Stuntebeck, “Wireless underground sensor networks: Research challenges,” *Ad Hoc Networks*, vol. 4, no. 6, pp. 669–686, Nov. 2006.
- [19] I. F. Akyildiz, Z. Sun, and M. C. Vuran, “Signal propagation techniques for wireless underground communication networks,” *Physical Communication*, vol. 2, no. 3, pp. 167–183, Sep. 2009.
- [20] F. Zhang, Z. Gong, S. Wang, *et al.*, “A rotating-permanent-magnet array for ULF through-the-sea magnetic communications,” *IEEE Trans. Antennas Propag.*, vol. 71, no. 3, pp. 2300–2310, 2023.
- [21] S. Yarkan, S. Guzelgoz, H. Arslan, *et al.*, “Underground mine communications: A survey,” *IEEE Commun. Surveys Tuts.*, vol. 11, no. 3, pp. 125–142, 2009.
- [22] A. E. Forooshani, S. Bashir, D. G. Michelson, *et al.*, “A survey of wireless communications and propagation modeling in underground mines,” *IEEE Commun. Surveys Tuts.*, vol. 15, no. 4, pp. 1524–1545, 2013.
- [23] S. Sheikhpour, A. Mahani, and H. F. Rashvand, *Agricultural Applications of Underground Wireless Sensor Systems: A Technical Review*. Wiley Semiconductors, 2017, pp. 351–379.
- [24] N. Saeed, M.-S. Alouini, and T. Y. Al-Naffouri, “Toward the internet of underground things: A systematic survey,” *IEEE Commun. Surveys Tuts.*, vol. 21, no. 4, pp. 3443–3466, 2019.
- [25] G. P. Hancke and B. J. Silva, “Wireless positioning in underground mines: Challenges and recent advances,” *IEEE Industrial Electronics Magazine*, vol. 15, no. 3, pp. 39–48, 2021.
- [26] D. Wohwe Sambo and A. Förster, “Wireless underground sensor networks: A comprehensive survey and tutorial,” *ACM Computing Surveys*, vol. 56, no. 4, pp. 1–44, 2023.
- [27] U. Raza and A. Salam, “A survey on subsurface signal propagation,” *Smart Cities*, vol. 3, no. 4, pp. 1513–1561, 2020.
- [28] A. Hrovat, G. Kandus, and T. Javornik, “A survey of radio propagation modeling for tunnels,” *IEEE Commun. Surveys Tuts.*, vol. 16, no. 2, pp. 658–669, 2014.
- [29] S. M. Riurean, M. Leba, and A. C. Ionica, *Conventional and Advanced Technologies for Wireless Transmission in Underground Mine*. Cham: Springer International Publishing, 2021, pp. 41–125.
- [30] E. Liu, Z. Sun, R. Wang, *et al.*, *Magnetic Communications: Theory and Techniques*. New York, NY, USA: Cambridge University Press, 2024.
- [31] A. K. Sharma, S. Yadav, S. N. Dandu, *et al.*, “Magnetic induction-based non-conventional media communications: A review,” *IEEE Sensors Journal*, vol. 17, no. 4, pp. 926–940, 2017.
- [32] Y. Li, S. Wang, C. Jin, *et al.*, “A survey of underwater magnetic induction communications: Fundamental issues, recent advances, and challenges,” *IEEE Communications Surveys Tutorials*, vol. 21, no. 3, pp. 2466–2487, Feb. 2019.
- [33] A. R. Silva and M. Moghaddam, “Strategic frequency adaptation for mid-range magnetic induction-based wireless underground sensor networks,” in *IEEE SysCon Proceedings*, Vancouver, BC, Canada, Apr. 2015, pp. 758–765.
- [34] Z. Sun, P. Wang, M. C. Vuran, *et al.*, “Mise-pipe: Magnetic induction-based wireless sensor networks for underground pipeline monitoring,” *Ad Hoc Networks*, vol. 9, no. 3, pp. 218–227, 2011.
- [35] C. B. Jenkins and A. Kiourti, “Wearable dual-layer planar magnetoinductive waveguide for wireless body area networks,” *IEEE Trans. Antennas Propag.*, vol. 71, no. 8, pp. 6893–6905, 2023.
- [36] S. Li, Y. Sun, and W. Shi, “Capacity of magnetic-induction MIMO communication for wireless underground sensor networks,” *International Journal of Distributed Sensor Networks*, vol. 11, no. 10, Jan. 2015.
- [37] H. Guo, Z. Sun, J. Sun, *et al.*, “M²I channel modeling for metamaterial-enhanced magnetic induction communications,” *IEEE Trans. Antennas Propag.*, vol. 63, no. 11, pp. 5072–5087, Nov. 2015.
- [38] Z. Wang, J. Wang, and W. Cheng, “Multi-frequency resonant circuit based multi-user emergency through-the-earth communication with magnetic induction,” in *Ucom*, 2024, pp. 152–157.
- [39] Z. Sun and I.F.Akyildiz, “On capacity of magnetic induction-based wireless underground sensor networks,” in *IEEE INFOCOM*, Orlando, FL, Mar. 2012, pp. 370–378.
- [40] U. Azad, H. C. Jing, and Y. E. Wang, “Link budget and capacity performance of inductively coupled resonant loops,” *IEEE Trans. Antennas Propag.*, vol. 60, no. 5, pp. 2453–2461, 2012.
- [41] J. Jiang, K. Song, G. Wei, *et al.*, “Capacity and bandwidth analysis of symmetric two-coil resonant magnetic communication using frequency divarication,” *IEEE Antennas Wireless Propag. Lett.*, vol. 14, pp. 370–373, 2015.
- [42] J. Zhou and J. Chen, “Maximum distance estimation of far-field model for underwater magnetic field communication,” in *2017 CCWC*, 2017, pp. 1–5.
- [43] H. Guo and Z. Sun, “Inter-media backscatter communications with magnetic induction,” in *IEEE ICC*, 2019, pp. 1–6.
- [44] Y. Liu, Q. Liu, S. Gong, *et al.*, “Chirp-rate shift keying modulation for mechanical antenna based on rotating dipoles,” *IEEE Trans. Antennas Propag.*, vol. 71, no. 4, pp. 2989–2999, 2023.
- [45] S. Kisseleff, I. F. Akyildiz, and W. Gerstacker, “On modulation for magnetic induction based transmission in wireless underground sensor networks,” in *IEEE ICC*, Sydney, NSW, Australia, Jun. 2014, pp. 71–76.

[46] Z. Chen, G. Liu, H. Zhang, *et al.*, “A novel polar code construction for magnetic induction-based wireless underground communications,” *IEEE Commun. Lett.*, vol. 27, no. 11, pp. 2884–2888, 2023.

[47] A. A. Alshehri, S.-C. Lin, and I. F. Akyildiz, “Optimal energy planning for wireless self-contained sensor networks in oil reservoirs,” in *IEEE ICC*, Paris, France, May 2017, pp. 1–7.

[48] H. Guo and Z. Sun, “Channel and energy modeling for self-contained wireless sensor networks in oil reservoirs,” *IEEE Trans. Wireless Commun.*, vol. 13, no. 4, pp. 2258–2269, Apr. 2014.

[49] J. Ma, X. Zhang, M. Liao, *et al.*, “Topology of magneto-inductive communication system based on the regular hexagonal array,” *IET Microwaves, Antennas & Propagation*, vol. 9, no. 5, pp. 389–398, 2015.

[50] R. A. Khalil and N. Saeed, “Optimal relay placement in magnetic induction-based internet of underwater things,” *IEEE Sensors Journal*, vol. 21, no. 1, pp. 821–828, 2021.

[51] Y. Zhang, “Cooperative magnetic induction communications: Performance analysis and power-location optimization,” in *IEEE WCNC*, 2024, pp. 1–6.

[52] S. C. Lin, I. F. Akyildiz, P. Wang, *et al.*, “Distributed cross-layer protocol design for magnetic induction communication in wireless underground sensor networks,” *IEEE Trans. Wireless Commun.*, vol. 14, no. 7, pp. 4006–4019, Jul. 2015.

[53] T. Li, Y. Zhao, Z. Hu, *et al.*, “Resource allocation strategy in auv-assisted edge computing uwsn with hybrid acoustic and mi communication,” in *IEEE VTC*, 2024, pp. 1–6.

[54] N. Ahmed, Y. R. Zheng, and D. Pommerenke, “Multi-coil mi based mac protocol for wireless sensor networks,” in *OCEANS 2016 MTS/IEEE Monterey*, 2016, pp. 1–4.

[55] N. Ahmed, G. Qiao, Y. R. Zheng, *et al.*, “Design and implementation of medium access control protocol for magneto-inductive wireless sensor networks using low power sensor nodes,” *IEEE Journal of Oceanic Engineering*, vol. 49, no. 2, pp. 572–582, 2024.

[56] S. Wang, T. L. N. Nguyen, and Y. Shin, “Data collection strategy for magnetic induction based monitoring in underwater sensor networks,” *IEEE Access*, vol. 6, pp. 43 644–43 653, 2018.

[57] G. Liu, “Frequency-switchable routing protocol for dynamic magnetic induction-based wireless underground sensor networks,” *IEEE Journal of Selected Areas in Sensors*, vol. 1, pp. 1–8, 2024.

[58] P. Singh, R. P. Singh, and Y. Singh, “An optimal energy-throughput efficient cross-layer solution using naked mole rat algorithm for wireless underground sensor networks,” *Materials Today: Proceedings*, vol. 48, pp. 1076–1083, 2022.

[59] V. Parameswaran, H. Zhou, and Z. Zhang, “Irrigation control using wireless underground sensor networks,” in *ICST*, Kolkata, India, Dec. 2012, pp. 653–659.

[60] Z. Li, Z. Sun, T. Singh, *et al.*, “Large range soil moisture sensing for inhomogeneous environments using magnetic induction networks,” in *IEEE GLOBECOM*, Waikoloa, HI, USA, Dec. 2019, pp. 1–6.

[61] S. Sugumar and S. M. Santhanam, “Design of filamentary planar spiral coils with enhanced channel model for magnetic induction based underground communication,” *Transactions on Emerging Telecommunications Technologies*, vol. 32, no. 10, p. e4282, 2021.

[62] C. Cariou, L. Moiroux-Arviz, F. Pinet, *et al.*, “Internet of underground things in agriculture 4.0: Challenges, applications and perspectives,” *Sensors*, vol. 23, no. 8, 2023, doi: 10.3390/s23084058. [Online]. Available: <https://www.mdpi.com/1424-8220/23/8/4058>

[63] X. Tan and Z. Sun, “An optimal leakage detection strategy for underground pipelines using magnetic induction-based sensor networks,” in *Proc. of WASA*, Berlin, Heidelberg, 2013, pp. 2780–2785.

[64] X. Tan, Z. Sun, and P. Wang, “On localization for magnetic induction-based wireless sensor networks in pipeline environments,” in *IEEE ICC*, London, UK, Jun. 2015, pp. 2780–2785.

[65] Y. Dong, J. Wu, X. Zhang, *et al.*, “A novel dual-permanent-magnet mechanical antenna for pipeline robot localization and communication,” *Sensors*, vol. 23, no. 6, p. 3228, 2023.

[66] X. Li, Q. Li, Q. Yu, *et al.*, “A rotating permanent magnets positioning system for laying underground pipelines,” *IEEE Trans. Instrum. Meas.*, vol. 73, pp. 1–9, 2024.

[67] C. Park, Q. Xie, P. Chou, *et al.*, “DuraNode: wireless networked sensor for structural health monitoring,” in *SENSORS, 2005 IEEE*, Irvine, CA, USA, 2005, pp. 1–4.

[68] P. Singh, R. P. Singh, Y. Singh, *et al.*, “Magnetic induction technology-based wireless sensor network for underground infrastructure, monitoring soil conditions, and environmental observation applications: Challenges and future aspects,” *Journal of Sensors*, vol. 2022, pp. 1–18, Jan. 2022.

[69] A. Markham and N. Trigoni, “Magneto-inductive networked rescue system (miners): Taking sensor networks underground,” in *2012 ACM/IEEE 11th IPSN*, Beijing China, Apr. 2012, pp. 1–11.

[70] S. A. Meybodi, M. Dohler, A. N. Askarpour, *et al.*, “The feasibility of communication among pumps in a district heating system,” *IEEE Antennas and Propagation Magazine*, vol. 55, no. 3, pp. 118–134, 2013.

[71] Domingo and C. Mari, “Magnetic induction for underwater wireless communication networks,” *IEEE Trans. Antennas Propag.*, vol. 60, no. 6, pp. 2929–2939, 2012.

[72] B. Gulbahar and O. B. Akan, “A communication theoretical modeling and analysis of underwater magneto-inductive wireless channels,” *IEEE Trans. Wireless Commun.*, vol. 11, no. 9, pp. 3326–3334, 2012.

[73] L. Erdogan and J.-F. Bousquet, “Dynamic bandwidth extension of coil for underwater magneto-inductive communication,” in *IEEE APSURSI*, 2014, pp. 1576–1577.

[74] I. F. Akyildiz, P. Wang, and Z. Sun, “Realizing underwater communication through magnetic induction,” *IEEE Communications Magazine*, vol. 53, no. 11, pp. 42–48, Nov. 2015.

[75] H. Guo, Z. Sun, and P. Wang, “Channel modeling of MI underwater communication using tri-directional coil antenna,” in *IEEE GLOBECOM*, San Diego, CA, USA, 2015, pp. 1–6.

[76] —, “Multiple frequency band channel modeling and analysis for magnetic induction communication in practical underwater environments,” *IEEE Trans. Veh. Technol.*, vol. 66, no. 8, pp. 6619–6632, 2017.

[77] D. Wei, S. S. Soto, J. Garcia, *et al.*, “ROV assisted magnetic induction communication field tests in underwater environments,” in *Proc. ACM Int. Conf. WUWNet*. Shenzhen China: ACM, Dec. 2018, pp. 1–5.

[78] Y. Liu, S. Gong, Q. Liu, *et al.*, “A mechanical transmitter for undersea magnetic induction communication,” *IEEE Trans. Antennas Propag.*, vol. 69, no. 10, pp. 6391–6400, 2021.

[79] H. Guo, Z. Sun, and P. Wang, “Joint design of communication, wireless energy transfer, and control for swarm autonomous underwater vehicles,” *IEEE Trans. Veh. Technol.*, vol. 70, no. 2, pp. 1821–1835, 2021.

[80] D. Wei, C. Huang, X. Li, *et al.*, “Power-efficient data collection scheme for AUV-assisted magnetic induction and acoustic hybrid internet of underwater things,” *IEEE Internet Things J.*, vol. 9, no. 14, pp. 11 675–11 684, 2022.

[81] C. Wang, Y. Cui, X. Song, *et al.*, “A novel underwater target detection method based on low-frequency magnetic signal generated by portable transmitter,” *IEEE Sensors Journal*, vol. 23, no. 8, pp. 8459–8465, 2023.

[82] X. Wang, D. Cui, W. Zhang, *et al.*, “Radiation study of low-power ultracompact rotating permanent magnetized mechanical antenna array,” *IEEE Trans. Antennas Propag.*, vol. 72, no. 7, pp. 5458–5468, 2024.

[83] X. He, Q. Zhou, and J. Zhang, “Rotating magnet-based mechanical antenna for magnetic inductive communications,” *IEEE Trans. Antennas Propag.*, vol. 72, no. 7, pp. 5502–5510, 2024.

[84] W. Zhang, Z. Cao, X. Wang, *et al.*, “Design, array, and test of super-low-frequency mechanical antenna based on permanent magnet,” *IEEE Trans. Antennas Propag.*, vol. 71, no. 3, pp. 2321–2329, 2023.

[85] S. Wang and Y. Shin, “Efficient routing protocol based on reinforcement learning for magnetic induction underwater sensor networks,” *IEEE Access*, vol. 7, pp. 82 027–82 037, 2019.

[86] L. Alsalmi and E. Alotaibi, “A balanced routing protocol based on machine learning for underwater sensor networks,” *IEEE Access*, vol. 9, pp. 152 082–152 097, 2021.

[87] Y. Zhang, D. Chen, Guanghua, *et al.*, “Performance analysis of two-hop active relaying for dynamic magnetic induction based underwater wireless sensor networks,” *IEEE Trans. Commun.*, vol. 70, no. 10, pp. 6938–6949, Oct. 2022.

[88] I. V. Zhilin, O. M. Bushnaq, G. D. Masi, *et al.*, “A universal multimode (Acoustic, Magnetic Induction, Optical, RF) software defined modem architecture for underwater communication,” *IEEE Trans. Wireless Commun.*, vol. 22, no. 12, pp. 9105–9116, 2023.

[89] G. Dumphart and A. Wittneben, “Stochastic misalignment model for magneto-inductive SISO and MIMO links,” in *IEEE PIMRC*, Valencia, Spain, Sep. 2016, pp. 1–6.

[90] A. Farhad, Y. Zia, S. Farid, *et al.*, “D-Mac: A dynamic MAC algorithm for the body area sensor networks based on ieee 802.15.4,” *IJCSNS International Journal of Computer Science and Network Security*, vol. 16, no. 5, pp. 29–35, May 2016.

[91] J. I. Agbinya and M. Masihpour, “Power equations and capacity performance of magnetic induction body area network nodes,” in *2010 Fifth International Conference on Broadband and Biomedical Communications*, Malaga, Spain, Dec. 2010, pp. 1–6.

[92] N. Thilak and R. Braun, “Near field magnetic induction communication in body area network,” in *ICDCS*, Coimbatore, India, Mar. 2012, pp. 124–125.

[93] M. Masihpour, D. Franklin, and M. Abolhasan, "Multihop relay techniques for communication range extension in near-field magnetic induction communication systems," *Journal of Networks*, vol. 8, no. 5, pp. 999–1011, May 2013.

[94] S. Kisseleff, I. F. Akyildiz, and W. Gerstacker, "Distributed beamforming for magnetic induction based body area sensor networks," in *IEEE GLOBECOM*, Washington, DC, USA, Dec. 2016, pp. 1–7.

[95] G. Dumphart, B. I. Bitachon, and A. Wittneben, "Magneto-inductive powering and uplink of in-body microsensors: Feasibility and high-density effects," in *IEEE WCNC*, Marrakesh, Morocco, Apr. 2019, pp. 1–6.

[96] N. Golestan and M. Moghaddam, "Theoretical modeling and analysis of magnetic induction communication in wireless body area networks (WBANs)," *IEEE Journal of Electromagnetics, RF and Microwaves in Medicine and Biology*, vol. 2, no. 1, pp. 48–55, 2018.

[97] S. Banou, K. Li, and K. Chowdhury, "Magic: Magnetic resonant coupling for intra-body communication," in *IEEE INFOCOM*, 2020, pp. 1549–1558.

[98] N. Golestan and M. Moghaddam, "Human activity recognition using magnetic induction-based motion signals and deep recurrent neural networks," *Nature Communications*, vol. 11, no. 1, p. 2879, 2020.

[99] V. Mishra and A. Kiourtzi, "Wearable planar magnetoinductive waveguide: A low-loss approach to wbans," *IEEE Trans. Antennas Propag.*, vol. 69, no. 11, pp. 7278–7289, 2021.

[100] L. Huang, Z. Wei, B. Chen, *et al.*, "Field-circuit combination method for solving the detuning problem of magnetic resonance human body communication," *IEEE Journal of Electromagnetics, RF and Microwaves in Medicine and Biology*, vol. 8, no. 2, pp. 94–101, 2024.

[101] M. Xu, P. S. Traore, and A. Asfour, "A high sensitivity digital giant magneto-impedance (GMI) sensor for magnetic communication," *Measurement Science and Technology*, vol. 35, no. 10, p. 104001, 2024.

[102] Z. Sun, P. Wang, M. C. Vuran, *et al.*, "BorderSense: Border patrol through advanced wireless sensor networks," *Ad Hoc Networks*, vol. 9, no. 3, pp. 468–477, 2011.

[103] S. Kisseleff, I. F. Akyildiz, and W. Gerstacker, "Disaster detection in magnetic induction based wireless sensor networks with limited feedback," in *2014 IFIP WD*. Rio de Janeiro, Brazil: IEEE, 2014.

[104] T. E. Abrudan, Z. Xiao, A. Markham, *et al.*, "Distortion rejecting magneto-inductive three-dimensional localization (MagLoc)," *IEEE J. Sel. Areas Commun.*, vol. 33, no. 11, pp. 2404–2417, Nov. 2015.

[105] O. Kypris, T. E. Abrudan, and A. Markham, "Magnetic induction-based positioning in distorted environments," *IEEE Trans. Geosci. Remote Sens.*, vol. 54, no. 8, pp. 4605–4612, 2016.

[106] S.-C. Lin, A. A. Alshehri, P. Wang, *et al.*, "Magnetic induction-based localization in randomly deployed wireless underground sensor networks," *IEEE Internet Things J.*, vol. 4, no. 5, pp. 1454–1465, 2017.

[107] N. Saeed, M.-S. Alouini, and T. Y. Al-Naffouri, "3d localization for internet of underground things in oil and gas reservoirs," *IEEE Access*, vol. 7, pp. 121 769–121 780, 2019.

[108] A. Sheinker, B. Ginzburg, N. Salomonski, *et al.*, "Localization of a mobile platform equipped with a rotating magnetic dipole source," *IEEE Trans. Instrum. Meas.*, vol. 68, no. 1, pp. 116–128, 2019.

[109] B. Wei, N. Trigoni, and A. Markham, "iMag+: An accurate and rapidly deployable inertial magneto-inductive slam system," *IEEE Trans. Mobile Comput.*, vol. 21, no. 10, pp. 3644–3655, 2022.

[110] Q. Li, X. Li, C. Wang, *et al.*, "An inertial magneto-inductive positioning system based on GWO-PF algorithm," *IEEE Trans. Instrum. Meas.*, vol. 71, pp. 1–10, 2022.

[111] A. Pal and K. Kant, "MagLoc: A magnetic induction based localization scheme for fresh food logistics," *Internet of Things*, vol. 19, p. 100552, 2022.

[112] M. Chavda, M. Zeeshan, C. O'Sullivan, *et al.*, "Magnetic-induction-based positioning system using dual multiplexing technique," *IEEE Sensors Letters*, vol. 7, no. 9, pp. 1–4, 2023.

[113] Y.-L. Chen, Z.-C. Liu, A. Li, *et al.*, "3-D positioning method of pipeline robots based on a rotating permanent magnet mechanical antenna," *IEEE Sensors Journal*, vol. 23, no. 7, pp. 7095–7104, 2023.

[114] A. T. Abraha and B. Wang, "A survey on scalable wireless indoor localization: Techniques, approaches and directions," *Wireless Personal Communications*, vol. 136, no. 3, pp. 1455–1496, 2024.

[115] W. Su, E. Liu, A. M. Calveras Augé, *et al.*, "Design and realization of precise indoor localization mechanism for Wi-Fi devices," *KSII Transactions on Internet and Information Systems*, vol. 10, no. 12, pp. 5422–5441, 2016.

[116] Z. Zhang, E. Liu, X. Qu, *et al.*, "Effective coverage for the connectivity of magnetic induction-based Ad Hoc networks," in *IEEE GLOBECOM*, San Diego, CA, USA, Dec. 2015, pp. 1–6.

[117] W. Ni, I. B. Collings, X. Wang, *et al.*, "Radio alignment for inductive charging of electric vehicles," *IEEE Trans. Ind. Informatics*, vol. 11, no. 2, pp. 427–440, 2015.

[118] (2012, Dec.) Through-the-Earth, Post-Accident Communications - an emerging technology. CDC. [Online]. Available: <https://www.cdc.gov/niosh/mining/UserFiles/Works/pdfs/2013-105.pdf>

[119] Canarycommis - vital alert — vital alert. Vital Alert. Accessed 08-04-2025. [Online]. Available: <https://vitalalert.com/product/canarycommis/>

[120] G. Liu, "A Q-learning-based distributed routing protocol for frequency-switchable magnetic induction-based wireless underground sensor networks," *Future Gener. Comput. Syst.*, vol. 139, pp. 253–266, 2022.

[121] S. Kisseleff, B. Sackenreuter, I. F. Akyildiz, *et al.*, "On capacity of active relaying in magnetic induction based wireless underground sensor networks," in *IEEE ICC*, London, UK, Jun. 2015, pp. 6541–6546.

[122] H. Guo, Z. Sun, and C. Zhou, "Practical design and implementation of metamaterial-enhanced magnetic induction communication," *IEEE Access*, vol. 5, pp. 17 213–17 229, 2017.

[123] Z. Li and Z. Sun, "Optimal active and reconfigurable meta-sphere design for metamaterial-enhanced magnetic induction communications," *IEEE Trans. Antennas Propag.*, vol. 70, no. 9, pp. 8148–8163, 2022.

[124] H. Rezaei, V. Khilkevich, S. Yong, *et al.*, "Mechanical magnetic field generator for communication in the ULF range," *IEEE Trans. Antennas Propag.*, vol. 68, no. 3, pp. 2332–2339, 2020.

[125] C. A. Balanis, *Antenna Theory: Analysis and Design*, 3rd ed. Hoboken, New Jersey, USA: John Wiley & Sons, Inc., 2005.

[126] H. Guo and A. A. Ofori, "Joint channel and antenna modeling for magnetic induction communication in inhomogeneous media," *IEEE Open Journal of the Communications Society*, vol. 1, pp. 1457–1469, 2020.

[127] O. C. Fawole and M. Tabib-Azar, "An electromechanically modulated permanent magnet antenna for wireless communication in harsh electromagnetic environments," *IEEE Trans. Antennas Propag.*, vol. 65, no. 12, pp. 6927–6936, 2017.

[128] M. Dionigi and M. Mongiardo, "Multi band resonators for wireless power transfer and near field magnetic communications," in *IEEE MTT-S IWPT Workshop*, Kyoto, Japan, 2012, pp. 61–64.

[129] J. Agbinya and H. Nguyen, "Principles and applications of frequency splitting in inductive communications and wireless power transfer systems," *Wireless Personal Communications*, vol. 107, pp. 987–1017, Apr. 2019.

[130] Z. Sun, I. F. Akyildiz, S. Kisseleff, *et al.*, "Increasing the capacity of magnetic induction communications in RF-challenged environments," *IEEE Trans. Commun.*, vol. 61, no. 9, pp. 3943–3952, 2013.

[131] J. Sogade, Y. Vichabian, A. Vandiver, *et al.*, "Electromagnetic cave-to-surface mapping system," *IEEE Trans. Geosci. Remote Sens.*, vol. 42, no. 4, pp. 754–763, Apr. 2004.

[132] M. K. Simon and M. S. Alouini, "Digital communications over fading channels: A unified approach to performance analysis," 1st ed. WileySeries in Telecommunications and Signal Processing Ed. New York, NY, USA: John Wiley & Sons, 2000.

[133] D. Tse and P. Viswanath, *Fundamentals of wireless communication*. New York, NY, USA: Cambridge university press, 2005.

[134] T. Ma, X. Jiang, and H. Hu, "A novel FBMC/QAM scheme with interference mitigation over multipath time-varying fading channels," *China Commun.*, vol. 22, no. 7, pp. 138–155, July 2025.

[135] A. A. Farid and S. Hranilovic, "Diversity gain and outage probability for MIMO free-space optical links with misalignment," *IEEE Trans. Commun.*, vol. 60, pp. 479–487, 2012.

[136] A. Jurado-Navas, J. M. Garrido-Balsells, J. F. Paris, *et al.*, "A unifying statistical model for atmospheric optical scintillation," in *Numerical simulations of physical and engineering processes*. InTech Rijeka, Croatia, 2011, vol. 181, no. 8, pp. 181–205.

[137] J.-Y. Wang, Y. Ma, R.-R. Lu, *et al.*, "Hovering UAV-based FSO communications: Channel modelling, performance analysis, and parameter optimization," *IEEE J. Sel. Areas Commun.*, vol. 39, pp. 2946–2959, 2021.

[138] M. Najafi, H. Ajam, V. Jamali, *et al.*, "Statistical modeling of the FSO fronthaul channel for UAV-based communications," *IEEE Trans. Commun.*, vol. 68, pp. 3720–3736, 2020.

[139] T. B. Aik, Q. S. Sen, and Z. Nan, "Characterization of multipath acoustic channels in very shallow waters for communications," in *OCEANS 2006 - Asia Pacific*, Singapore, 2006, pp. 1–8.

[140] A. G. Zajic, "Statistical modeling of MIMO mobile-to-mobile underwater channels," *IEEE Trans. Veh. Technol.*, vol. 60, no. 4, pp. 1337–1351, 2011.

[141] J. Wang, W. Cheng, W. Zhang, *et al.*, "Multi-frequency access for magnetic induction-based swift," *IEEE J. Sel. Areas Commun.*, vol. 40, no. 5, pp. 1679–1691, 2022.

[142] M. Chen, X. Qu, E. Liu, *et al.*, "Statistical channel modeling and estimation for pmma-based vehicle-mounted magnetic communication systems," *IEEE Trans. Veh. Technol.*, pp. 1–6, 2025, early access, doi: 10.1109/TVT.2025.3574843.

[143] S. Gang, *Vehicle noise, vibration, and sound quality*. SAE international, apr 2012.

[144] S. Kisseleff, I. F. Akyildiz, and W. Gerstacker, "Transmitter-side channel estimation in magnetic induction based communication systems," in *IEEE BlackSeaCom*. Odessa, Ukraine: IEEE, May 2014, pp. 16–21.

[145] X. Tan and Z. Sun, "On environment-aware channel estimation for wireless sensor networks using magnetic induction," in *IEEE INFOCOM WKSHPS*, Atlanta, GA, USA, 2017, pp. 217–222.

[146] J. S. Glickstein, J. Liang, S. Choi, *et al.*, "Power-efficient ELF wireless communications using electro-mechanical transmitters," *IEEE Access*, vol. 8, pp. 2455–2471, 2020.

[147] M. Golkowski, J. Park, J. Bittle, *et al.*, "Novel mechanical magnetic shutter antenna for ELF/VLF radiation," in *IEEE APS/URSI Symp. & NRSM*, Boston, MA, USA, 2018, pp. 65–66.

[148] F. Sun, F. Zhang, X. Ma, *et al.*, "Research on ultra-low-frequency communication based on the rotating shutter antenna," *Electronics*, vol. 11, no. 4, p. 596, 2022.

[149] E. Slevin, M. B. Cohen, N. Opalinski, *et al.*, "Broadband electrically small VLF/LF transmitter via time-varying antenna properties," *IEEE Trans. Antennas Propag.*, vol. 70, no. 1, pp. 97–110, 2022.

[150] R. Zhu, Z. Cheng, X. Lv, *et al.*, "Piezo-turned magnet rotation for ELF/SLF cross-medium communication in omni-direction," *Advanced Optical Materials*, vol. 12, no. 20, p. 2400461, 2024.

[151] Z. Cheng, J. Zhou, B. Wang, *et al.*, "A bionic flapping magnetic-dipole resonator for ELF cross-medium communication," *Advanced Science*, vol. 11, no. 30, p. 2403746, 2024.

[152] Y. Cui, Y. Pei, Z. Yuan, *et al.*, "The optimization of multilayer spacing for miniaturization of mechanical antenna based on unipolar electrets," *IEEE Trans. Dielectr. Electr. Insul.*, vol. 31, no. 1, pp. 50–57, 2024.

[153] H. Guo and Z. Sun, "M²I: communication: From theoretical modeling to practical design," in *IEEE ICC*, Kuala Lumpur, Malaysia, May 2016, pp. 1–6.

[154] P. Sharma, D. Bhatia, and R. S. Meena, "Metamaterial enhanced magnetization induced communication for wireless applications," in *ICICIC*, Indore, India, 2017, pp. 1–5.

[155] Z. Li and Z. Sun, "Antenna system optimization for active metamaterial-enhanced magnetic induction communications," in *EuCAP*, Krakow, Poland, Mar. 2019, pp. 1–5.

[156] J. A. Bickford, R. S. McNabb, P. A. Ward, *et al.*, "Low frequency mechanical antennas: Electrically short transmitters from mechanically-actuated dielectrics," in *IEEE APS/URSI Symp. & NRSM*, San Diego, CA, USA, 2017, pp. 1475–1476.

[157] Z. Sun and I. F. Akyildiz, "Optimal deployment for magnetic induction-based wireless networks in challenged environments," *IEEE Trans. Wireless Commun.*, vol. 12, no. 3, pp. 996–1005, 2013.

[158] E. Shamonina, V. Kalinin, R. K.H., *et al.*, "Magneto-inductive waveguide," *Electronics Letters*, vol. 38, no. 8, pp. 371–373, Apr. 2002.

[159] M. Ishtiaq and S. H. Hwang, "Performance analysis of multihop underground magnetic induction communication," *Electronics*, vol. 10, no. 11, p. 1255, 2021.

[160] Z. Sun and I. F. Akyildiz, "Deployment algorithms for wireless underground sensor networks using magnetic induction," in *IEEE GLOBECOM*, Miami, FL, USA, 2010, pp. 1–5.

[161] S. Wang, T. L. N. Nguyen, and Y. Shin, "Energy-efficient clustering algorithm for magnetic induction-based underwater wireless sensor networks," *IEEE Access*, vol. 7, pp. 5975–5983, 2019.

[162] M. Masihpour and J. I. Agbinya, "Cooperative relay in near field magnetic induction: A new technology for embedded medical communication systems," in *2010 Fifth International Conference on Broadband and Biomedical Communications*, Malaga, Spain, Dec. 2010.

[163] Y. W. P. Hong, W. J. Huang, and K. C. C. Jay, *Cooperative communications and networking: technologies and system design*. New York: Springer Science & Business Media, 2010.

[164] R. Li, J. Zhang, and A. Dang, "Cooperative system in free-space optical communications for simultaneous multiuser transmission," *IEEE Commun. Lett.*, vol. 22, no. 10, pp. 2036–2039, 2018.

[165] S. Li, P. Wang, W. Pang, *et al.*, "Performance analysis for cooperative communication system in optical IoT network with hdafl strategy," *IEEE Photonics Journal*, vol. 13, no. 3, pp. 1–22, 2021.

[166] Z.-Y. Liu, B.-Q. Ding, B.-Q. Wu, *et al.*, "Adaptive combining multi-branch frequency-domain detector for underwater acoustic cooperative communication," in *2015 12th ICCWAMTIP*, Chengdu, China, Dec. 2015, pp. 26–29.

[167] F. Ye, H. Xu, and J. Gao, "Relay selection in underwater acoustic sensor networks for QoS-based cooperative communication using game theory," *Computer communications*, vol. 219, no. Apr., pp. 104–115, 2024.

[168] N. Ahmed, A. Radchenko, D. Pommerenke, *et al.*, "Design and evaluation of low-cost and energy-efficient magneto-inductive sensor nodes for wireless sensor networks," *IEEE Systems Journal*, vol. 13, no. 2, pp. 1135–1144, 2019.

[169] Z. Sun, I. F. Akyildiz, and G. P. Hancke, "Dynamic connectivity in wireless underground sensor networks," *IEEE Trans. Wireless Commun.*, vol. 10, no. 12, pp. 4334–4344, 2011.

[170] Z. Xing, R. Wang, J. Wu, *et al.*, "Achievable rate analysis and phase shift optimization on intelligent reflecting surface with hardware impairments," *IEEE Trans. Wireless Commun.*, vol. 20, no. 9, pp. 5514–5530, 2021.

[171] Z. Xing, R. Wang, and X. Yuan, "Joint active and passive beamforming design for reconfigurable intelligent surface enabled integrated sensing and communication," *IEEE Trans. Commun.*, vol. 71, no. 4, pp. 2457–2474, 2023.

[172] —, "An efficient solution to phase-shift optimization for ris enabled joint communication and sensing," *IEEE Trans. Veh. Technol.*, pp. 1–6, 2024.

[173] J. M. Daladier and M. A. Labrador, "An adaptive logical link layer protocol for underwater acoustic communication channels," in *OCEANS*, Biloxi, MS, USA, 2009, pp. 1–8.

[174] S. Kisseleff, I. F. Akyildiz, and W. Gerstacker, "Interference polarization in magnetic induction based wireless underground sensor networks," in *IEEE PIMRC Workshops*, London, UK, 2013, pp. 71–75.

[175] B. Parrein, N. Morozs, and L. Toutain, "An internet protocol adaptation layer for underwater acoustic networks," in *Forum Acusticum 2023*, Turin, Italy, Sep. 2023.

[176] T. Matsuda and M. Yamamoto, "Performance analysis of TCP fairness between wired and wireless sessions," in *IEEE PIMRC*, vol. 5, Lisbon, Portugal, 2002, pp. 2429–2433 vol.5.

[177] J. M. Daladier and M. A. Labrador, "A data link layer in support of swarming of autonomous underwater vehicles," in *OCEANS 2009-EUROPE*, Bremen, Germany, 2009, pp. 1–10.

[178] A. Dahlberg, M. Skrzypczyk, T. Coopmans, *et al.*, "A link layer protocol for quantum networks," in *ACM SIGCOMM*, Beijing, China, Aug. 2019, pp. 159–173.

[179] P. Gupta and P. Kumar, "Critical power for asymptotic connectivity," in *Proc. 37th IEEE Conf. Decision Control*, vol. 1, Tampa, FL, USA, 1998, pp. 1106–1110.

[180] R. Wattenhofer, L. Li, P. Bahl, *et al.*, "Distributed topology control for power efficient operation in multi-hop wireless ad hoc networks," in *IEEE INFOCOM*, vol. 3, Anchorage, AK, USA, 2001, pp. 1388–1397.

[181] C. Bettstetter, "On the minimum node degree and connectivity of a wireless multihop network," in *ACM MOBIHOC*, Lausanne Switzerland, 2002.

[182] X. Wang, X. Lin, Q. Wang, *et al.*, "Mobility increases the connectivity of wireless networks," *IEEE/ACM Transactions on Networking*, vol. 21, no. 2, pp. 440–454, 2013.

[183] J. Postel, "Internet protocol (IP)," IETF, RFC 791, Sep. 1981. [Online]. Available: <https://www.rfc-editor.org/info/rfc791>

[184] S. Deering and R. Hinden, "Internet protocol, version 6 (IPv6) specification," IETF, RFC 8200, Jul. 2017. [Online]. Available: <https://www.rfc-editor.org/info/rfc8200>

[185] W.-K. Jia, L.-T. Chen, and Z.-X. Xu, "An end-to-end IP header compressed packet forwarding framework for bandwidth-constrained networks," *IEEE Transactions on Green Communications and Networking*, vol. 6, no. 4, pp. 2156–2167, 2022.

[186] J. Postel, "Transmission control protocol," IETF, RFC 793, Sep. 1981. [Online]. Available: <https://www.rfc-editor.org/rfc/rfc793>

[187] J. Xu, B. Ai, L. Chen, *et al.*, "When high-speed railway networks meet multipath tcp: Supporting dependable communications," *IEEE Wireless Communications Letters*, vol. 9, no. 2, pp. 202–205, 2020.

[188] Z. Shelby, K. Hartke, and C. Bormann, "The constrained application protocol (CoAP)," IETF, RFC 7252, June 2014. [Online]. Available: <https://www.rfc-editor.org/info/rfc7252>

[189] V. Cerf, S. Burleigh, A. Hooke, *et al.*, "Delay-tolerant networking architecture," IRTF, RFC 4838, April 2007. [Online]. Available: <https://www.rfc-editor.org/info/rfc4838>

[190] L.-E. Jonsson and G. Pelletier, "RObust Header Compression (ROHC): A Compression Profile for IP," IETF, RFC 3843, Jun. 2004. [Online]. Available: <https://www.rfc-editor.org/info/rfc3843>

[191] J. C. Mankins, *et al.*, "Technology readiness levels," Tech. Rep., 6 1995, advanced Concepts Office, NASA HQ.

[192] C. Zhao, H. Du, D. Niyato, *et al.*, "Generative AI for secure physical layer communications: A survey," *IEEE Trans. on Cogn. Commun. Netw.*, vol. 11, no. 1, pp. 3–26, 2025.

[193] M. A. Ferrag, O. Friha, B. Kantarci, *et al.*, “Edge learning for 6G-enabled internet of things: A comprehensive survey of vulnerabilities, datasets, and defenses,” *IEEE Commun. Surveys Tuts.*, vol. 25, no. 4, pp. 2654–2713, 2023.

[194] J. Corbet, A. Rubini, and G. K. Hartman, *Linux Device Drivers*, 4th ed. O’Reilly Media, Inc., Feb. 2015.

[195] C. Benvenuti, *Understanding Linux Network Internals: Guided Tour to Networking on Linux*, 1st ed., A. Oram, Ed. 1005 Gravenstein Highway North, Sebastopol, CA: “O’Reilly Media, Inc.”, 2005.

[196] DSR Corporation, “ZBOSS: Open-source ZigBee protocol stack,” Online, DSR Corporation, 2023, version 1.0. [Online]. Available: <https://dsr-iot.com/downloads/open-sourcezigbee>

[197] Rockchip, “airrockchip/rknn-toolkit2,” Github, Rockchip, 2025. [Online]. Available: <https://github.com/airrockchip/rknn-toolkit2>

[198] Y. Liu, M. Hou, and S. Gong, “A rotating permanent magnet transmitter for magnetic induction communication in RF-impenetrable environment,” in *IEEE NEMO*, Hangzhou, China, 2020, pp. 1–3.

[199] M. T. B. Tarek, S. Dharmasena, A. Madanayake, *et al.*, “Power-efficient data modulation for all-mechanical ULF/VLF transmitters,” in *IEEE MWSCAS*, 2018, pp. 759–762.

[200] Q. Zhang and Z. Hao, “Research on ask modulation method for rotating magnet based mechanical antenna array system,” in *ICEMS*, Chiang Mai, Thailand, 2022, pp. 1–5.

[201] S. Kisseleff, I. F. Akyildiz, and W. Gerstacker, “Beamforming for magnetic induction based wireless power transfer systems with multiple receivers,” in *IEEE GLOBECOM*, San Diego, CA, USA, Dec. 2015, pp. 1–7.

[202] H. J. Kim, J. Park, K. S. Oh, *et al.*, “Near-field magnetic induction MIMO communication using heterogeneous multipole loop antenna array for higher data rate transmission,” *IEEE Trans. Antennas Propag.*, vol. 64, no. 5, pp. 1952–1962, May 2016.

[203] Z. Li and Z. Sun, “Enabling magnetic beamforming in MIMO wireless power transfer using reconfigurable metasurface,” in *IEEE GLOBECOM*, 2020, pp. 1–6.

[204] G. Yang, M. R. V. Moghadam, and R. Zhang, “Magnetic MIMO signal processing and optimization for wireless power transfer,” *IEEE Trans. Signal Process.*, vol. 65, no. 11, pp. 2860–2874, Jun. 2017.

[205] Z. Xu and E. Rodriguez-Villegas, “A wireless power transfer mattress based system for perpetually operating physiological monitoring wearables,” *IEEE Trans. Biomed. Circuits Syst.*, vol. 18, no. 2, pp. 460–473, 2024.

[206] J. Wang, W. Cheng, W. Zhang, *et al.*, “Backscatter based bidirectional full-duplex magnetic induction communications,” *IEEE Trans. Commun.*, vol. 71, pp. 6258–6271, 2023.

[207] V. Pasku, A. De Angelis, G. De Angelis, *et al.*, “Magnetic field-based positioning systems,” *IEEE Commun. Surveys Tuts.*, vol. 19, no. 3, pp. 2003–2017, 2017.

[208] M. A. Khan, J. Sun, B. Li, *et al.*, “Magnetic sensors-a review and recent technologies,” *Engineering Research Express*, vol. 3, no. 2, p. 022005, Jun 2021.

[209] Z. Xing, R. Wang, X. Yuan, *et al.*, “Location information assisted beamforming design for reconfigurable intelligent surface aided communication systems,” *IEEE Trans. Wireless Commun.*, vol. 22, no. 11, pp. 7676–7695, 2023.

[210] R. Wang, Z. Xing, E. Liu, *et al.*, “Joint localization and communication study for intelligent reflecting surface aided wireless communication system,” *IEEE Trans. Commun.*, vol. 71, no. 5, pp. 3024–3042, 2023.

[211] F. Zhai, Y. Eisenberg, and A. K. Katsaggelos, “Joint source-channel coding for video communications,” in *Handbook of Image and Video Processing*, 2nd ed., A. Bovik, Ed. Burlington MA, USA: Academic, 2005, pp. 1065–1082.

[212] E. Bourtsoulatze, D. Burth Kurka, and D. Gündüz, “Deep joint source-channel coding for wireless image transmission,” *IEEE Trans. on Cogn. Commun. Netw.*, vol. 5, no. 3, pp. 567–579, 2019.

[213] J. Xu, B. Ai, W. Chen, *et al.*, “Deep joint source-channel coding for image transmission with visual protection,” *IEEE Trans. on Cogn. Commun. Netw.*, vol. 9, no. 6, pp. 1399–1411, 2023.

[214] H. Wu, Y. Shao, C. Bian, *et al.*, “Deep joint source-channel coding for adaptive image transmission over MIMO channels,” *IEEE Trans. Wireless Commun.*, vol. 23, no. 10, pp. 15 002–15 017, 2024.

[215] M. Zhang, H. Wu, G. Zhu, *et al.*, “Semantics-guided diffusion for deep joint source-channel coding in wireless image transmission,” *IEEE Trans. Wireless Commun.*, pp. 1–1, 2025, early access, doi: 10.1109/TWC.2025.3591456.

[216] H. Xie, Z. Qin, G. Y. Li, *et al.*, “Deep learning enabled semantic communication systems,” *IEEE Trans. Signal Process.*, vol. 69, pp. 2663–2675, 2021.

[217] J. Huang, K. Yuan, C. Huang, *et al.*, “D2-JSCC: Digital deep joint source-channel coding for semantic communications,” *IEEE J. Sel. Areas Commun.*, vol. 43, no. 4, pp. 1246–1261, 2025.

[218] X. Chen, Z. Zhao, and H. Zhang, “Stochastic power adaptation with multiagent reinforcement learning for cognitive wireless mesh networks,” *IEEE Trans. Mobile Comput.*, vol. 12, no. 11, pp. 2155–2166, Nov. 2013.

[219] D. Shi, F. Tian, and S. Wu, “Energy efficiency optimization in heterogeneous networks based on deep reinforcement learning,” in *IEEE ICC Workshops*, 2020, pp. 1–6.

[220] F. G. Ortiz-Gomez, D. Tarchi, R. Martinez, *et al.*, “Cooperative multi-agent deep reinforcement learning for resource management in full flexible VHTS systems,” *IEEE Trans. on Cogn. Commun. Netw.*, vol. 8, no. 1, pp. 335–349, 2022.

[221] ISO/IEC, *Information Technology-Telecommunications and Information Exchange between Systems-Near Field Communication-Interface and Protocol (NFCIP-1)*, ISO/IEC International Standard 18 092, 2013. [Online]. Available: <https://webstore.ansi.org/standards/iso/isoiec180922013>

[222] X. Tan, Z. Sun, and I. F. Akyildiz, “A testbed of magnetic induction-based communication system for underground applications,” *arXiv preprint arXiv:1503.02519*, 2015.



Honglei Ma received the Ph.D. degree from the School of Electronics and Information Engineering, Tongji University, China, in 2020. He is currently with School of Electronic and Electrical Engineering, Shanghai University of Engineering Science. From 2009 to 2015, he served as a Senior Engineer with the Chinese Academy of Sciences. His current research interests include magnetic induction communications, ad-hoc network, wireless sensor network, and object detection for embedded systems.



Erwu Liu (Senior Member, IEEE) received the Ph.D. degree from Huazhong University of Science and Technology, China, in 2001. He has been a Professor with Tongji University since 2011. Previously he was with Alcatel-Lucent (2001-2007) and Imperial College London (2007-2011). He studies localization & sensing, AI & blockchain, and wireless communications & IoT, with 120+ papers published and 70+ patents granted/pending. Prof. Liu won the Microsoft Indoor Localization Competition (IPSN) in 2016 and 2018, and developed the indoor navigation system for China International Import Expo (CIIE). He is the Community Dev. Co-Chair of IEEE Blockchain Technical Community (BCTC), and leads the local group development of the IEEE BCTC in Asia/China. He leads the Shanghai Engineering Research Center for Blockchain Applications and Services (SERCBAAS). He is an IET Fellow, the Founding Editor-in-Chief of IET Blockchain, and the Founding Chair of the IEEE Global Blockchain Conference (GBC).



Wei Ni (Fellow, IEEE) received the B.E. and Ph.D. degrees in Electronic Engineering from Fudan University, Shanghai, China, in 2000 and 2005, respectively. He is the Associate Dean (Research) in the School of Engineering, Edith Cowan University, Perth, and a Conjoint Professor at the University of New South Wales, Sydney, Australia. He was a Deputy Project Manager at the Bell Labs, Alcatel/Alcatel-Lucent from 2005 to 2008; a Senior Research Engineer at Nokia from 2008 to 2009; and a Senior Principal Research Scientist and Group

Leader at the Commonwealth Scientific and Industrial Research Organisation (CSIRO) from 2009 to 2025. He has been an Editor for IEEE Transactions on Wireless Communications since 2018, IEEE Transactions on Vehicular Technology since 2022, IEEE Transactions on Information Forensics and Security and IEEE Communication Surveys and Tutorials since 2024, and IEEE Transactions on Network Science and Engineering since 2025. He served as Secretary, Vice-Chair, and Chair of the IEEE VTS NSW Chapter from 2015 to 2022, Track Chair for VTC-Spring 2017, Track Co-chair for IEEE VTC-Spring 2016, Publication Chair for BodyNet 2015, and Student Travel Grant Chair for WPMC 2014.



Dusit Niyato (M'09-SM'15-F'17) is a professor in the College of Computing and Data Science, at Nanyang Technological University, Singapore. He received B.Eng. from King Mongkuts Institute of Technology Ladkrabang (KMITL), Thailand and Ph.D. in Electrical and Computer Engineering from the University of Manitoba, Canada. His research interests are in the areas of mobile generative AI, edge general intelligence, quantum computing and networking, and incentive mechanism design.



Zhijun Fang (Senior Member, IEEE) received the Ph.D. degree from Shanghai Jiao Tong University, Shanghai, China. He is currently a Professor and the Dean with the School of Electronic and Electrical Engineering, Shanghai University of Engineering Science. His current research interests include image processing, video coding, and pattern recognition. He was the General Chair of the Joint Conference on Harmonious Human Machine Environment (HHME) 2013 and the General Co-Chair of the International Symposium on Information Technology Convergence (ISITC) in 2014, 2015, 2016, and 2017. He received the “Hundred, Thousand and Ten Thousand Talents Project” in China. He received several major program projects of the National Natural Science Foundation of China and the National Key Research and Development Project of the Ministry of Science and Technology of China.



Rui Wang (Senior Member, IEEE) received the Ph.D. degree from Shanghai Jiao Tong University, China, in 2013. From August 2012 to February 2013, he was a Visiting Ph.D. Student with the Department of Electrical Engineering, University of California at Riverside. From October 2013 to October of 2014, he was a Post-Doctoral Research Associate with the Institute of Network Coding, The Chinese University of Hong Kong. He is currently a Professor with the College of Electronics and Information Engineering, Tongji University. He is also with the Shanghai Institute of Intelligent Science and Technology, Tongji University. He has published over 60 articles. His research interests include wireless communications, artificial intelligence, and wireless positioning. He is also an Associate Editor of IEEE ACCESS and an Editor of IEEE WIRELESS COMMUNICATIONS LETTERS.



Ekram Hossain (Fellow, IEEE) is a Professor and the Associate Head (Graduate Studies) of the Department of Electrical and Computer Engineering, University of Manitoba, Canada. He is a Member (Class of 2016) of the College of the Royal Society of Canada. He is also a Fellow of the Canadian Academy of Engineering and the Engineering Institute of Canada. He has won several research awards, including the 2017 IEEE Communications Society Best Survey Paper Award and the 2011 IEEE Communications Society Fred Ellersick Prize Paper Award. He was listed as a Clarivate Analytics Highly Cited Researcher in Computer Science in 2017-2025. Previously, he served as the Editor-in-Chief (EiC) for the IEEE Press (2018-2021) and the IEEE Communications Surveys and Tutorials (2012-2016). He was a Distinguished Lecturer of the IEEE Communications Society and the IEEE Vehicular Technology Society. He served as the Director of Magazines (2020-2021) and the Director of Online Content (2022-2023) for the IEEE Communications Society.



Yongbin Gao received the Ph.D. degree from Jeonbuk National University, South Korea. He is currently an Associate Professor with the School of Electronic and Electrical Engineering, Shanghai University of Engineering Science, Shanghai, China. He has published 30 SCI articles in prestigious journals.